

JUACEP Program

at University of Michigan & UCLA

2016 Long/Medium/Short



Table of Contents

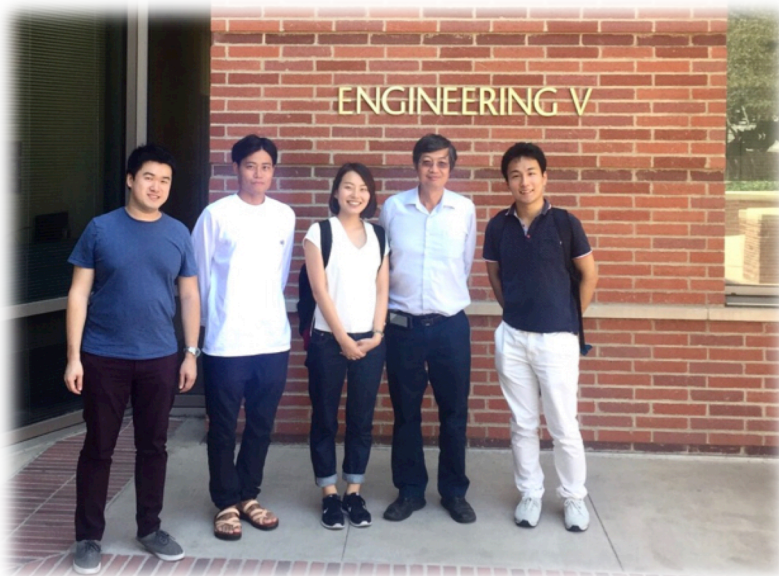
<1> About the Program	
(a) Overview	2
(b) Participants	3
(c) Schedule	4
<2> Research Reports	5
<3> Research Presentations	
● For 2016 Short-term course	42
● For 2016 Medium- and Long-term course	47
<4> Findings through JUACEP	
● Students' reviews	60
● Questionnaires (in Japanese)	68

<1> About the Program

- (a) Overview
- (b) Participants
- (c) Schedule



With Prof. Kurabayashi (leftmost) at Univ. Michigan



With Prof. Yang (second from the right) at UCLA

(a) Overview

JUACEP provides three program courses for students of the Graduate School of Engineering at Nagoya University to study abroad: a short-term (two months) course; a medium-term (six months) course; a long-term (eight months) course. Choosing one of those courses the selected students are offered an opportunity to work together with faculty and other researchers or students from all over the world at the world's top universities.

Each student works on a research project related to his/her own master's thesis topic while belonging to a specialized research group of the University of Michigan or UCLA. In addition to research implementation, the students are expected to attend lab seminars, lab discussions and other events. At the end of each course, the students are required to submit a research report to their mentors at the host institution, then give a research presentation based on their achievements in front of the faculty and peer students at JUACEP Workshop held in Nagoya University. The report and the presentation are primary requisites for course credits of the program.

This publication is compiling the activities of the following students.

- [a] One student of short-term course from August to September 2016 at Univ. Michigan
- [b] Two students of short-term course from August to September 2016 at UCLA
- [c] Three students of medium-term course from August 2016 to January 2017 at Univ. Michigan
- [d] One student of medium-term course from August 2016 to January 2017 at UCLA
- [e] One student of Long-term course from August 2016 to March 2017 at Univ. Michigan

JUACEP 2016 Short-, Medium- and Long-term Courses Flowchart

	Short-term course	Medium-term course	Long-term course
January 2016	Public announcement and accepting application (Jan. - Mar.)		
February			
March			
April	Screening candidates		
May	Selected students approach UM/UCLA faculty to get post of 'Visiting Scholar' (called *VGR at UCLA). After acceptance by faculty, **DS-2019 procedure starts including examination of CV, English proficiency and other qualification.		
June			
July	J-1 Visa application		
August	[a,b] Short-term course study at UM/UCLA from Aug. to Sep. 2016	[c,d] Medium-term course study at UM/UCLA from Aug. 2016 to Jan. 2017	[e] Long-term course study at UM from Aug. 2016 to Mar. 2017
September			
October	18 th Workshop, Oct. 6 2016		
November			
January 2017			
February			
March			
April		19 th Workshop, Mar. 31, 2017	

*VGR: Visiting Graduate Researcher for UCLA

**DS-2019: Certificate of eligibility to obtain J-1 Visa

(b) Participants

University of Michigan

Short-term (Program period: August 8, 2016 – September 23, 2016)

Name		Advisor at NU	Advisor at UM
Kazuya Sato	M1	Prof. Akira Uritani Quantum Science and Energy Engineering	Prof. Zhong He Nuclear Engineering and Radiological Science

Medium-term (Program period: August 8, 2016 – January 27, 2017)

Kota Konishi	M1	Prof. Noritsugu Umehara Mechanical Science and Engineering	Prof. Wei Lu, Mechanical Engineering
Toshiya Sawaki	M1	Prof. Noritsugu Umehara Mechanical Science and Engineering	Prof. Richard Laine Materials Science and Engineering
Akira Tsuji	M1	Prof. Hosei Nagano Mechanical Science and Engineering	Assoc. Prof. Pramod Reddy Mechanical Engineering

Long-term (Program period: August 5, 2016 – March 24, 2017)

Keisuke Goto	M1	Prof. Jiro Kasahara Aerospace Engineering	Prof. Katsuo Kurabayashi Mechanical Engineering
--------------	----	--	--

UCLA

Short-term (Program period: August 8, 2016 – September 23, 2016)

Takaharu Katsu	M1	Prof. Chikara Ohtsuki Crystals Materials Science	Prof. Benjamin Wu Bioengineering
Chisato Atsumi	M1	Prof. Chikara Ohtsuki Crystals Materials Science	Prof. Yu Huang Materials Science and Engineering

Medium-term (Program period: August 8, 2016 – January 27, 2017)

Naoki Kamimura	M1	Prof. Yahachi Saito Quantum Engineering	Prof. Ya-Hong Xie Materials Science and Engineering
----------------	----	--	--

Coordinators at Partner Universities

Prof. Katsuo Kurabayashi Mechanical Engineering, University of Michigan
Prof. Jenn-Ming Yang Materials Science and Engineering, UCLA

JUACEP Members

Prof. Noritsugu Umehara Mechanical Science and Engineering
Prof. Yang Ju Mechanical Science and Engineering
Assoc. Prof. Yasumasa Ito Mechanical Science and Engineering
Tomoko Kato Administrative Staff

(c) JUACEP Research Abroad 2016 Schedule

Period	Short-term course	Medium-term course	Long-term course
2016/08/03~2016/08/08	Departure from Japan and starting of JUACEP research activity at Univ. Michigan and UCLA		
~2016/09/15	Research activity at each lab		
2016/09/16~2016/09/28	Submitting research report to the advisor and receiving evaluation sheet from the advisor	Research activity at each lab	Research activity at each lab
~2016/09/30	Departure from US/ arrival at Nagoya	Research activity at each lab	Research activity at each lab
2016/10/03	Submission deadline for 3 reports and evaluation sheet to JUACEP Office	Research activity at each lab	Research activity at each lab
2016/10/06	The 18th Workshop for Short-term course	Research activity at each lab	Research activity at each lab
~2017/01/18		Research activity at each lab	Research activity at each lab
2017/01/19~2017/01/27		Submitting research report to the advisor and receiving evaluation sheet from the advisor	Research activity at each lab
~2017/01/31		Departure from US/ arrival at Nagoya	Research activity at each lab
2017/02/02		Submission deadline for 3 reports and evaluation sheet to JUACEP Office	Research activity at each lab
TBA			Research activity at each lab
~2016/03/15			Research activity at each lab
2017/03/16~2017/03/24			Submitting research report to the advisor and receiving evaluation sheet from the advisor
~2017/03/27			Departure from US/ arrival at Nagoya
2017/03/29			Submission deadline for 3 reports and evaluation sheet to JUACEP Office
2017/03/31	The 19th Workshop for Long- and Short-term course		

<2> Research Reports

Studies at University of Michigan

[S] **Kazuya Sato**, *mentored by Prof. Zhong He* (P.6)
Effect of Scatter Angle Overestimation in Compton Images of Partial Deposited Energy

[M] **Kota Konishi**, *mentored by Prof. Wei Lu* (P.7)
Development of Three Dimensional Imaging Techniques Using Optical Microscope

[M] **Toshiya Sawaki**, *mentored by Prof. Richard Laine* (P.15)
Development of Transparent YSZ Thin Films

[M] **Akira Tsuji**, *mentored by Prof. Pramod Reddy* (P.22)
3D-Printing of Porous and Solid Silicone Structures

[L] **Keisuke Goto**, *mentored by Prof. Katsuo Kurabayashi* (P.23)
Therapeutic Sepsis Biomarker Screening with Localized Surface Plasmon Resonance Biosensors

Studies at UCLA

[S] **Takaharu Katsu**, *mentored by Prof. Benjamin Wu* (P.29)
Synthesis of Biopolymer Compound with Selective Antimicrobial Activity for Denture Applications

[S] **Chisato Atsumi**, *mentored by Prof. Yu Huang* (P.34)
Synthesis of Octahedral Platinum-copper Nanocrystals

[M] **Naoki Kamimura**, *mentored by Prof. Ya-Hong Xie* (P.35)
Local Feeding APCVD Graphene Growth on Cu and Cu:Ni Foils

**[S]; Short-term course, [M]; Medium-term course, [L]; Long-term course*

EFFECT OF SCATTER ANGLE OVERESTIMATION IN COMPTON IMAGES OF PARTIAL DEPOSITED ENERGY

Kazuya Sato

Department of Quantum Energy Engineering, Nagoya University
Satou.kazuya@f.mbox.nagoya-u.ac.jp

Supervisor: Zhong He

Nuclear Engineering & Radiological Sciences, University of Michigan
hezhong@umich.edu

ABSTRACT

When we create a gamma-ray image of a point source using Compton camera, the image of partial energy deposition events has a shape which we do not completely understand. Most notably, there is a dip in intensity, or a “hole” the direction where the hot spot should be. When another, smaller-intensity photopeak exists in the Compton continuum of another source, it can be difficult to observe the small peak’s image against the high intensity image of the continuum. It is of interest to be able to predict the shape of the continuum image so we can remove it from the small photopeak image in this case. Through measurement, simulation and hand calculation, we have gained a better understanding about how the continuum image changes as a function of energy for 662 keV gamma rays incident on a single pixelated CdZnTe crystal.

Undisclosed

DEVELOPMENT OF THREE DIMENSIONAL IMAGING TECHNIQUES USING OPTICAL MICROSCOPE

Kota Konishi

Graduate School of Engineering, Nagoya University
konishi.kouta@g.mbox.nagoya-u.ac.jp

Supervisor: Prof. Wei Lu

Department of Mechanical Engineering, University of Michigan
weilu@umich.edu

ABSTRACT

In recent years, three-dimensional (3D) imaging techniques have been developed in several fields. Since 3D images provide more information than 2D images, many applications are expected. Here, we focus on 3D imaging techniques using an optical microscope. We develop two techniques for opaque material and transparent material, respectively.

For opaque material, we use shape from focus (SFF) method. In SFF, reflective material can cause a noisy result. To address this problem, we propose a new method to correct the error and noise using different contrast-level images. Consequently, noisy results are successfully reduced.

For transparent material, we use optical projection tomography (OPT) method. OPT has been developed mainly for biomedical applications, and its applications to other fields has not been explored. We arranged an OPT set-up using an ordinary optical microscope, and successfully generated 3D image of transparent samples.

1 INTRODUCTION

In recent years, three-dimensional (3D) imaging techniques have been developed in several fields such as the medical applications, geometry, biology and material science. 3D imaging allows us to obtain information which cannot be obtained from 2D imaging. There is a remarkable variety of 3D imaging and their applications depend on samples [1][2]. For small samples, micro computed tomography (μ -CT), confocal laser microscope, scanning electron microscope (SEM) have been used. These techniques, however, are very expensive and time-consuming. Thus, 3D imaging using optical microscope has been developed because of its accessibility [3].

In this paper, two types of 3D imaging techniques using optical microscope has been developed. One is for opaque samples, while the other is for transparent samples.

2 OPAQUE MATERIAL

2.1 BACKGROUND

There are a variety of 3D imaging methods using optical light. For example, as commonly used techniques, there are laser triangulation, stereo vision, structured light, shape from X, and so on [4]. These techniques can be classified into active and passive method. The active methods involve specifically controlled lightning or illumination to obtain the 3D data whereas the passive methods depend only on the ambient light. Based on the accuracy, computational time, and cost, each technique varies with strengths and weaknesses. These techniques have been widely applied in various fields.

In this paper, Shape from focus method has been developed. The details of this method are described in 2.2.1. Basically, the procedure is divided into two steps. The first step is image acquisition, and the second step is a calculation of the degree of focus. According to the degree of focus at each point, the most focused point in an image sequence is decided. The value of the degree of focus is called focus measure. In the literature, many focus measure methods has been proposed. However, the result of these focus measure method is affected by the type of sample, the camera, the noise level, and the window size (a parameter for calculating focus measure)[5]. Hence, which focus measure method is the best in general is indefinable.

To evaluate and improve the focus measure at certain situation, a reflective sample shown in Fig. 2.1 was used. At first, appropriate focus measure operator was selected by comparing the performance of four different software and then MATLAB code was written based on the best operator's algorithm to decrease noisy results. To realize this, new method using different contrast-level images is proposed.

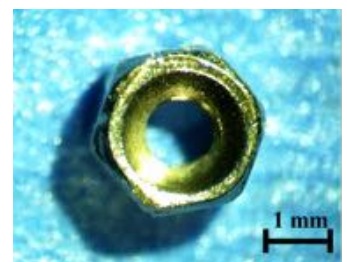


Fig. 2.1 Specimen for SFF

2.2 METHOD

2.2.1 SHAPE FROM FOCUS

SFF is a 3D imaging method estimating depth information from an image sequence. Since this technique employs a monocular image acquisition method, it is not confronted with the correspondence problem, which happens with the stereo vision method [6]. Moreover, the hardware complexity is low and no special equipment is required.

Here, we first explain the defocused images in order to explain the principle of SFF [7]. The image formation is illustrated in Fig. 2.2.

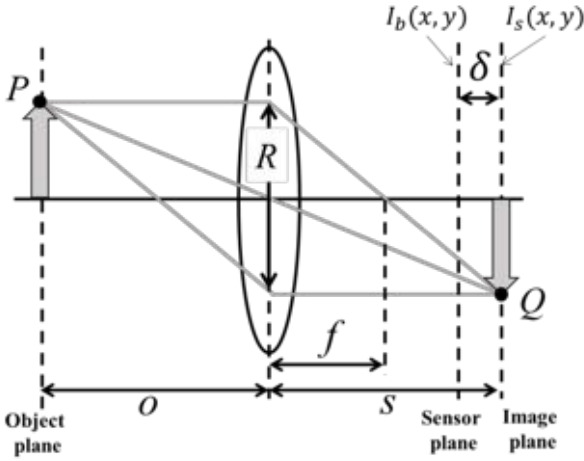


Fig. 2.2 Optical image formation

The object point P is imaged into point Q by a lens with an aperture R . The point Q lies in the image plane of a lens. The distance between the object and the lens, o , and the distance between the lens and the image plane, s , have a relation shown in Eq. (1)

$$\frac{1}{o} + \frac{1}{s} = \frac{1}{f} \quad (1)$$

where f is the focal length of the lens. A focused image $I_s(x, y)$ is formed in the image plane. If the image plane does not coincide with the sensor plane, where the distance between them is δ , the energy received from the object by the lens is distributed on the sensor plane in a circular shape. The radius of this shape can be calculated by Eq. (2).

$$r = \frac{\delta \cdot R}{s} \quad (2)$$

The blurred image $I_b(x, y)$ which is formed on the sensor plane can be considered as a result of the convolution between a focused image $I_s(x, y)$ and a blur function $h(x, y)$.

$$I_b(x, y) = I_s(x, y) * h(x, y) \quad (3)$$

It is not possible to calculate analytically the blur function for a circular aperture. However, for an approximate calculation, this blur function can be approximated by a low pass filter, and the circular aperture can be replaced by a Gaussian function.

$$h(x, y) = \frac{1}{2\pi\sigma_h^2} \exp\left(-\frac{x^2 + y^2}{2\sigma_h^2}\right) \quad (4)$$

The spread parameter σ_h is proportional to the radius r . The larger the δ is, the higher frequencies are cut off. As a result, a blurred image is obtained.

According to Eqs. (3) and (4), a blurred image has lower frequency. In the image processing field, an image with low frequency means an image with low variation. In other words, it is possible to figure out the degree of focus by calculating the image variation at each pixel. Comparing those values with the other images in a whole image sequence, one can estimate which image is the most focused. A lot of focus measure algorithm have been proposed and the details of focus measure methods are described in 2.2.3.

As described in 2.1, there are two main steps in SFF. In the first step, a sequence of images of a sample is acquired as the level of focus of the object is changed. This is conducted by moving the sample stage in the direction of the z axis. Each object point is gradually focused until it is completely focused and then it is gradually defocused. In the second stage, the focus measure is calculated at each pixel in a whole image sequence and then maximum focus measure is calculated out at each pixel. Finally, the height at the pixel can be estimated according to the movement distance of the stage.

2.2.2 SET-UP

The SFF acquisition system is set up based on a normal microscope. The schematic overview of the image acquisition system is shown in Fig. 2.3. To acquire an image sequence, the displacement of the stage is the z -axis movement of the stage controlled by a stepping motor (PKP546MN18A, ORIENTAL MOTOR). This motor makes it possible to control the displacement of the stage by $0.2 \mu\text{m}$ adjustments. The setting of the number of images and the displacement was conducted using a macro plugin in Micro-Manager 1.4, and those parameters can be changed easily in the software. The images are captured by a CCD camera (MU1000, AmScope) with a resolution of 896 by 684 pixels. Additional LED light is used to illuminate the sample to brighten the image field. In this experiment, 50 images were acquired at the intervals

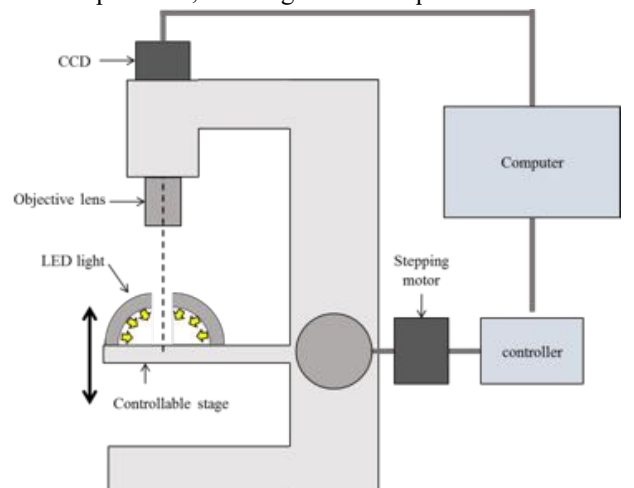


Fig. 2.3 Schematic of SFF system

of 0.04 mm. Total displacement was 2 mm which was enough to produce both a focused image and a defocused image in the image sequence.

2.2.3 FOCUS MEASURE METHOD

There are numerous solutions of focus measure methods in the literature. Pertuz investigated the performances of several focus measure operators [5]. Pertuz concluded that it is difficult to determine which focus measure operators have the best performance for various conditions. Depending on the condition, an appropriate focus measure operator should be selected. The three most commonly used focus measure operators are Sum of Modified Laplacian (SML), Tenenbaum gradient (TEN), and Gray Level Variance (GLV) [8]

SML is based on Laplace filter. Second derivatives in x and y directions are calculated and these absolute values are added at each pixel (Eq. (5)). This is called Modified Laplacian (ML).

$$ML(x_0, y_0) = \left| \frac{d^2 g(x, y)}{dx^2} \right| + \left| \frac{d^2 g(x, y)}{dy^2} \right| \quad (5)$$

where $g(x, y)$ is the gray value for the coordinates (x, y) . In SML, the focus measure at pixel (x_0, y_0) is defined as a sum of ML in a local window (Eq. (6)).

$$SML(x_0, y_0) = \sum_{p(x, y) \in U(x_0, y_0)} ML(x, y) \quad (6)$$

TEN is based on Sobel gradient operator which is commonly used to detect edges. The focus measure method used sum of squares of horizontal Sobel mask G_x and vertical Sobel mask G_y (Eq. (7)). These values also summed in a local window. In TEN, the focus measure at pixel (x_0, y_0) is defined as Eq. (8).

$$G_x = [-1 \ 0 \ 1 : -2 \ 0 \ 2 : -1 \ 0 \ 1], G_y = G_x^T \quad (7)$$

$$TEN(x_0, y_0) = \sum_{p(x, y) \in U(x_0, y_0)} [G_x(x, y)^2 + G_y(x, y)^2] \quad (8)$$

GLV is based on variations in a gray level values in an image. The focused image has more variation than the blurred image. The variation at pixel (x_0, y_0) is calculated as a square of the result of subtracting mean value of the pixels around (x_0, y_0) from the gray value at (x_0, y_0) . These values are described as $\mu_{U(x_0, y_0)}$ and $g(x_0, y_0)$ respectively. Next, the variation at pixel (x_0, y_0) is averaged by its neighborhood pixels (Eq. (9)).

$$GLV(x_0, y_0) = \frac{1}{N-1} \sum_{p(x, y) \in U(x_0, y_0)} [g(x, y) - \mu_{U(x_0, y_0)}]^2 \quad (9)$$

In addition to these methods, many other methods are proposed in the literature. For example, there are some focus measure operators which are based on the discrete wavelet transform [9], or those which are based on discrete cosine transform [10] and so on. In this research, first of all, 4 different freeware [11] (Expanded-Depth-of-Field, Focus stacker, CombineZM, Picolay) are used to calculate a focus

measure and to generate depth map which is an image including depth information, and the results were compared each other. As a result, Picolay showed the best result among the four software. Since these software showed only the result, the reconstruction should be conducted without these software to investigate into focus measure. The 3D reconstruction in the following experiments was conducted using MATLAB, whose algorithm was created based on the TEN focus operator as well as Picoley.

2.2.4 3D VISUALIZATION

Based on the depth map, 3D visualization is completed using 3D surface plot plugin in ImageJ. This plugin also allows us to apply texture of the surface. For example, the 3D image created from the depth map which is generated by MATLAB are shown in Fig. 2.4. The red area shows high area. In addition, the 3D image with its texture is shown in Fig. 2.4

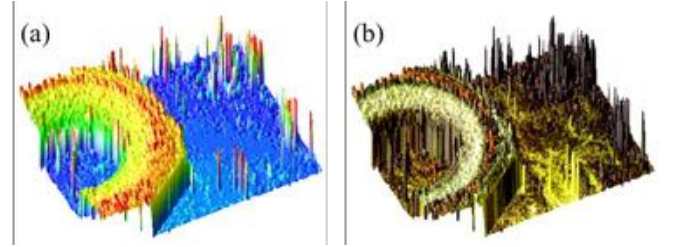


Fig. 2.4 (a) 3D image, (b) 3D image with its texture

2.2.5 REMOVAL OF ERROR

As shown in Fig. 2.4, the 3D visualization is successfully completed. However, some area showed error results, especially in the dark area of the top surface of the specimen. Because the dark areas show low variance, the focus measure is easily disturbed by unexpected errors. To address this problem, high-contrast images created from the original image sequence by ImageJ are used. By increasing the image contrast, it is assumed that the variance of the dark areas grows while the errors which derive from bright areas shrinks. However, the image saturation might cause inaccuracies in the focus measure in bright areas. Consequently, a depth map made by high-contrast images includes better results and worse results. In order to extract only accurate results from several results, the reliability of focus measure was calculated and compared among the different images at each pixel [12]. By then picking up the most reliable result, a combined depth map was created.

Focus measure function $f(x)$ is defined as a function of the experimental results at each pixel. Some researchers have proposed to assume the focus measure function as a Gaussian function. In this way, the idealized focus function corresponds to a bell-shaped peak whose maximum corresponds to the position of the best focus. Following this assumption, the focus function $f(x)$ was fitted as the Gaussian function $F(x)$ (Eq. (10)).

$$F(x) = F_{peak} \exp \left\{ -\frac{1}{2} \left(\frac{d - \bar{d}}{\sigma_F} \right)^2 \right\} \quad (10)$$

where \bar{d} and σ_F are the mean and standard deviation of the Gaussian distribution. To calculate \bar{d} and σ_F , the maximum focus measure point (d_m, f_m) and its adjacent two points (d_{m-1}, f_{m-1}) , (d_{m+1}, f_{m+1}) are used (Eq. (11) (12))[7]. These points are also shown in .

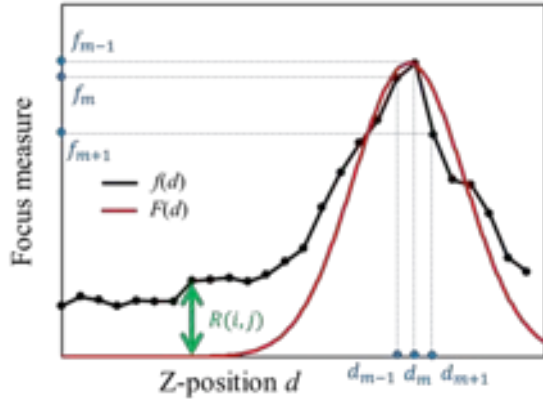


Fig. 2.5 Gaussian fitting

$$\bar{d} = \frac{(\ln f_m - \ln f_{m+1})(d_m^2 - d_{m-1}^2) - (\ln f_m - \ln f_{m-1})(d_m^2 - d_{m+1}^2)}{2\{(\ln f_m - \ln f_{m-1}) + (\ln f_m - \ln f_{m+1})\}} \quad (11)$$

$$\sigma_F^2 = -\frac{(d_m^2 - d_{m-1}^2) + (d_m^2 - d_{m+1}^2)}{2\{(\ln f_m - \ln f_{m-1}) + (\ln f_m - \ln f_{m+1})\}} \quad (12)$$

The reliability function $R(i, j)$ is defined by Eq. (13)

$$R(i, j) = 1 - \max\{|F(x) - f(x)|\} \quad (13)$$

where $\max\{*\}$ means denotes the supremum operator. The value shows how small the difference between $f(x)$ and $F(x)$. The maximum value is 1, which means that $f(x)$ matches perfectly to $F(x)$. In this experiment, four different reliability maps were generated and the depthmap information which has the biggest $R(i, j)$ is used to create a new depthmap. That calculation is perfumed using MATLAB.

2.3 RESULT AND DISCUSSION

2.3.1 RELIABILITY OF FOCUS MEASURE

All focused images, corresponding depth maps, and corresponding reliability maps are shown in Fig. 2.6. (a) is an original image and (b), (c), and (d) are contrasted images. (d) is the most contrasted one, while (b) is the least contrasted one. The white area in depthmap means high position and the black area means low positon. In the reliability map, the white area means high accuracy and the black area means low accuracy. The more contrasted the image is, the less accurate the result is. However, the result at some points became more accurate.

2.3.2 3D VISUALIZATION

The new depth map and the 3D reconstructed image are shown in Fig. 2.7. Compared with Fig. 2.6 (c), the noise in the top area of the specimen was greatly removed. However, there is still remaining noise which was not removed.

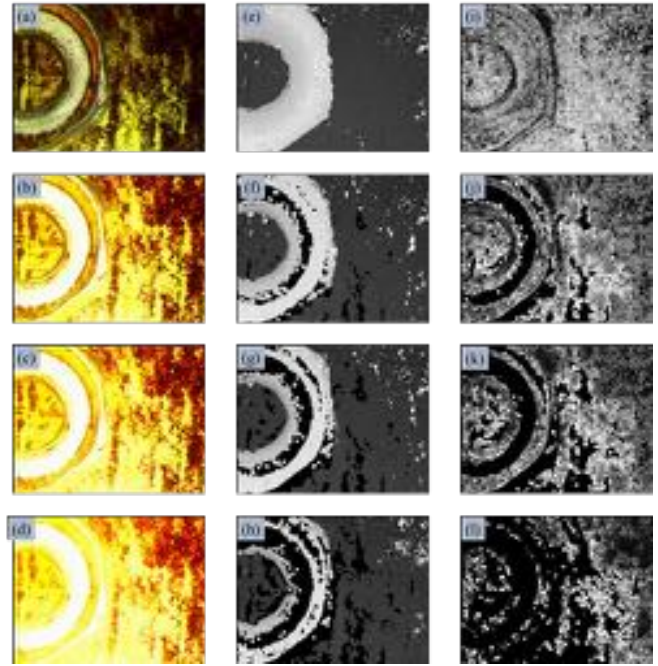


Fig. 2.6 left row: all-focused image
middle row: depth map, right row: reliability map

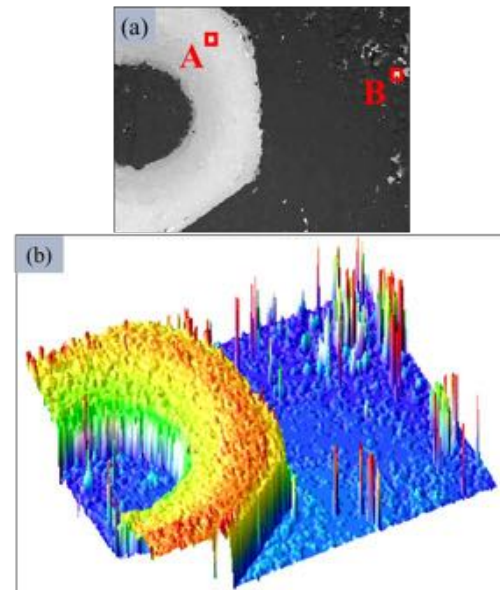


Fig. 2.7 (a) New depth map, (b) Revised 3D image

In SFF, too-dark area and too-bright area can show noisy result because such area has less texture. In addition, even on the surface with texture, if the image variation of a point is smaller than the image variance caused by burred image, the result can be noisy. For example, the variance of the focus measure at point A is shown in Fig. 2.8. The red one is from the original image. The black one is from the high-contrast image. As you can see, there are some big values around 50 in the original one, but in the high-contrast image, the noise is removed. On the other hand, the variance of the focus measure at point B is shown in Fig. 2.8 as well. Even when high-contrast image are used, the focus measure did not change. This means this point does not have enough texture.

In such case, the noise cannot be removed. Using high-contrast images, the noise like point A which comes from a bright point can be removed but the noise like point B which

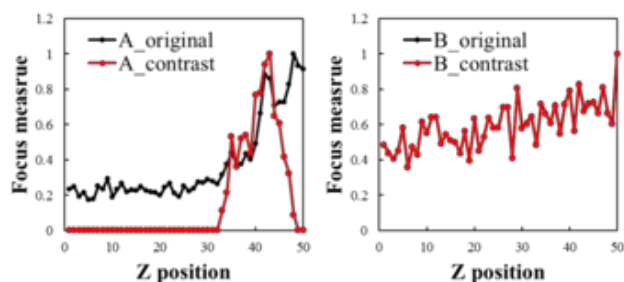


Fig. 2.8 Variance of focus measure (Left: A, Right: B)

is caused by a lack of texture cannot be removed.

To improve the result of SFF, first of all, the enough illumination to make texture on the surface is required. Then our correction method would work well to remove the noise .

2.4 IMPROVEMENT

As described in 2.3.2, the most importance factor is making sure the surface has enough texture. To realize this, brightness and illumination also play important roles, however, the reflective property is different from materials. That results in the existence of dark area which does not have enough texture like this time. This can be improved by developing illumination system of hardware.

Secondary, in this research, the three-different contrast level image are used. The method to decide effective contrast has not been investigated. In other words, there is a room to make it computationally efficient.

3 TRANSPARENT MATERIAL

3.1 BACKGROUND

We developed the 3D imaging method for opaque samples using SFF. Since SFF cannot be applied for transparent materials, another method needs to be developed. As a sample, we used a fabric which consists of a lot of single fibers (Fig. 3.1).

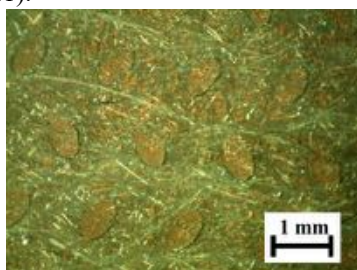


Fig. 3.1 transparent specimen

First of all, we tried to apply photogrammetry, which is a one of 3D reconstruction methods based on triangulation. It is reported that 3D reconstruction of SEM images is successfully done by mean of photogrammetry [13]. However, if specimen has a complicated structure, it become difficult to detect overlapped points between 2D images

accurately. That results in inaccurate 3D reconstruction. To realize 3D reconstruction of our sample which is transparent and has complicated structure, we adapted a concept of optical projection tomography to reconstruct our transparent specimen. In this research, we designed the image acquisition set-up based on an ordinal optical microscope and performed 3D reconstruction.

3.2 METHOD

3.2.1 OPTICAL PROJECTION TOMOGRAPHY

Optical projection tomography (OPT) is a relatively new technology that provides a novel approach to reconstruct 3D images. This new method has been developed mainly in the biomedical field. In the literature, it is reported that researchers successfully have conducted the 3D reconstruction of different kinds of species including human brain, zebrafish, drosophila, mouse embryos, and Arabidopsis [14]. On the other hand, OPT has not been explored in the other fields.

The method is based on projection tomography which is used successfully for CT and electron tomography. The main difference between those techniques and OPT is what is projected on the detector. X-ray is used for CT and electron is used for electron tomography, while optical light is used for OPT. The OPT procedure mainly consists of two steps which are image acquisition and 3D reconstruction.

At the first step, a sequence of the images from different angles is acquired. The typical OPT image acquisition system is outlined in Fig. 3.2 [15].

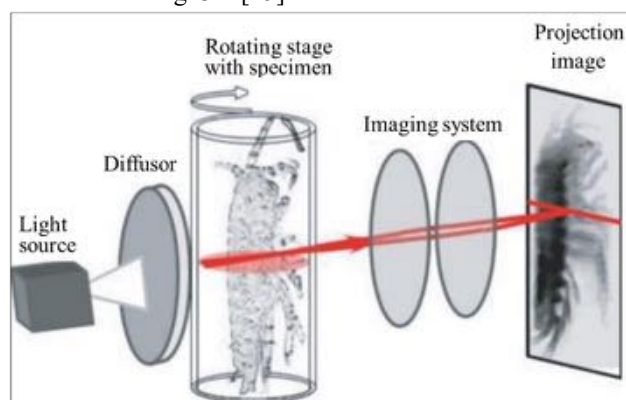


Fig. 3.2 Principle of OPT system

The specimen to be visualized is typically embedded in a matching fluid, then fixed to the rotating stage. The position of the stag is intentionally located at the focal point of the objective lens along the optical axis. The specimen is illuminated by the light source from the other direction to the lens. At first, the light is transmitted through a diffuser in order to provide a uniform illumination to the sample. The uniform light goes through the sample, and the transmitted light from the specimen is detected by a camera. This image is so-called projection image that is dependent on the attenuation coefficients of the specimen. To acquire a sequence of projection images, the specimen is rotated through 360 degrees. Usually, 400 images are recorded by

360 degrees. It is apparent that a higher angular resolution would result in a higher image resolution.

At the next step, 3D reconstruction is computationally performed using the sequence of projection images. To carry out this work, the filtered back-projection algorithm is typically used and has shown a good result. The principle of the back-projection algorithm is shown in Fig. 3.3 [16]. The acquired projection images are imaged back as stripe images. If there is an object in a pixel, those stripe images are accumulated and get to show an object. The more images are used, the clearer the reconstructed object becomes. This calculation is performed at each plane and many slice images are generated. Those slice images are stacked up in the z direction, and then 3D reconstruction is visualized.

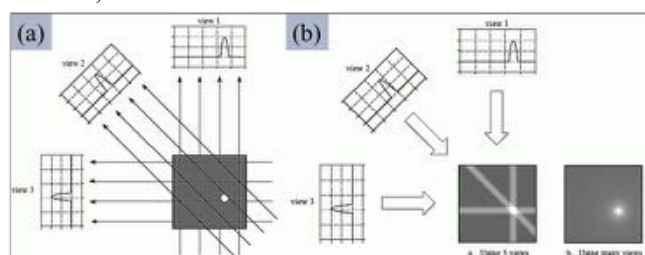


Fig. 3.3 Back-projection algorithm

3.2.2 IMAGE ACQUISITION

In this research, the OPT system is set up based on normal optical microscope. OPT system mainly consists of two parts, which are the imaging unit and the rotation unit. The schematic of our system is shown in Fig. 3.4.

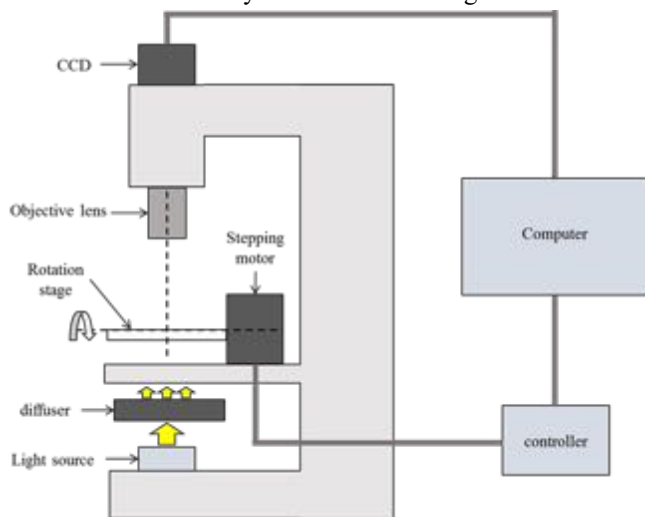


Fig. 3.4 Schematic of OPT system

For imaging unit, the lens of the optical microscope was employed. To illuminate the sample, the broadband lamp equipped with the microscope was used and a diffuser is located before the rotation stage. The light transmitted through the specimen is eventually detected by CCD camera (MU 300, AmScope) attached to the top of the microscope. For specimen rotation unit, the rotation of the stage is controlled by a stepping motor (SY70PB9701, ORIENTALMOTOR) with rotational step size of 0.36 degrees. As described in 3.2.1, the specimen is usually embedded in a cylinder of agarose. However, the process

might affect the structure of the specimen. In this research, a slide glass is attached to the motor as the stage, and the sample is attached to the stage directly with a tape. The rotation stage is controlled by Arduino, and the manipulation can be easily conducted using developed software in the lab. Once the number of the acquired images and steps are input, the images are automatically as the stage rotates.

In this research, 500 images are acquired by 0.36 degrees through 180 degrees, and 300 images are used for 3D reconstruction in order to get rid of the error from glass stage. In addition, the images without the specimen are acquired to conduct flat-field correction which is a correction to remove the effect of the difference of the background brightness. One of images acquired in this experiment is shown in Fig. 3.5 (a).

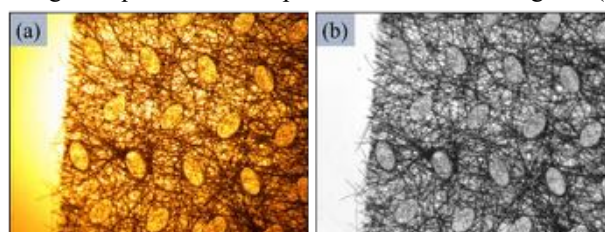


Fig. 3.5 (a) projection image (b) flat-field correction

3.2.3 3D RECONSTRUCTION

A 3D reconstruction is computed using a filtered back-projection algorithm as well as a typical OPT reconstruction. To conduct the filtered back-projection algorithm, Nrecon V1.7.0.4 (SkyScan) are used. Since Nrecon is basically software for specific hardware, pre-image processing is required, which includes flat-field corrections and the alternations of the file names [17]. The flat-field corrections on our dataset are performed using macro plugin in ImageJ (Fig. 3.5(b)). The calibration is performed at the same time. Nrecon requires 16-bit TIFF files with specific sequent file names, so the alternations of the file names are conducted in Bulk Name Utility. When the pre-processed data are input in Nrecon, 'log file' is required at the same time. It provides important information such as the number of images, the number of pixels and so on. After these data is successfully recognized, Nrecon automatically input the settings and slice images starts to be generated. The number of slices depends on the number of pixel in original image. 763 slice images are generated this time. Those slice data was stacked in ImageJ and finally visualized in a three-dimensional coordination using 3D viewer plugin in ImageJ.

3.3 RESULT AND DISCUSSION

3.3.1 3D VISUALIZATION

Following the procedure as described in 3.2, the 3D image of a thin fabric was successfully reconstructed from a sequence of 2D images. The 3D reconstruction image, the side view, the top view and the front view are respectively shown in Fig. 3.6(a)-(d). Using this data, it is possible to observe any cross-section from any angle. Also, we can measure a length between points which can be freely selected.

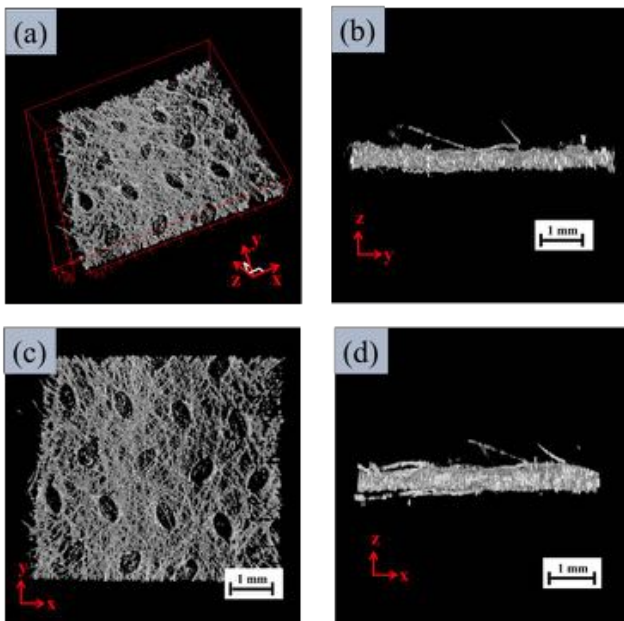


Fig. 3.6 (a) 3D image, (b) side, (c) top, (d) front view

As you can see, the closer a position is to the center line, the denser and clearer the 3D image is. This is because a lens has a certain depth of focus. Principally, a lens has only one focal plane. However, the regions near a focal place also appear close to a focused image. The distance which can be regarded as a focused plane is called a depth from focus and it is decided depending on whole optical imaging system. In this method, the distance from the lens changes as the stage rotates and some regions are out of the depth from focus. The information of the sample in such regions decrease and it results in an unclear image. However, the general shape was successfully visualized even though its region includes unfocused images.

Fig. 3.7 shows the enlarged 3D reconstruction image and its corresponding 2D image. Now we can see even a single fiber and easily confirm which fiber is in the higher or lower position.

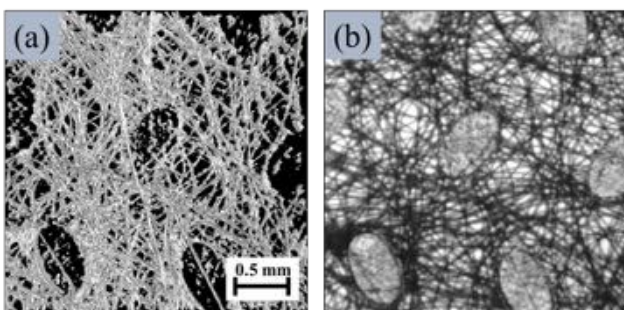


Fig. 3.7 (a)enlarged image (b) corresponding 2D image

3.3.2 APPLICATION

One of possible applications of this method is evaluations of fabric composites. Friction and wear may result in damage on a surface. 3D imaging can be an evaluation method of surface condition.

To confirm the possibility that this method works as an evaluation method of surface condition, the following experiment was conducted. At first, a specimen without damage was 3D reconstructed using the method explained in this paper. Next, the surface of specimen was scratched. Then, 3D reconstruction for the same place was conducted again. This process was repeated twice and the 3D images are shown in Fig. 3.8.

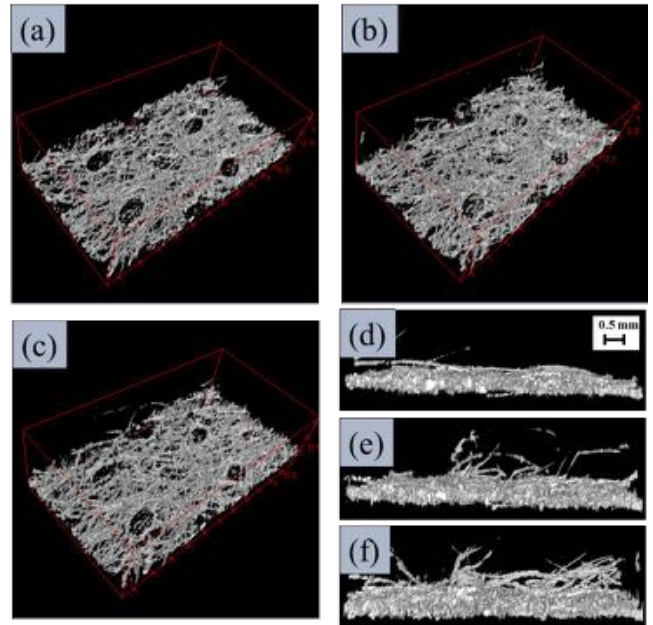


Fig. 3.8 (a), (d) 3D image and side view of original
(b), (e) after 1st abrasion, (c), (f) after 2nd abrasion

To visualize the surface morphology clearly, the height map was generated (Fig. 3.9 (a)-(c)).

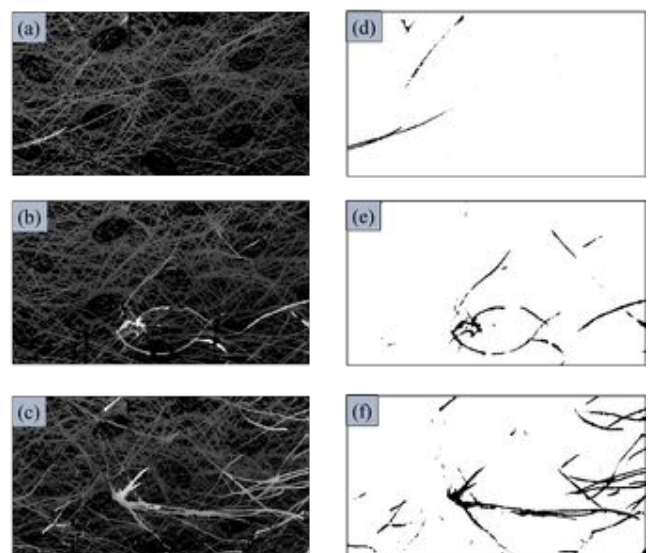


Fig. 3.9 (a), (d) height map and binary image of original
(b), (e) after 1st abrasion, (c), (f) after 2nd abrasion

This process was calculated using MATLAB. White area means high area while black area means low area. Using this height map, the area over certain height can be extracted by setting a certain threshold and making a binary image. This

time, thread hold of the height is set to 120 out of 255, those binary images are shown in Fig. 3.9 (d)-(f). The high-area rate was respectively 0.89%, 2.17%, 6.29%. It was confirmed that the high-area rate increased in accordance with the amount of scratch.

3.4 IMPROVEMENT

In this method, the most important factor is how accurate the center line of rotation crosses stage matches to the optical axis perpendicularly. If the distance between them is big, the slice image will be burred. One of possible solutions is to apply a XY positioning stage to set the position of the motor accurately. It will be more helpful if it can set the same position repeatedly.

Secondary, since the projection image is acquired by microscope, the depth of focus has to be taken into consideration. In this research, the image close to the center is reconstructed very well, while the image far away from the center didn't show dense 3D image. According to the specimen, the lens with appropriate depth of focus should be used.

4 CONCLUSION

In this research, two kinds of 3D reconstruction method for opaque and transparent material have been developed.

For opaque material, shape from focus was used. In SFF, the surface texture is an important factor, and dark image generally has pure texture. Since pure texture doesn't provide enough image variation, the result of the focus measure operator becomes noisy. To remove the error result, the correction method using high-contrast images has been proposed and conducted. As a result, the error caused by bright area was removed well, however, the error caused by the lack of texture could not be removed.

For transparent material, optical projection tomography was used. OPT system was developed based on ordinary optical microscope, and 3D reconstruction was successfully performed.

5 ACKNOWLEDGEMENT

This project was conducted at Prof. Wei Lu's group at the department of Mechanical Engineering, University of Michigan. I would like to sincerely thank Prof. Lu, and the members of the laboratory for their great guidance and support. I am also grateful to Prof. Noritsugu Umehara, Prof. Kurabayashi and the staff of JUACEP office for their support at Nagoya University.

6 REFERENCE

[1] G. Sansoni, M. Trebeschi, and F. Docchio, "State-of-the-art and applications of 3D imaging sensors in industry, cultural heritage, medicine, and criminal investigation," *Sensors*, vol. 9, no. 1, pp. 568–601, 2009.

[2] O. H. Karatas and E. Toy, "Three-dimensional imaging techniques: A literature review," *Eur. J. Dent.*, vol. 8, no. 1, pp. 132–140, 2014.

[3] M. Niederoest, J. Niederoest, and J. \vSCUCKA, "Shape From Focus: Fully Automated 3D Reconstruction and Visualization of Microscopic Objects," *6th Int. Conf. Opt.*, vol. 8790, pp. 236–243, 2003.

[4] D. S. Pankaj, R. R. Nidamanuri, and P. B. Prasad, "3-D Imaging Techniques and Review of Products," *Int. Conf. "Innovations Comput. Sci. Eng. (ICICSE 2013)*, vol. 3, no. Icicse, pp. 21–27, 2013.

[5] S. Pertuz, D. Puig, and M. A. Garcia, "Analysis of focus measure operators for shape-from-focus," *Pattern Recognit.*, vol. 46, no. 5, pp. 1415–1432, 2013.

[6] B. Billiot, F. Cointault, L. Journaux, J. C. Simon, and P. Gouton, "3D Image Acquisition System Based on Shape from Focus Technique," *Sensors*, vol. 13, no. 4, pp. 5040–5053, 2013.

[7] S. Nayar, "Shape from focus," *Cmu-Ri-Tr-89-27*, vol. 16, no. 8, pp. 824–831, 1989.

[8] J. Florczak and M. Petko, "Usage of Shape From Focus Method For 3D Shape Recovery And Identification of 3D Object Position," *Int. J. Image Process.*, vol. 8, no. 8, pp. 116–124, 2014.

[9] B. Forster, D. Van De Ville, J. Berent, D. Sage, and M. Unser, "Complex wavelets for extended depth-of-field: A new method for the fusion of multichannel microscopy images," *Microsc. Res. Tech.*, vol. 65, no. 1–2, pp. 33–42, 2004.

[10] M. T. Mahmood, W. J. Choi, and T. S. Choi, "DCT and PCA based method for shape from focus," *Lect. Notes Comput. Sci. (including Subser. Lect. Notes Artif. Intell. Lect. Notes Bioinformatics)*, vol. 5073 LNCS, no. PART 2, pp. 1025–1034, 2008.

[11] a Bercovici, A. Hadley, and U. Villanueva-Amadoz, "Improving Depth of Field Resolution for Palynological Photomicrography," *Palaeontol. Electron.*, vol. 12, no. 2, 2009.

[12] S. Pertuz, D. Puig, and M. A. Garcia, "Reliability measure for shape-from-focus," *Image Vis. Comput.*, vol. 31, no. 10, pp. 725–734, 2013.

[13] L. C. Gontard, R. Schierholz, S. Yu, J. Cintas, and R. E. Dunin-Borkowski, "Photogrammetry of the three-dimensional shape and texture of a nanoscale particle using scanning electron microscopy and freeware software," *Ultramicroscopy*, vol. 169, pp. 80–88, 2016.

[14] C. Jean-François and S. James, "Live optical projection tomography," *Organogenesis*, vol. 6278, no. April 2015, pp. 211–216, 2009.

[15] Sharpe J., "Optical Projection Tomography," 2004.

[16] S. W. Smith, "25 Special Imaging Techniques," *Sci. Eng. Guid. to Digit. Signal Process.*, pp. 423–450, 1997.

[17] B. Microct, "NRecon User Manual NRecon User Manual 2016 User manual for SkyScan reconstruction program NRecon Index Introduction: NRecon in a nutshell," 2016.

DEVELOPMENT OF TRANSPARENT YSZ THIN FILMS

Toshiya Sawaki

Department of Mechanical Engineering, Graduate School of Engineering, Nagoya University
sawaki@ume.mech.nagoya-u.ac.jp

Eongyu Yi, Richard Laine

Department of Materials Science and Engineering, Graduate School of Engineering, University of Michigan
eonyi@umich.edu, talsdad@umich.edu

ABSTRACT

Optical ceramics has been studied by many researchers for applications to high power lasers, transparent armor and cellphone surface. In particular, yttria stabilized zirconia (YSZ) is one good that shows high transparency and mechanical properties. The purpose of this report is to develop the highly transparent YSZ thin films using less pressure in sintering. In this work, nanopowders synthesized by liquid-feed flame spray pyrolysis (LF-FSP) method were used as the starting material for fabricating thin films. A dispersion of YSZ was made by mixing powders, plasticizer, binder, dispersant and solvent. After the suspension was ball-milled for 12-24 h, suspensions were cast on mylar and dried to obtain green films. The green debindered films were sintered at selected temperatures. The microstructures of the sintered thin films were characterized using SEM and XRD. To reduce porosity YSZ thin films were doped with TiO₂ dopant.

1. INTRODUCTION

Transparent ceramic materials are attracting the interests in optical applications and expected to be used as high power laser, cameras lenses and cellphone surface. Ceramic materials have excellent mechanical and thermal properties. Moreover, they can be produced in a large volume because they are fabricated by heating at much lower temperature than the melting point.¹

Among the many optical ceramic materials like YAG and Al₂O₃, several researchers have studied zirconium oxide (zirconia) ceramics. This is because zirconia shows flexural strength, good fracture toughness and high melting point of 2700°C. In general, zirconia has monoclinic structure at room temperature and changes the phase from monoclinic into tetragonal and cubic as the temperature increases (tetragonal 1170°C and cubic 2370°C). Therefore, increasing temperature breaks zirconia in sintering process because change in phase causes change in volume. It has been well known that adding Y₂O₃, CaO, MgO and CeO₂ to zirconia stabilizes cubic phase even at room temperature.²⁻⁴ Cubic

structure has optical isotropy and prevent light scattering in crystalline grain, which provides transparency.

For applications of yttria stabilized zirconia (YSZ), Tsukuma et al. reported that they were successful in fabricating highly transparent 8 mol % Y₂O₃-ZrO₂ ceramic materials by the hot isostatic pressing method.⁵ They revealed that residual pores and grain sizes affect light transmission strongly. Moreover, it is broadly reported that thin YSZ films have been successfully prepared by several kinds of deposition methods. Hisanori et al. were successful in preparing YSZ thin films by chemical vapor deposition (CVD).⁶ Heiroth et al. grew YSZ layers by pulsed laser deposition (PLD).⁷ However, these deposition processes need large scale equipment, take a lot of time and are expensive.

The optical and mechanical properties of ceramic materials are highly dependent on their grain sizes and residual porosity. Grain size is closely related to mechanical properties following the Hall-Petch equation. The Hall-Petch equation is given by

$$\sigma = \sigma_0 + k \cdot d^{-0.5} \quad (1)$$

where σ is the yield stress, d is the average grain diameter, and σ_0 and k are empirical constants, strength or hardness should increase as grain size decrease.^{8,9} Moreover, light is scattered at grain boundaries, pores and impurities, which decreases the transparency. Therefore, various strategies have been employed to control the grain sizes and minimize residual porosity.

In this report, we aimed to fabricate transparent YSZ thin films by tape-casting. We sintered YSZ films with several composition and sintering methods, and evaluated crystal structure, grain sizes and porosity by using XRD and SEM.

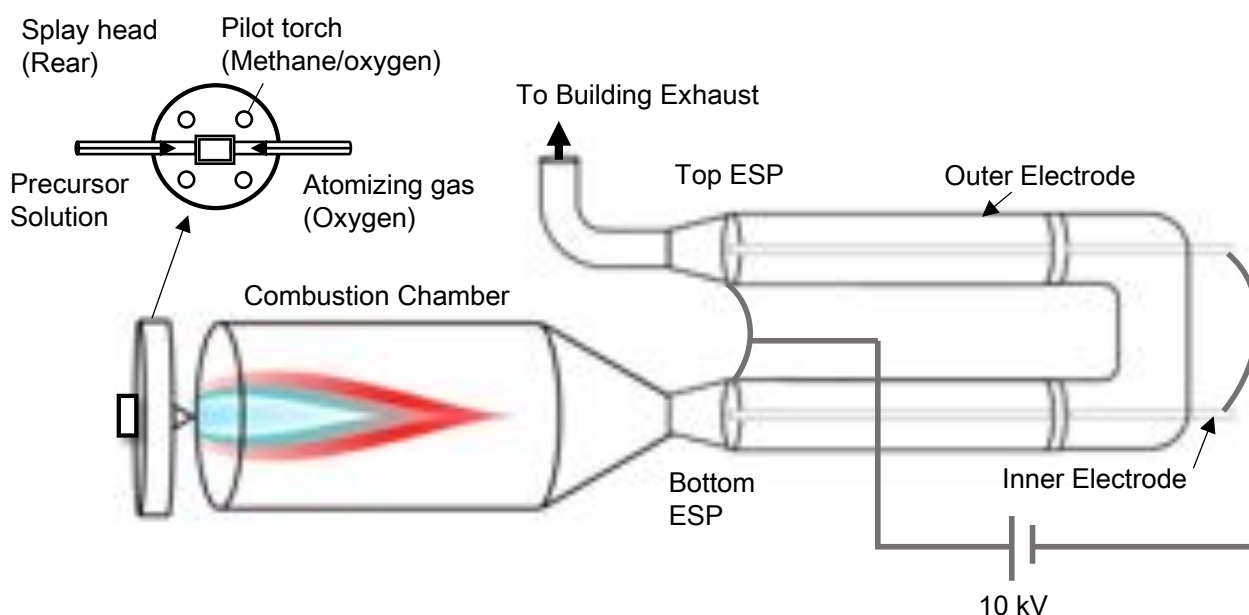


Figure 1. Schematic of Liquid Feed Flame Spray Pyrolysis

2. EXPERIMENTAL

Liquid-Feed Flame Spray Pyrolysis (LF-FSP). The ZrO_2 and Y_2O_3 nanopowders were prepared by the method called liquid-feed flame spray pyrolysis (LF-FSP), which was developed at University of Michigan.¹⁰⁻¹⁹ The LF-FSP apparatus consists of a precursor reservoir, an ultrasonic atomizer, a combustion chamber, and electrostatic precipitators (ESPs) as shown in Figure 1. The precursor was dissolved in ethanol with a selected molar ratio that makes 3 wt. % ceramic yield. The precursor solution was pumped into an ultrasonic atomizer, aerosolized and combusted with methane/oxygen pilot torches on the spray head. Combustion at ≥ 1500 °C produced ZrO_2 and Y_2O_3 nanopowders and byproducts like H_2O and CO_2 . The nanopowders were collected down-stream in ESPs operated at a DC potential of 10 kV. The as-produced powders were dispersed and cleaned in ethanol (200 proof, Decon Labs) with 2 wt.% bicine as a dispersant by an ultrasonic horn (Vibra cell VC-505, Sonics & Mater. Inc.) at 100 W for 15 min. The suspension was allowed settle for 4 h to allow larger particles to settle. The supernatant was decanted into a container and the recovered powder dried in an oven.

Precursors synthesis. Zirconium isobutyrate $\{Zr[O_2-CCH(CH_3)_2(OH)_2]\}$ precursor and yttrium propionate $(CH_3CH_2COO)_3Y$ precursor were prepared for synthesizing ZrO_2 and Y_2O_3 nanopowders, respectively.

Zirconium isobutyrate was synthesized by reacting zirconium basic carbonate with isobutyric acid (Pfaltz and Bauer, Waterbury, Connecticut) and isobutyric anhydride (Sigma-Aldrich, ST. Louis, Missouri) in a 1 L round bottom flask equipped with a still head at 140 °C in N_2 atmosphere.²⁰

Once transparent liquid was obtained, heat was removed and zirconium isobutyrate crystallized on cooling which was filtered off.

Yttrium propionate was prepared by reacting Y_2O_3 (PIDC, Ann Arbor, Michigan) with propionic acid (Acros Organics, Geel, Belgium)⁵ in the same manner as with zirconium isobutyrate synthesis.

Dispersion tests. The dispersion tests were conducted for ZrO_2 and Y_2O_3 powders, respectively to determine solvent and dispersant. 16 vials were prepared with dispersed powders and dispersant in respective kinds of solvent. Solvent included ethanol, propanol, acetone and methyl ethyl ketone (MEK). Dispersant included bicine, poly acryl acid, blank (no dispersant) and polyvinyl butyral. Both 50 mg of each powder and 2~5 mg of each dispersant were added in vials with solvent to fill up to a half of the vial and dispersed by an ultrasonic horn (Vibra cell VC-505, Sonics & Mater. Inc.). The dispersive condition was observed after 1.5h and 18h later.

Film processing. Collected powders, polyvinyl butyral, benzyl butyl phthalate, acetone, and ethanol at selected wt. ratios were added to a 20 mL vial. Three types of suspension were prepared including 8YSZ, 15YSZ and 8YSZ doped 3 mol % TiO_2 (8YSZ/ TiO_2) as shown in Table 1, 2 and 3. The suspension was ball-milled with 3.0 mm diameter spherical 99% zirconia beads for 12-24 h to homogenize the suspension. One fifth of the vial was filled with the milling beads. A ball mill (Rotary Tumbler Model B, Tru-Square Metal Products, Auburn, WA, UK) was used for ball-milling. The suspensions were cast using a wire wound rod coater (Automatic Film Applicator-1137, Sheen Instrument, Ltd UK). The gap between the rod and the substrate was adjusted in order to control films thickness. After films evaporate, two dried green films were manually pressed together, peeled off the

Mylar substrate, and cut to selected sizes. Green films were uniaxially pressed between stainless steel dies at 80-100 °C under a pressure of 50-80 MPa for 0-5 min. using a heated bench top press (Carver, Inc) in order to improve packing density.

Table 1. Starting materials and composition for 8YSZ suspension.

Components	Roles	Mass (g)	Wt. %	Vol. %
ZrO ₂	Powder	0.863	27.9	5.5
Y ₂ O ₃	Powder	0.137	4.4	1.0
Benzyl butyl phthalate	Plasticizer	0.095	3.1	3.1
Polyvinylbutyral	Binder	0.095	3.1	3.2
Bicine	Dispersant	0.005	0.2	0.2
Ethanol	Solvent	0.947	30.6	43.5
Acetone	Solvent	0.949	30.7	43.5

Table 2. Starting materials and composition for 15YSZ suspension.

Components	Roles	Mass (g)	Wt. %	Vol. %
ZrO ₂	Powder	0.756	24.4	4.8
Y ₂ O ₃	Powder	0.244	7.9	1.8
Benzyl butyl phthalate	Plasticizer	0.097	3.1	3.2
Polyvinylbutyral	Binder	0.097	3.1	3.2
Bicine	Dispersant	0.005	0.2	0.2
Ethanol	Solvent	0.947	30.6	43.4
Acetone	Solvent	0.949	30.7	43.4

Table 3. Starting materials and composition for 8YSZ/3 mol % TiO₂ suspension.

Components	Roles	Mass (g)	Wt. %	Vol. %
ZrO ₂	Powder	0.847	28.9	5.8
Y ₂ O ₃	Powder	0.135	4.6	1.1
TiO ₂	Powder	0.018	0.6	0.2
Benzyl butyl phthalate	Plasticizer	0.096	3.3	3.5
Polyvinylbutyral	Binder	0.096	3.3	3.5
Bicine	Dispersant	0.005	0.2	0.2
Ethanol	Solvent	0.868	29.6	42.9
Acetone	Solvent	0.870	29.7	42.9

Film sintering. Green films were placed between YSZ or Al₂O₃ plates and sintered at selected temperatures and times with a ramp rate of 3~5 °C/min in a furnace. The plates were used to prevent films from warping through all the process.

Thermal etching. Sintered films were manually snapped getting new fracture surfaces, then heated to designed temperatures for 30 min in air. Thermal etching temperatures are generally 100 °C lower than sintering temperatures. Since fracture provides a uniform two-dimensional surface, no grinding or polishing was necessary. Average grain sizes were calculated by the lineal intercept method.

XRD analysis. Measurements were carried out using a Rigaku Rotating Anode Goniometer (Rigaku Denki., LTD., Tokyo, Japan) at 40 kV and 100 mA with Cu K α radiation (1.541 Å). Scans range was between 10 and 70° 2 θ , using a scan rate at 2°/min with 0.02° intervals. The Jade program 2010 (Version 1.1.5 from Materials Data, Inc.) was used to determine the presence of crystallographic phases, wt.

fraction, and to refine lattice constants. Peak positions and intensities were evaluated by comparison with ICDD files of zirconium oxide (01-070-6627), baddeleyite (03-065-1024), yttrium oxide (98-001-8238) and yttrium zirconium oxide (00-030-1468).

Scanning electron microscopy (SEM). Sample morphologies were observed by Philips XL30 SEM and SEM (NOVA Nanolab, FEI Inc.). Because all the samples lack of conductivity, they were sputter coated with a gold film using a Technics Hummer VI sputtering system (Anatech Ltd., Alexandria, VA) to improve resolution.

3. RESULTS AND DISCUSSION

3.1 Characterization of as-produced Powders.

Figure 2 shows SEMs of as-produced ZrO_2 and Y_2O_3 powders synthesized by LF-FSP method. The average powder sizes are under 100 nm. The XRD analysis of as-produced powders are shown in Figure 3. Although Y_2O_3 powders had only one phase corresponding to cubic yttrium oxide, ZrO_2 powders had two phases corresponding to tetragonal ZrO_2 and monoclinic ZrO_2 . Some ZrO_2 powders retain metastable tetragonal phase even at room temperature through rapid quenching of LF-FSP method. It is reported that as particles become smaller, the whole particles are likely to melt at lower temperature. Nanopowder sintering leads to the reduction in sintering temperature and time when compared to micron sized powders.

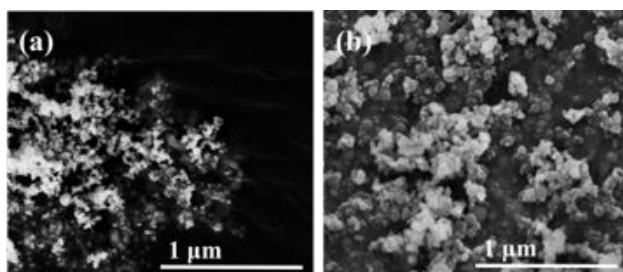


Figure 2. SEM images of as-produced powders synthesized by LF-FSP. Shown are (a) ZrO_2 and (b) Y_2O_3 powders.

3.2 Characterization of thin films of 8 mol % yttria doped zirconia (8YSZ) and 15 mol % yttria doped zirconia (15YSZ).

8YSZ and 15YSZ green films were prepared by using ZrO_2 and Y_2O_3 powders synthesized by LF-FSP. The components shown in Table 1 and Table 2 were ball-milled and tape-cast to make 8YSZ and 15YSZ suspension. Green films were obtained through pressing after the suspension dried. These films were sintered to 1400°C/5h, 1500°C/2h and 1600°C/1h in air in the furnace. Figure 4 shows the XRD patterns of sintered thin films. All peaks showed almost the same peak positions as cubic yttrium zirconium oxide even if the yttria dopant or sintering temperatures were changed.

The SEM images of fracture surfaces are shown in Figure 5. Average grain sizes were calculated using the linear intersection method as shown in Table 4. Higher sintering temperatures induced more densification and grain growth. Moreover, increasing yttria dopant also led to grain growth. Grain growth makes it difficult to fabricate thin films because increasing grain sizes promotes reduction of the mechanical strength and hardness properties as explained above by Hall-Petch equation. However, the transparency of 15 YSZ thin films was higher than that of 8YSZ thin films because of lower porosity as shown in Figure 6.

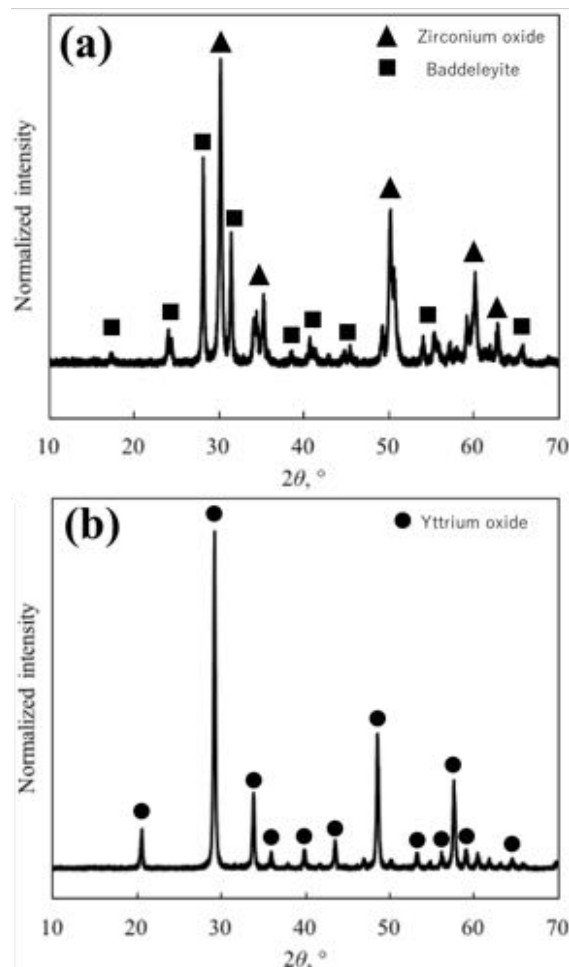


Figure 3. XRD patterns of as-produced powders by LF-FSP. Shown are (a) ZrO_2 and (b) Y_2O_3 powders

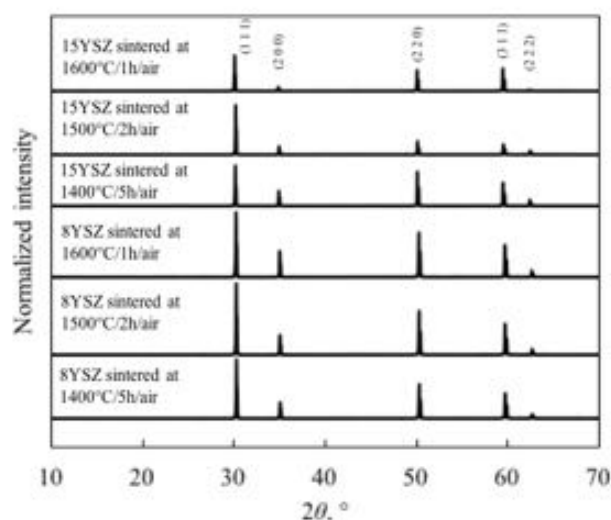


Figure 4. XRD patterns of sintered YSZ thin films.

Table 4. Grain sizes of YSZ thin films.

	8YSZ	15YSZ
Sintered at 1400/5h/air	1.2 μm	4.0 μm
Sintered at 1500/2h/air	1.6 μm	5.0 μm
Sintered at 1600/1h/air	2.1 μm	8.9 μm

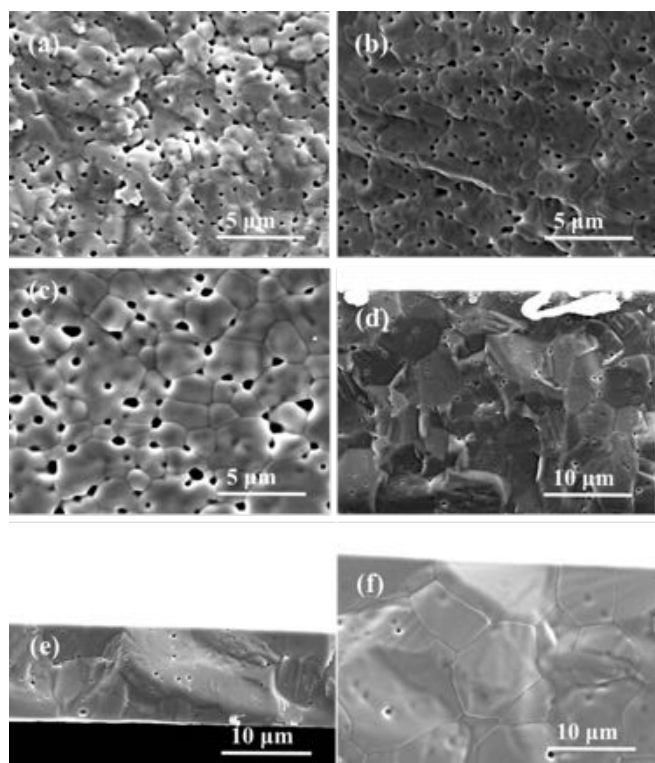


Figure 5. SEM fracture surface images of (a) ~ (c) 8YSZ and (d) ~ (f) 15YSZ thin films sintered to (a) to 1400°C/5h, (b) to 1500°C/2h, (c) to 1600°C/1h, (d) to 1400°C/5h, (e) to 1500°C/2h and (f) to 1600°C/1h.

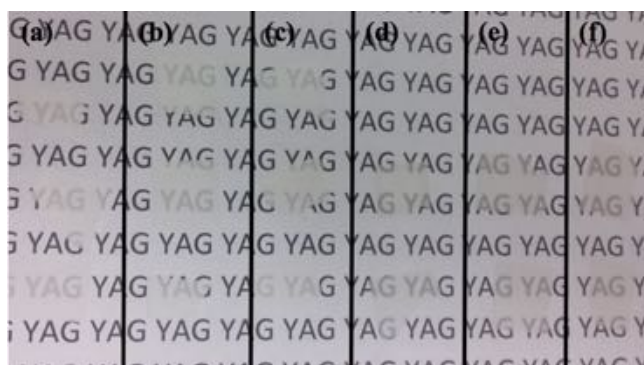


Figure 6. The images of (a) ~ (c) 8YSZ and (d) ~ (f) 15YSZ thin films sintered to (a) to 1400°C/5h, (b) to 1500°C/2h, (c) to 1600°C/1h, (d) to 1400°C/5h, (e) to 1500°C/2h and (f) to 1600°C/1h.

3.3 Characterization of TiO₂ doped YSZ thin films.

Previously, TiO₂ dopant was found to be an effective aid for densification.^{5,21} Therefore, TiO₂ was added to YSZ suspension as shown in Table 3 for 8YSZ doped 3 mol % TiO₂ (8YSZ/TiO₂). Green films were dried and pressed from the suspension in the same way as above. Afterward, the green bodies were sintered to 1350°C/5h between Al₂O₃ plates in air. Unfortunately, XRD analysis could not be

conducted because the thin films stuck to plates strongly and fell apart. It is because TiO₂ diffused to plate. Figure 7 shows SEM fracture surface image of 8YSZ/TiO₂ thin film. Small particles were observed among big particles, which had not been observed in no dopant 8YSZ thin films. Figure 8 shows the image of 8YSZ/TiO₂ thin film. Visual observation confirmed that 8YSZ/TiO₂ thin films were the most transparent among undoped 8YSZ and 15YSZ thin films sintered at respective temperatures. It is considered that the small particle has an important role in covering pores and increased the transparency. In order to investigate the difference between small particle and big particle, the EDS analysis was conducted. The image of EDS analysis area and EDS result are shown in Figure 9 and 10. The element ratio is shown in Table 5. The EDS peaks showed almost the same positions. Moreover, no big difference was obtained in the element ratio. Further work is necessary to find out the mechanism of TiO₂ for covering pores.

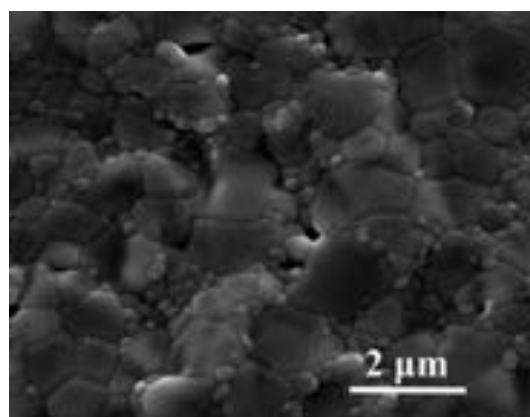


Figure 7. SEM fracture surface image of 8YSZ doped 3 mol % TiO₂ sintered at 1350°C/5h/air between Al₂O₃ plates.

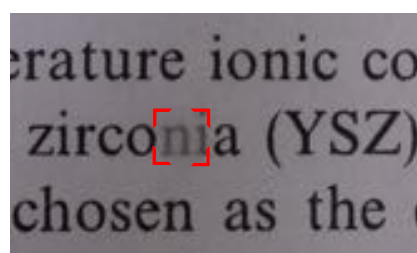


Figure 8. The image of 8YSZ doped 3 mol % TiO₂ sintered at 1350°C/5h/O₂ between Al₂O₃ plates.

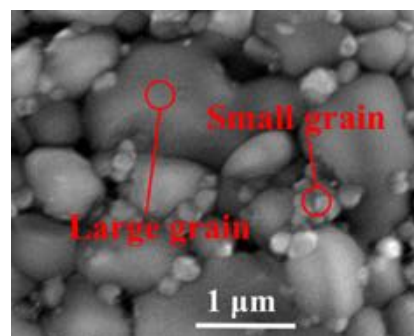


Figure 9. The EDS analysis area of 8YSZ/TiO₂ thin films.

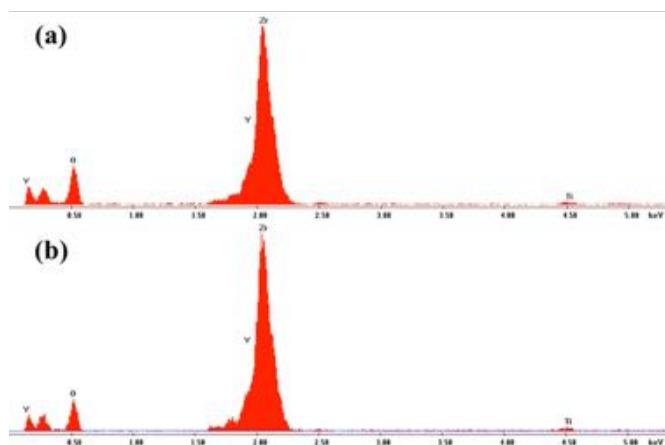


Figure 10. EDS patterns of (a) small particle and (b) large particle formed on 8YSZ/TiO₂ thin films.

Table 5. Element ratio of small particle and large particle formed on 8YSZ/TiO₂ thin films.

Element	Small grain		Large grain	
	Wt. %	At. %	Wt. %	At. %
O	20.40	58.88	19.90	58.13
Y	13.08	6.79	13.94	7.33
Zr	65.05	32.92	64.76	33.18
Ti	1.46	1.41	1.40	1.37

4. CONCLUSIONS

We have synthesized ZrO₂ and Y₂O₃ nanopowders by LF-FSP and fabricated transparent YSZ thin films. The XRD analysis showed every film had only one cubic phase (yttrium zirconium oxide) even when the dopant volume or sintering temperature were changed. The SEMs showed that the sintered thin films were dense but had a lot of pores. Moreover, it is confirmed that adding TiO₂ dopant to 8YSZ reduced the pores and increased the transparency. However, 8YSZ/TiO₂ films fell apart easily. Some problems have yet to be solved about how to make thin films intact and the mechanism of TiO₂.

ACKNOWLEDGEMENTS

I would like to thank Professor Richard M. Laine for giving me such a valuable opportunity to study at University of Michigan. I would like to thank Eongyu Yi for giving me a lot of advice. Moreover, I would like to thank the administrators of equipment which I used for helping me to master those devices. Finally, this work was supported by Japan-US Advanced Collaborative Education Program. I would like to thank all office workers for processing my studying abroad.

REFERENCES

- [1] Akio I., Yan Lin A., Ceramic laser materials, *Nature Photonics* 2, pp. 721 - 727 (2008)
- [2] Basu B., Toughening of yttria-stabilised tetragonal zirconia ceramics, *International Material review*, 18, pp. 239-256, (2013)
- [3] Kim M, Laine R. M., Sintering behavior of ZrO₂/δ-Al₂O₃ core shell nanopowders, *J. Am. Ceram. Soc.*, 93, pp. 709-715, (2010)
- [4] Lange F. F., Transformation toughening, *Journal of Materials Science*, 17, pp. 225-234, (1982)
- [5] Koji T., Isao Y., Transparent 8 mol % Y₂O₃-ZrO₂ (8Y) Ceramics, *J. Am. Ceram. Soc.*, 91 [3] pp. 813-818 (2008)
- [6] Hisanori Y., Toshio H., Yttria stabilized zirconia transparent films prepared by chemical vapor deposition, *Journal of Crystal Growth*, 94, 4, pp. 880-884 (1989)
- [7] S. Heirotha, R., Ghislenib, T., Lipperta, J., Michlerb, A., Wokauna, Optical and mechanical properties of amorphous and crystalline yttria-stabilized zirconia thin films prepared by pulsed laser deposition, *Acta Materialia*, 59, 6, pp. 2330-2340, (2011)
- [8] Nieh, T. G. and Wadsworth, J., Hall-Petch relation in nanocrystalline solids, *Scripta metallurgica et Materialia*, 25, pp. 955-958 (1991)
- [9] Chokshi, A. H., Rosen, A., Karch, J. and Gleiter, H., On the validity of the Hall-Petch relationship in nanocrystalline materials, *Scripta Metallurgica*, 23, pp. 1679-1684 (1989)
- [10] Nathan J. T., Laine R. M., Bart M. B., John W. H., Pierre F. P., Liquid-feed flame spray pyrolysis synthesis of oxide nanopowders for the processing of ceramic composites
- [11] Kim, M., Hinklin, T. R. and Laine, R. M., Core-shell nanostructured nanopowders along (CeO_x)_x(Al₂O₃)_{1-x} tie-line by Liquid-Feed Flame Spray Pyrolysis (LF-FSP), *Chem. Mater.*, 20, pp. 5154-5162 (2008)
- [12] Bickmore, C. R., Waldner, K. F., Baranwal, R., Hinklin, T. and Laine, R. M., Ultrafine titania by Flame Spray Pyrolysis of a titanatran complex, *JECS*, 18, pp. 287-296 (1998)
- [13] Marchal, J., Johns, T., Baranwal, R., Hinklin, T. and Laine, R. M., Yttrium aluminium garnet nanopowders produced by Liquid-Feed Flame Spray Pyrolysis (LF-FSP) of metalloorganic precursors, *Chem. Mater.*, 16, pp. 822-831 (2004)
- [14] Kim, S., Gislason, J. J., Morton, R. W., Pan, X. Q. and Laine, R. M., Liquid-Feed Flame Spray Pyrolysis of nanopowders in the alumina-titania system, *Chem. Mater.*, 26, pp. 2336-2343 (2004)
- [15] Azurdia, J., Marchal, J. and Laine, R. M., Synthesis and characterization of mixed-metal oxide nanopowders along the CoO_x-Al₂O₃ tie line using Liquid-Feed Flame Spray Pyrolysis, *JACM*, 89, pp. 2749-2756 (2006)
- [16] Kim, M. and Laine, R. M., One-step synthesis of core-shell (Ce_{0.7}Zr_{0.3}O₂)_x(Al₂O₃)_{1-x} [(Ce_{0.7}Zr_{0.3}O₂)Al₂O₃] nanopowders via Liquid-Feed Flame Spray Pyrolysis (LF-FSP), *JACS*, 8, pp. 9920-9929 (2007)

- [17] Laine, R. M., Hinklin, T., Williams, G. and Rand, S. C., Low-cost nanopowders for phosphor and laser applications by Flame Spray Pyrolysis, *Materials Science Forum*, 343-346, pp. 500-510 (2000)
- [18] Hinklin, T., Toury, B., Gervais, C., Babonneau, F., Gislason, J. J., Morton, R. W. and Laine, R. M., Liquid-Feed Flame Spray Pyrolysis of metalloorganic and inorganic alumina sources in the production of nanoalumina powders, *Chem. Mater.*, 16, pp. 21-30 (2004)
- [19] Azurdia, J. A., Marchal, J., Shea, P., Sun, H., Pan, X. Q. and Laine, R. M., Liquid-Feed Flame Spray Pyrolysis as a method of producing mixed-metal oxide nanopowders of potential interest as catalytic materials. Nanopowders along NiO-Al₂O₃ tie line including (NiO)_{0.22}(Al₂O₃)_{0.78}, a new inverse spinel composition, *Chem. Mater.*, 18, pp. 731-739 (2006)
- [20] Eongyu Y., Weimin W., John K. and Richard M. Laine, Flame made nanoparticles permit processing of dense, flexible, Li⁺ conducting ceramic electrolyte thin films of cubic-Li₇La₃Zr₂O₁₂ (c-LLZO), *Journal of Materials Chemistry A*, 4, pp. 12947–12954 (2016)
- [21] Koji T., Transparent titania-yttria-zirconia ceramics, *JOURNAL OF MATERIALS SCIENCE LETTERS*, 5, pp. 1143-1144, (1986)

HIGH RESOLUTION RESISTIVE CALORIMETRY MADE OF A CAPILLARY TUBE

Akira Tsuji
Sunghoon Hur
Rohith Mittapally

Department of Aerospace Engineering, Nagoya University
tsuji@prop2.nuae.nagoya-u.ac.jp

Department of Mechanical Engineering, University of Michigan
hur@umich.edu

Department of Mechanical Engineering, University of Michigan
mrohith@umich.edu

Supervisor: Pramod Sangi Reddy, Edgar Meyhofer

Department of Mechanical Engineering, University of Michigan
pramodr@umich.edu
meyhofer@umich.edu

ABSTRACT

High resolution calorimetry is fabricated in this study. The device is achieved by combining high resolution calorimetry using high performance resistive thermometry material, niobium nitride (NBN_x), and silica tube. The temperature coefficient of resistance (TCR) of NBN_x is measured (the value is $\sim 0.8\%/K$ at room temperature which is 5 times larger than TCR of Pt). Then optimum frequency is determined in order to obtain a high signal while avoid $1/f$ noise. Using the frequency, modulated temperature in the device is measured using modulated sensing electrical current. The result shows that the thermal conductance of the calorimetry is $\sim 42 \mu\text{W}/K$ and heat flow resolution of the calorimetry is $\sim 7.1 \text{ nW}$.

Undisclosed

THERAPEUTIC SEPSIS BIOMARKER SCREENING WITH LOCALIZED SURFACE PLASMON RESONANCE BIOSENSORS

Keisuke Goto

(Affiliation) Department of Micro-Nano System Engineering, Graduate School of Engineering, Nagoya University
goto@prop2.nuae.nagoya-u.ac.jp

Supervisor: Katsuo Kurabayashi

(Affiliation) Department of Mechanical Engineering, Graduate School of Engineering, University of Michigan Ann Arbor
katsuo@umich.edu

ABSTRACT

Circulating citrullinated histone H3 is a new potential biomarker for early screening of sepsis. However, conventional immunoassay ELISA takes more than 3 hours to output the result, and it prevents from evaluating early onset and transient status of sepsis. Localized surface plasmon resonance based microfluidic optical biosensing have a great promise to fill this technological gap. We demonstrated the ability to complete the assay within 40 min and got the calibration curve to evaluate the concentration of CitH3.

1. INTRODUCTION

Biomarkers play important role in disease prediction and monitoring^[1-3] and biological research.^[1] For example, cytokines are soluble low-molecular-weight proteins secreted by immune cells. They serve as mediators and modulators in the immune system to regulate the differentiation, growth and inflammatory response of cells.^[2,3] Quantification of cytokine dynamics allows immune response to be monitored, and it provides clinically and immunologically useful information related to acute inflammation and acute infectious diseases^[4]. Moreover, Monitoring and understanding these immunodynamics are attractive way to evaluate the impact of drug or therapy on the immune system for future immunotherapy.^[5,6] Immunotherapy does not target the tumour, but the host immune system and might cure various types of cancer.^[5] The enzyme-linked immunosorbent assay (ELISA) is a conventional method to quantify cytokines. However, the need for sample incubation, secondary antibodies binding to the target analytes as well as multiple washing step require a long sample preparation from 3 to 8 hours. Furthermore, the fluorescent based measurement requires a large amount of sample volume.^[7] This long labelled immunoassay inherently results in the lack of providing the demanding cytokine-based immune status information since dynamic transition of the immune status from pro-inflammatory

phase to anti-inflammatory phase occurs within a short period of time (several hours to a few days).^[3] To capture this dynamics, the biosensors should be rapid, sensitive enough to detect and capable of measuring various kinds of biomarkers simultaneously for a comprehensive understanding of immune functional behaviours.^[3]

Generally, labelling-based methods experience signal decay over time due to photobleaching and could be only qualitative because of the inconsistent binding of labels to target analytes. However, Label-free biosensing can eliminate labelling step and achieve quantitative measurements. Furthermore, label-free biosensing can acquire signals continuously during assay, which provides real-time information of the binding events. Among various label-free biosensors, plasmonic biosensors have the greatest promise to achieve high sensitivity and rapid assay.^[2,3] The principle of plasmonic biosensors is based on the interaction of electromagnetic radiation on a noble metal surrounding dielectric medium. When the collective motion of the free electrons in a metal resonates with a certain wavelength of the incident light, it gives rise to surface confined electromagnetic modes referred to as “surface plasmons (SPs).” The evanescent field of SPs decays exponentially into the dielectric region, which is quite sensitive to the local refractive (RI) index change induced by the temporal or irreversible adsorption of biomolecules in the vicinity of metal surface.^[2] This RI change can be interpreted to binding events and enables label-free real time quantitative measurement. Plasmonic biosensors are mainly categorized into two: (1) surface plasmon resonance (SPR), which monitors the resonance condition for SPs in thin gold films and (2) localized surface plasmon resonance (LSPR), which monitors SPs in sub-wavelength-sized goldnanoparticles (GNPs) surface. However, SPR is not widely used in clinical immunoassays because of the complexity of optical setup such as bulky optical components and the temperature sensitivity.^[10] LSPR sensing takes advantage of simple optical instrument and elimination of temperature control. Moreover, the LSPR

technique takes yields precise and quick responses to local RI changes due to the surface adsorption of analytes.^{[2][7]}

In this report, we developed a label-free biosensor platform integrating plasmonic microarray in microfluidic system to expand the capability of detection of a potential new biomarkers for early diagnosis of sepsis. Recently, circulating citrullinated histone H3 (CitH3) was revealed as a potential biomarker for accurate sepsis screening and treatment target.^{[12][13]} However, a long clinical test by conventional immunoassay hinders detection of the early onset and temporally varying status of sepsis. This work establishes scalable biosensor platform for high speed, high-throughput, multiplexed analysis^[14] of CitH3 and other biomarkers.

2. MATERIAL AND METHOD

2-1. LSPR Microarray Chip Preparation

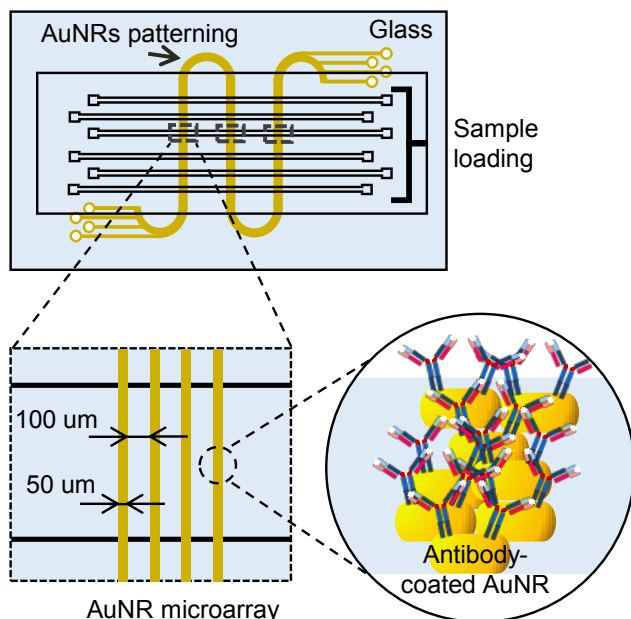


Fig. 1 Schematic of LSPR microarray chip

Our LSPR microarray biochip consists several microfluidic channels which run orthogonal to four meandering stripes of antibody-functionalized gold nanorods (AuNR) patterns. (Fig. 1) We used AuNRs from NanoSeedz in aqueous cetrimonium bromide (CTAB, 0.1M) buffer. An average length and width of AuNRs are 80 ± 5 nm and 40 ± 3 nm. At first, glass slides were treated with Piranha solution ($\text{H}_2\text{SO}_4:\text{H}_2\text{O}_2 = 3:1$ v/v) for 15 min to remove organic residues and make most surfaces highly hydrophilic. Then, glass slides were rinsed with deionized (DI) water, and kept in an ultrasonic bath for 15 min. We then treated the surfaces of the glass substrates under O_2 plasma for 2 min at 30 W. This process created a negatively charged glass surface owing to the dissociated hydroxyl groups existing on the surface, which attract the positively

charged, CTAB stabilized AuNRs onto the surface. After the surface treatment, we immediately we mount the microfluidic flow-patterning dimethylpolysiloxane (PDMS) mask layer onto each glass substrate by non-permanently bonding. PDMS mask layer was created from PDMS prepolymer (Sylgard-184, Dow Corning). We mixed a curing agent with a base monomer (wt : wt = 1: 10), onto the silicon mold and cured it in an oven at 110°C for 4 hours. We then loaded 2 μL of AuNRs diluted 16 times with DI water at a flow rate of 1 $\mu\text{L}/\text{min}$ and incubate overnight. After constructing AuNR microarray, we functionalized AuNRs with 16-carboxy-1-de-canetioli (C16) and activated following 1-ethyl-3-(3-dimethylaminopropyl)carbodiimide/N-hydroxysuccinimide (EDC/NHS) coupling chemistry.^[15] The activated carboxylic group on AuNRs could form esters with the amine groups on the primal antibody.

2-2. Optical Setup and LSPR Microarray Imaging Measurement

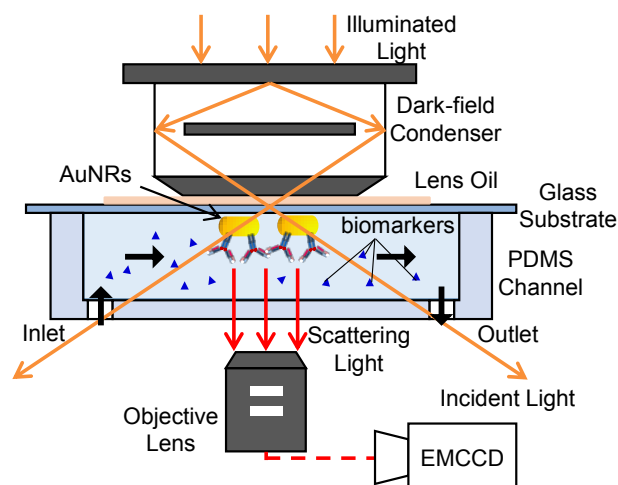


Fig. 2 Schematic of optical setup of dark-field imaging

Following the AuNR microarray antibody functionalization process, we replaced the PDMS mask layer with another PDMS layer with sample-loading microfluidic channel arrays. We bonded this new PDMS layer perpendicular to the LSPR microarray stripes. We then mounted the constructed LSPR microarray chip on a motorized X-Y stage (Proscan, Prior Scientific, Rockland, MA). The LSPR microarray imaging measurement started with guiding white incident light into dark-field condenser oil lens (n.a. 1.20 to 1.45, Mager Scientific) equipped on the inverted fluorescent microscope (Nikon Eclipse Ti-S, Nikon). (Fig. 2) Binding events of analyte molecules onto the AuNRs surface induced an increase in the scattering rate of light within a certain special band as well as red peak shift in the LSPR peak wavelength. (Fig. 3)

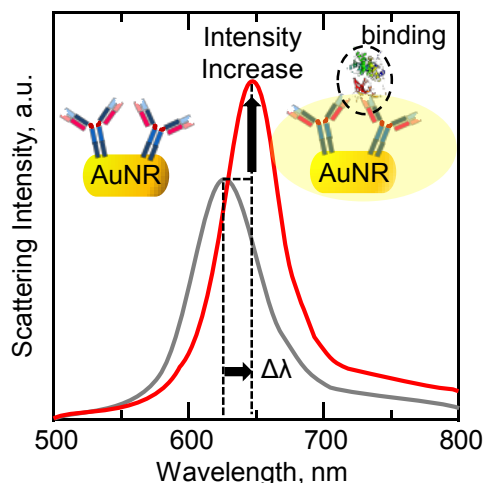


Fig. 3 Principle of LSPR measurement

We used band pass filter (610-680 nm) to capture the maximum intensity change during the observation. We obtained the time-lapse images of microarrays with the EMCCD camera and recorded them using NIS-Element BR analysis software. We used a special Matlab code to analyze and quantify the scattering intensity shift for each microarray.

3. RESULTS AND DISCUSSION

3-1. Real-Time LSPR immunoassay of CitH3

We measured real-time sensor signals associated with analyte binding onto the surface with CitH3 suspended in phosphate buffered saline (PBS) solution. We assigned different concentration levels at 2.5, 5, 10, 20 ng/mL. We infused the CitH3 mixture into one of the microfluidic channels of the LSPR microarray chip and subsequently observed the real-time response from the sensor surface. (Fig. 4)

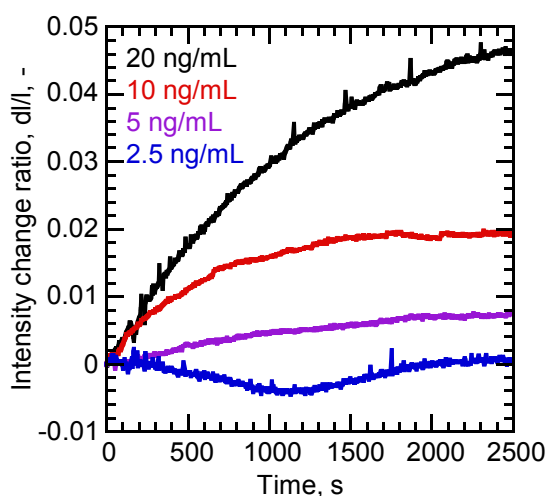


Fig. 4 Real-time AuNR microarray signal variations during the CitH3 detection.

Analyte binding events reached an equilibrium within 40 min after loading samples, as shown by signal plateaus. Then, we obtained the sensor calibration curve by plotting the normalized intensity shift dI/I as a function of analyte concentration.

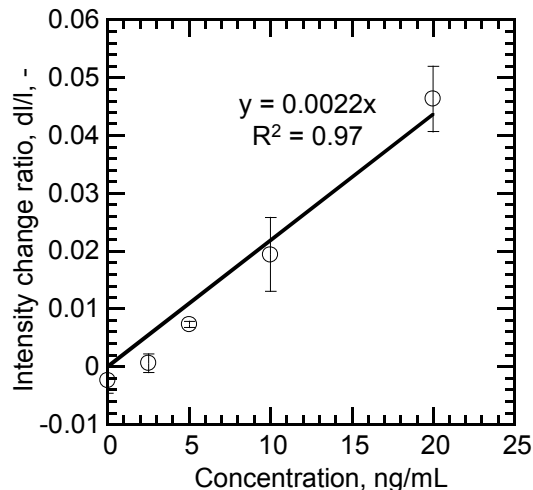


Fig. 5 Calibration curve of CitH3 obtained from the LSPR microarray intensity change.

We performed control experiment measuring the variance of the background signal with no analytes loaded for 30 min. I calculated the standard deviation of the 4 GNP bars from the control test.

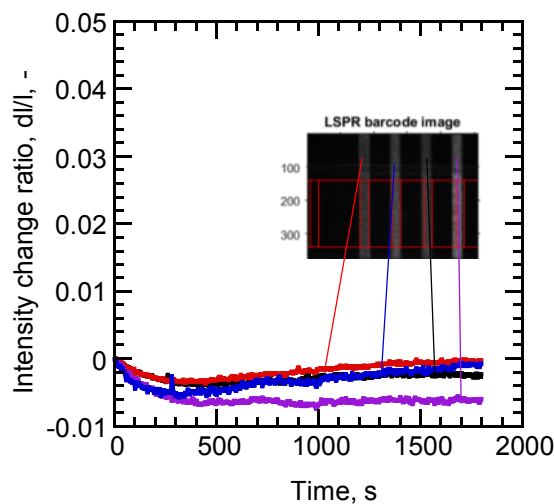


Fig. 6 Control test real-time signal.

This system uncertainty was calculated to be $\sim 0.66\%$, which was determined by the minimum distinguishable signal equivalent to a confidence factor set to 3 times the standard deviation of the background noise (σ).^[14] Then we obtained the detection limit (LOD) of the CitH3 detection from the equation below.

$$LOD = 3\sigma / k_{slope} \quad (1)$$

k_{slope} is the slope of the regression of the calibration curve that we obtained. Finally, we obtained LOD = 3 ng/mL for our microarray sensor platform. Since the typical LOD of ELISA for CitH3 is 0.1 ng/mL,^[16] ELISA still has a lower LOD. However, it requires at least 3.5 hours from sampling to reading the assay plate. Moreover, this assay needs multiple washing steps, so the assay time will be much longer than this minimum time. On the other hand, our chip's protocol is simpler because after fabricating antibody-coated AuNRs, we only have to wash channels with PBS once and load samples. Therefore, we could finish our assay within 40 min, which is 5 times shorter than ELISA. Although I did not demonstrate multiplex LSPR measurement in this work, but our LSPR microarray has 4 AuNR bars, hence our sensor is potentially capable of detecting several biomarkers from single sample. This advantage will enhance the reliability of the CitH3's information through monitoring several biomarkers simultaneously.

However, the deficit of sensor's dynamic range is a problem that we have to overcome. For this purpose, we need to investigate more sensitive gold patterning and sensor structure to enhance LSPR signal.

4. CONCLUSION

We have developed optofluidic biosensing platform to detect CitH3 for accurate sepsis screening. The biosensor used in our assay can achieve 40 min assay, which is approximately 5 times lower than that of goldstandard method, ELISA. We achieved LOD = 3 ng/mL, but ELISA still has a lower value. To overcome this deficit, we need a further improvement in dynamic range of the sensor.

ACKNOWLEDGEMENTS

I would like to express my deepest gratitude to my supervisor, Professor Katsuo Kurabayashi, for his supervision and mentorship throughout this JUACEP program. I learned a lot of important things to do research such as having clear vision and how to solve problems. His passion toward new research impressed me and change my idea of scientific and engineering research.

Also, I would like to thank the lab members in the Microsystems Technology and Science (MSTS) laboratory. Thanks to them, I could learn a lot to be a mature researcher. I would like to send my appreciation Dr. Young Geun Park, Dr. Bo-Ram Oh, Mr. Meng-Ting Chung, Mr. Yujing Song, Mr. Andrew Stephens, Mr. Ryan Rosario and Mr. Shane Berry. Especially, I would like to emphasize my gratitude to Mr. Yujing Song and Mr. Shane Berry as my mentor at the lab.

I would like to express deepest gratitude to my supervisor in Nagoya University, Jiro Kasahara. I cannot

send thanks enough to you. I would like to deeply contribute to drive our research with my attitude toward research, which I learned in Ann Arbor.

Finally, I would like to express my gratitude to everyone who supports this studying abroad and friends that I met in U.S.

REFERENCES

- [1] Younesi, E., Toldo, L., Müller, B., Friedrich, C., M., Novac, N., Scheer, A., Hofmann-Aptius, M., Fluck, J. Mining biomarker information in biomedical literature, *BMC Medical Informatics and Decision Making* Vol. 12, pp. 148 (2012)
- [2] Chen, P., Huang, N., T., Chung, M., T., Cornell, T., T., Kurabayashi, K., Label-free cytokine micro- and nano-biosensing towards personalized medicine of systemic inflammatory disorders, *Advanced Drug Delivery Reviews* Vol. 95, pp. 90-103 (2015)
- [3] Oh, B., R., Label-Free biosensors for Cytokine Detection, PhD dissertation, University of Michigan, Ann Arbor (2016)
- [4] Bienvenu, J., Monneret, G., Fabien, N., Revillard, J., P., The clinical Usefulness of the measurement of cytokines, *Clin Chem Lab Med* Vol. 38, pp.267-285 (2000)
- [5] Kohrt, H., E., Tume, P., C., Benson, D., Bhardwaj, N., Brody, J., Formenti, S., Fox, B., A., Galon, J., June, C., H., Kalos, M., Kirsch, I., Kleen, T., Kroemer, G., Lanier, L., Levy, R., Lyster, H., K., Maecker, H., Marabelle, A., Melenhorst, J., Miller, J., Melero, I., Odunsi, K., Palucka, K., Peoples, G., Ribas, A., Robins, H., Robinson, W., Serafini, T., Sondel, P., Vivier, E., Weber, J., Wolchok, J., Zitvogel, L., Disis, M., L., Cheeser, M., A., Cancer Immunotherapy Trial Network, Immunodynamics: a cancer immunotherapy trials network review of immune monitoring in immune-oncology clinical trials, *Journal of ImmunoTherapy of Cancer*, pp.4-15 (2016)
- [6] John, J., Pandha, H., Dalgleish, A., G., Detection of T cell cytokine production as a tool for monitoring immunotherapy, *Dis Markers*, Vol. 16(1-2), pp.71-75 (2000)
- [7] Oh, B., R., Huang, N., T., Chen, W., Seo, J., H., Chen, P., Cornell, T., T., Shanley, T., P., Fu, J., Kurabayashi, K., Integrated nanoplasmonic sensing for cellular functional immunoanalysis using human blood, *ACS NANO*, Vol.8 pp. 2667-2676 (2014)
- [8] Salata, O.V., Application of nanoparticles in biology and medicine, *Journal of Nanobiotechnology*, 2, 3 (2004)
- [9] Sackmann, E., K., Fulton, A., L., Beebe, D., J., The present and future role of microfluidics in biomedical research, *NATURE*, Vol. 507, pp.181-189 (2014)

- [10] Mayer, K., M., Lee, S., Liao, H., Rostro, B., C., Fuentes., A., Scully, P., T., Nehl, C., L., Hafner, J., H., A label-free immunoassay based upon localized surface plasmon resonance of gold nanolods, ACSNANO, Vol.2, NO.4, pp.687-692 (2008)
- [11] Haes, A., J., Duyne, R., P., V., Preliminary studies and potential applications of localized surface plasmon resonance spectroscopy in medical diagnostics, Expert Review of Molecular Diagnostics, Vol.4, pp.527-537, (2004)
- [12] Li, Y., Liu, B., Fukudome, E., Y., Lu, J., Chong, W., Jin, G., Liu, Z., Velmahos, G., C., deMoya, M., King, D., R., Alam, H., B., Identification of citrullinated histone H3 as a potential serum protein biomarker in a lethal model of lipopolysaccharide-induced shock, Surgery, Vol.150(3), pp.442-451, (2011)
- [13] Li, Y., Liu, Z., Liu, B., Zhao, T., Chong, W., Wang, Y., Alam, H., B., Citrullinated histone H3: a novel target for the treatment of sepsis, Surgery, Vol.156(2) pp.229-234, (2014)
- [14] Chen, P., Chung, M., T., MchHugh, W., Nidetz, R., Li, Y., Fu, J., Cornell, T., T., Shanley, T., P., Kurabayashi, K., Multiplex serum cytokine immunoassay using nanoplasmonic biosensor microarrays, ACSNANO, Vol.9, No.4, pp.4173-4181, (2015)
- [15] Hermanson, G., T., Bioconjugate Techniques, Academic Press, pp.219-223 (2008)
- [16] Citrullinated Histone H3 ELISA Kit, Cayman CHEMICAL, Item No.501440
- [17] O'Connor, R., S., Hao, X., Shen, K., Bashour, K., Akimova, T., Hancock, W., W., Kam, L., C., Milone, M., C., Substrate rigidity regulates human T cell activation and proliferation, The Journal of Immunology, Vol.189, pp.1330-1339 (2012)
- [18] Ma, Z., Finkel, T., H., T cell receptor triggering by force, Trend Immunol. Vol.31(1), pp.1-6 (2010)
- [19] Hu, K., H., Butte, M., J., T cell activation requires force generation, The Journal of Cell Biology, Vol.213(5), pp.535-542 (2016)
- [20] Li, Y., C., Chen, B., M., Wu, P., C., Cheng, T., L., Kao, L., S., Tao, M., H., Lieber, A., Roffler, S., R., Cutting edge: mechanical forces acting on T cells immobilized via the TCR complex can trigger TCR signaling, J Immunol. Vol.184(11), pp.5959-5963 (2010)
- [21] Kim, S., T., Takeuchi, K., Sun, Z., Y., J., Touma, M., Castro, C., E., Fahmy, A., Lang, M., J., Wagner, G., Reinherz, E., L., The $\alpha\beta$ T cell receptor is an anisotropic mechanosensor, The Journal of Biological Chemistry, Vol.284(45), pp.31028-31037 (2009)
- [22] Kim, S., T., Shin, Yongdae, S., Brazin, K., Mallis, R., J., Sun, Z., Y., J., Wagner, G., Lang, M., J., Reinherz, E., L., TCR mechanobiology: torques and tunable structures linked to early T cell signaling, Front. Immunol., Vol.18, pp.1-8 (2012)
- [23] Chen, W., Zhu, C., Mechanical regulation of T-cell functions, Immuno Rev., Vol.256(1), pp.160-176 (2013)
- [24] Beemiller, P., Krummel, M., F., Mediation of T cell activation by actin meshworks, Cold Spring Harb Perspect Biol., Vol.2(9), pp.1-14 (2010)
- [25] Hashimoto, K., Surface acoustic wave devices in telecommunications modeling and simulation, Springer (2000)
- [26] Ding, X., Li, P., Lin, Sz-C. S., Stratton, Z., S., Nama, N., Guo, F., Slotcavage, D., Mao, X., Shi, J., Costanzo, F., Huang, T., J., Surface acoustic wave microfluidics, Lab on a Chip, Vol.13, pp.3626-3649 (2013)
- [27] Schmid, L., Wixforth, A., Weitz, D., A., Franke, T., Novel surface acoustic wave (SAW)-driven closed PDMS flow chamber, Microfluid Nanofluid, Vol.12, pp.229-235 (2012)
- [28] A surface acoustic wave (SAW)-enhanced grating-coupling phase-integration surface plasmon resonance (SPR) microfluidic biosensor, Lab on a Chip, Vol.16, pp.1224-1233 (2016)

APPENDIX

In this appendix, my additional research work is described. I developed a new biological platform integrating LSPR biosensor with microfluidic pumping system, aiming to monitor T cell responses to mechanical shear force in real time. Central to immunotherapeutic approaches are controllable platform for ex vivo activation of T cells.^[17] T cell uses T cell receptors (TCRs) to probe their cognate peptides presented in major histocompatibility complexes (pMHCs) on the surface of antigen presenting cells (APCs). Recent work has suggested that TCR triggering requires force upon the TCR,^[17-124] especially, force must be applied to the TCR tangentially.^{[21][22]} However, previous studies are based on fluorescent measurements and lack of quantitative evaluation of tangential force and time-course information.^[21] Microfluidic shear force device can generate shear force upon multiple cells simultaneously, however, using syringe pump needs open flow pass and can lose cytokines secreted from T cells. To achieve quantitative real-time measurement, we develop novel platform integrating LSPR biosensor with surface acoustic wave (SAW) device. SAW are acoustic waves propagating along the surface of an elastic material, which is produced by applying a high-frequency voltage to a piezoelectric material.^{[25][26]} When a traveling SAW contacts a liquid, it generate a force and induce flow within the confined

channel.^[26-28] Previously, Integrating SPR technique with SAW device has been demonstrated,^[28] however, nobody has not demonstrated the integration of LSPR with SAW technology. Here, we fabricated SAW device and measured LSPR signals on SAW device platform.

Device design and fabrication of SAW-based fluidic pump

The device pumps the fluid in an enclosed PDMS chamber using surface acoustic streaming^[26] excited by an interdigital transducer (IDT). The IDT consist of two gold electrodes on a piezoelectric substrate. These gold electrodes were fabricated by vapor deposition and standard lithography. In this study we used Y-cut of LiNbO₃ with the crystal axis rotated around the X-axis by 128° (LN), which is widely used for SAW device.^{[25][26]} The IDT finger widths and spacing are all $\lambda/4$ ($\lambda = C_s/f$), where λ is the SAW wave length, $C_s = 3990\text{m/s}$, is the sound speed in LN and f is the operational frequency. Device has $\lambda/4 = 13\ \mu\text{m}$ finger widths and spacing and works at 76 MHz. We carefully aligned IDT fingers perpendicular to the X-axis. A function generator (33250A 80 MHz Function, Agilent) applied the high frequency voltage. To integrate SAW-based fluidic pump with LSPR microarray chip, we treated LN instead of glass substrate following 2-1 protocol. After the preparation of antibody-functionalized AuNRs, we assembled a PDMS chamber.

Results and discussion

We fabricated IDT on LiNbO₃ wafer (Fig. 7) and SAW device successfully worked at 76 MHz because it could generated local flow inside a droplet put on the substrate. (Figure not shown)

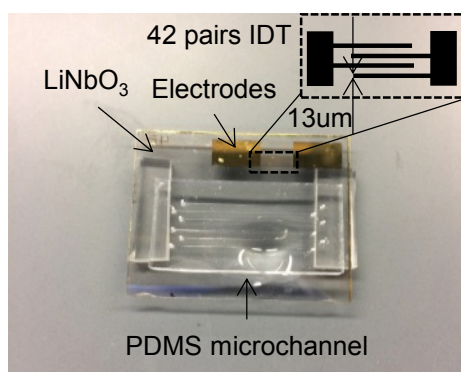


Fig. 7 SAW device integrated into LSPR microarray

However, Fluid was not pumped inside microchannel due to the high surface tension caused by small height (50 μm). On the other hand, we observed high initial peak wavelength with LiNbO₃ wafer due to the high refractive index of 2.3. Acquiring LSPR intensity change, we got a spectrum shift using spectrometer simultaneously. I did a quick test with IL-6 at 100ng/mL, which is one of the cytokines. After loading sample, binding caused peak shift of AuNRs. (Fig. 8) However, Intensity change was not observed for this test due to the non-appropriate band pass filter (610-680 nm).

(data not shown) For further improvement, we need to choose a correct filter.

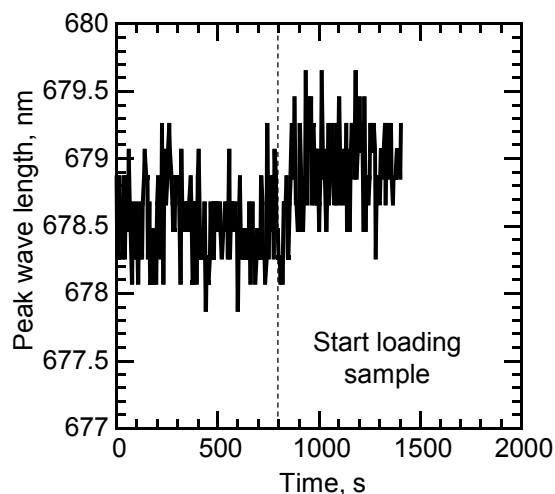


Fig. 8 Real-time peak wavelength of AuNRs on LiNbO₃. Sample is IL-6 (100ng/mL)

Although I could not complete this additional research project, I would like to show my research progress in this appendix for future research.

Synthesis of biopolymer compound with selective antimicrobial activity for denture applications

Takaharu Katsu

Department of Crystalline Materials Science, Graduate School of Engineering, Nagoya University
katsu.takaharu@g.mbox.nagoya-u.ac.jp

Supervisor: Benjamin M. Wu, DDS, PhD

Bioengineering, University of California, Los Angeles
benwu@ucla.edu

ABSTRACT

Biofilm formation on the denture resin, caused by microorganisms located in the oral cavity, is one of the problem within the dentistry field. To prevent this, several attempts have been carried out through antifungal or antiseptics agents. However, these compounds resulted in damages on the oral mucosa. As an alternative, cationic polymers have been used and they have shown good antimicrobial properties. Still, they do not have the selective antimicrobial activity against some microorganisms that should be eliminated. In this study, modified glycol chitosan was synthesized by grafting ethylene diamine tetra acetic acid disodium salt (EDTA-2Na) and ϵ -poly lysine (ϵ -PL) for selective antimicrobial activity against *Candida albicans* and *fusobacterium*. For the first step of synthesis, amino group of ϵ -PL was protected by di-tert-butyl dicarbonate ((Boc)₂O). The protection rate was about 17%. Then almost all the protected poly lysine was attached on the glycol chitosan.

1. INTRODUCTION

Many people have been wearing the denture for a long time. For denture fabrication, acrylic resins have been commonly used because they show high enough physical, mechanical, and esthetic properties^[1]. However, it has been shown that denture base acrylic resins may act as the reservoirs for microorganisms and have the potential to support biofilm formation^{[2],[3]}. They can also result in denture stomatitis, a big problem within the medical field.

In order to prevent the formation of biofilm on the resin surface, several antifungal agents or antiseptics were incorporated into tissue conditioners and denture acrylic resins^{[4]-[7]}. However, although they exhibited the antimicrobial activity, they also could have toxic effects on the oral mucosa, damage the mechanical properties, and lose their effectiveness over time^{[8],[9]}.

As a possible alternative, some other attempts have been carried out without the problems mentioned above. For example, cationic polymers, such as poly(2-tert-

butylaminoethyl) methacrylate and some ionic dimethacrylate monomers, were mixed with resins and they showed good microbial activity against some bacteria and fungi^{[1],[10]}. However, they sometimes killed the good microorganism as well, or did not kill ones intended. In other words, they did not have the selectivity required for the treatment. There are both some microorganisms which should not be killed, and others which should be killed, like *Candida albicans* and *fusobacterium*. It is known that *C. albicans* and *fuso* may cause stomatitis and bacterial acute pharyngitis, respectively^{[11],[12]}.

The objective of this study was to synthesize the biopolymer with selective antimicrobial activity for denture application. In this case, ethylene diamine tetra acetic acid (EDTA) and poly lysine (PL) must have the potential for such properties because based on previous research, they have antimicrobial activity against *C. albicans* and *fuso*. We intended to graft these compounds onto the biopolymer chitosan, selected due to its known antimicrobial activity, biocompatibility, and non-toxicity^[13]. EDTA and PL can be conjugated with chitosan through amide bonding between the carboxyl groups of EDTA and PL, and the amino groups of chitosan, which has multiple amino group per molecule.

As substitutes of chitosan and EDTA, glycol chitosan and EDTA disodium salt, 2-hydrate (EDTA-2Na) were used in order to increase their solubility in water. The synthesis in the water solvent should be better because it is easy to treat and organic solvent may damage the oral mucosa if not be removed.

Summarizing the above, in this study, glycol chitosan was modified by grafting EDTA-2Na and poly-lysine for selective antimicrobial activity. Almost all the synthesis was done in water, a better option over organic solvents.

2. EXPERIMENT

2.1 Materials

2-Morpholinoethane sulfonic acid (MES) was purchased from Acros Organics. ϵ -poly-L-lysine (ϵ -PL; M.W. 3500–4500 Da) was provided from Carbosynth LCC. Guanidine hydrochloride (Gu-HCl) was obtained from USB corporation. All other chemicals, Ethylene Diamine Tetra Acetic acid disodium salt 2-hydrate (EDTA-2Na), di-tert-butyl dicarbonate ((Boc)₂O), 1-Hydroxybenzotriazole (HOBT), N-[3-(Dimethylamino)propyl]-N'-ethyl carbodiimide (EDC) and glycol chitosan ($n \geq 400$), were purchased from Sigma-Aldrich, Inc., USA. They were used without further purification.

2.2 Evaluation of the antimicrobial activity of EDTA-2Na and ϵ -PL

The antimicrobial activity of EDTA-2Na and ϵ -PL was observed in order to evaluate which molecular ratio of EDTA-2Na and ϵ -PL would show the best antimicrobial activity. 5 mg of each EDTA-2Na and ϵ -PL was dissolved into the 5 mL of nano pure water. These solutions were filtered through 0.2 μ m filter by syringe in order to remove any cells. For these solution, antimicrobial testing was carried out, but the result was not obtained.

2.3 Synthesis of modified biopolymer

For the synthesis, there are two possible routes: attaching the poly lysine first, or attaching the EDTA first. We opted to implement the former where first, the amino groups of poly-lysine including the end of functional group

are protected and then attached to the glycol chitosan. After that, EDTA-2Na is attached and the amino groups are deprotected. The other one, attaching the EDTA first, then, attaching the protected poly lysine could have resulted in several carboxyl group of one EDTA-2Na molecule grafted on the chitosan's amino group. Therefore, we selected the former steps to synthesize the polymer. The scheme is shown below in Fig. 1.

2.3.1 Protection of amino group of PL

(Boc)₂O (1.27 g), Gu-HCl (0.556 g), H₂O (1.5 mL) and ethanol (1.5 mL) were mixed then ϵ -PL (0.250 g) was added to the solution [14]. Molecular ratio of ϵ -PL : (Boc)₂O : Gu-HCl was 1 : 35 : 35 because polymerization of ϵ -PL (M.W.3500–4500) should be about 35. It was stirred at room temperature overnight, dialyzed, and lyophilized. A small part of powder was evaluated by ¹H NMR and the rest of powder was used for the next step of synthesis.

2.3.2 Fabrication of the MES buffer [15],[16]

In order to keep the pH around 5.0–5.5 during the synthesis, maintaining EDC stability [17], 0.1 M MES buffer was prepared. MES (1.953 g, 10 mmol) and 100 mL nano pure water were mixed then pH was adjusted by adding about 10 mL of 0.1 N NaOH aq.

2.3.3 Attaching the protected PL on the glycol chitosan [13]

Glycol chitosan (0.010 g, 48.8 μ mol) was stirred with two molar equivalents of HOBT (0.013 g, 97.6 μ mol) in 1 mL of MES buffer, mentioned above, at room temperature until all the reagents dissolved. This was mixed with

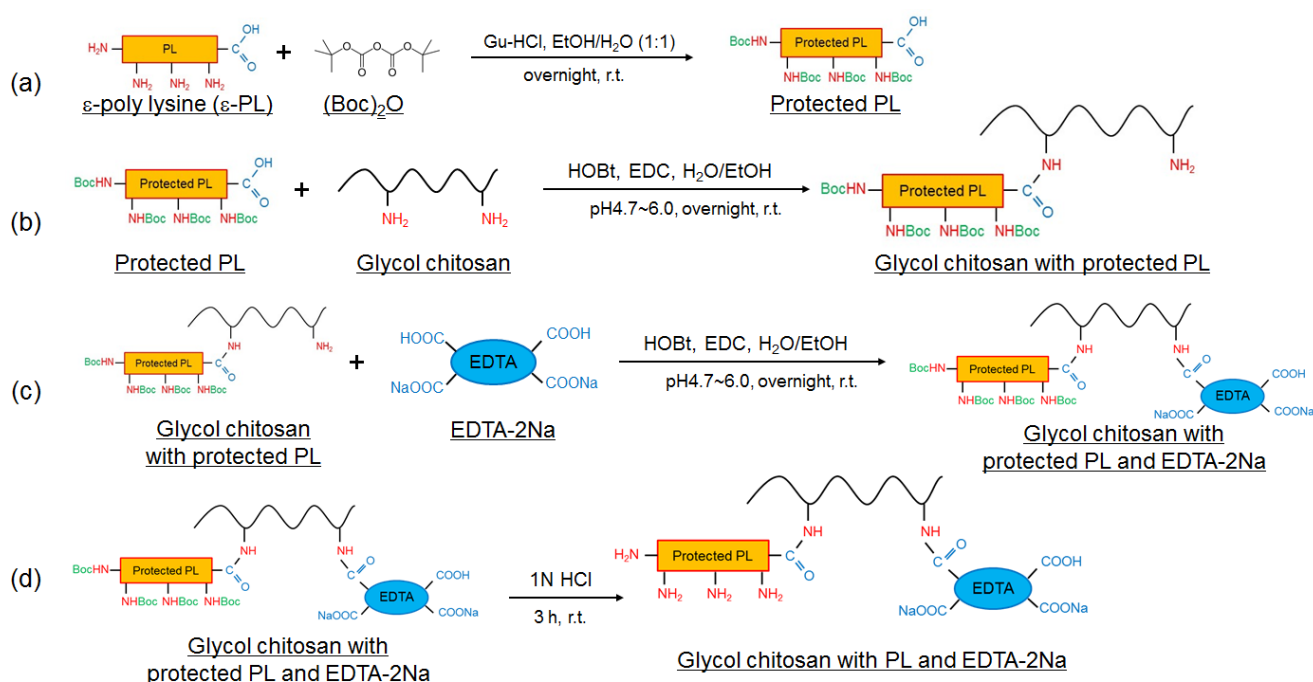


Fig. 1 The synthesis route scheme model (a) Protection of amino group of PL (2.3.2) (b) Attaching the polprotected PL on the glycol chitosan (2.3.3) (c) Attaching the EDTA-2Na on the glycol chitosan (2.3.4) (d) Deblocking of Boc protection (2.3.4)

protected PL (0.072 g, 1.6 μmol) in MES buffer (1 mL) followed by adding a solution of EDC in MES buffer (0.019 g, 97.6 μmol , 1 mL) dropwise. The reaction was carried out for 5 hours at room temperature. The crude product was dialyzed and lyophilized then evaluated by ^1H NMR.

2.3.4 Attaching the EDTA-2Na on the glycol chitosan and removal of Boc protection^[13]

This part will be done in the future in order to complete the synthesis. As well as above, glycol chitosan grafted the protected PL will be dissolved into the MES buffer with HOBt. This will be mixed with EDTA-2Na solution in MES buffer, then EDC solution will be added dropwise and stirred for 5 hours at room temperature. After the reaction, small part of the solution will be dialyzed and lyophilized, then the sample will be evaluated by ^1H NMR.

1N HCl will be added to the rest of solution and it will be stirred for 3 hours at room temperature. The Boc protection should be removed through this process. After the dialysis and lyophilization, the obtained sample will be observed by ^1H NMR as well.

3. RESULT AND DISCUSSION

3.1 Boc protection

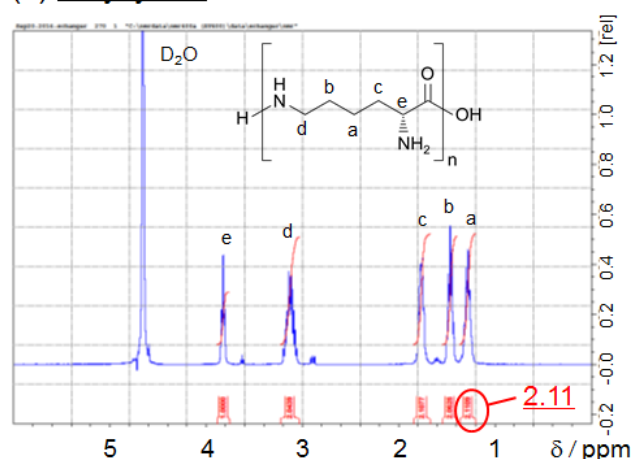
The amino group of PL was protected by $(\text{Boc})_2\text{O}$ and it was evaluated by ^1H NMR. The NMR peaks are shown in Fig. 2. Fig. 2(1) shows the peaks of ϵ -PL (observed), and Fig. 2(2) shows the peaks of product. ^1H NMR (D_2O) $\delta = 1.25$ (H-a), 1.45 (H-b), 1.78 (H-c), 3.14 (H-d), 3.81 (H-e) and 4.73 (D_2O). All other proton peaks should be exhibited above $\delta = 6$. The value around $\delta = 1.25$ (H-a) should be 2 because there are two protons. The obtained value, 2.11, was fine.

As for the product, the proton's peak of tert-butyl group should be $\delta = 1.32$, very closed to the peak of $\delta = 1.25$ (H-a). There are 9 protons in tert-butyl group (Boc group), then the value around $\delta = 1.3$ should be 11 if the reaction was completed 100%. However, it was just 3.52. Taking into account the above mentioned, the protection rate was calculated as below.

$$\text{Protection rate(\%)} = \frac{3.52 - 2}{9} \times 100 \cong 16.9 \text{ (\%)}$$

Gu-HCl works as a catalyst like Fig.3^[14]. Both $(\text{Boc})_2\text{O}$ and Gu-HCL must approach to the amino group of poly lysine for the reaction. It is not well-known of the 3D structure of ϵ -PL in the water, however, it is suggested that they form a lot of hydroxyl bonding between each molecule and it may be difficult for other chemicals to get closer. That is one of the possible reason why the protection rate was such a small amount.

(1) Poly lysine



(2) Protected poly lysine

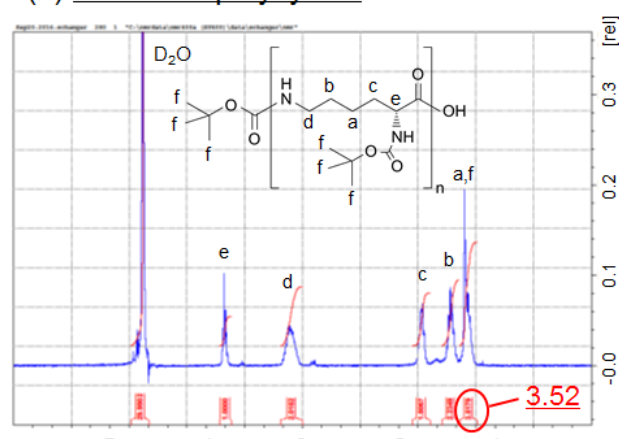


Fig. 2 ^1H NMR peaks (1) Observed poly lysine (2) Protected poly lysine (product)

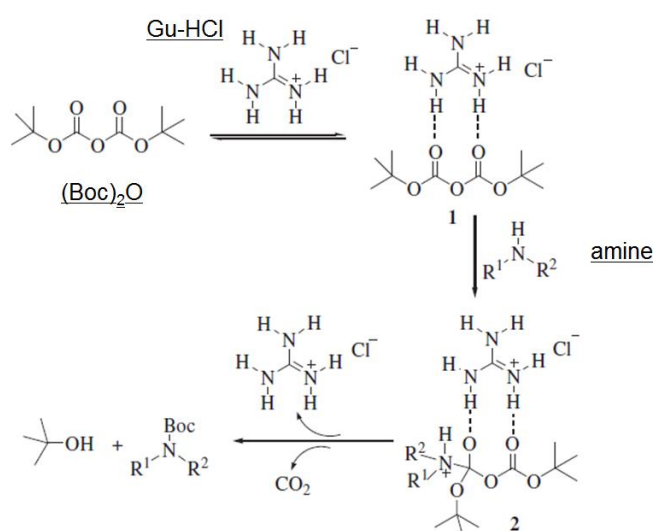


Fig. 3 The proposed mechanism for $(\text{Boc})_2\text{O}$ protection of amines^[14]

3.2 MES buffer

After the MES was dissolved in the water, pH value was about 4. It must be because MES has a sulfo group. The pH value was adjusted by adding NaOH aq dropwise and the final pH of obtained buffer was 5.16. The concentration was not 0.1 M perfectly, but this had no detrimental effects, since the aim of buffer was to maintain a specific pH through the synthesis process.

3.3 Attaching the protected PL on glycol chitosan

The protected PL was attached on the glycol chitosan and it was evaluated by ^1H NMR. The NMR peaks are shown in Fig. 4. Fig. 4(i) shows the peaks of glycol chitosan (observed). Fig. 4(ii) shows the peaks of protected poly lysine (same as above). And Fig. 4(iii) shows the peaks of product. The important peak of ^1H NMR (D_2O) of glycol chitosan (i) is; $\delta = 2.75$ (H-a), because when the amide bonding was produced, this peak shifted.

As it is seen in (iii), this peak almost disappeared. However, protected PL was added only enough to react 3% of the amino groups in glycol chitosan. Therefore, some of the amino group of chitosan should remain unreacted and this peak should not completely disappear. Furthermore, new peaks appeared around $\delta = 7.5\sim 8.0$ in (iii). There are both peaks of glycol chitosan and peaks of protected PL in the product.

These things suggest that HOBt, supporting chemical like a catalyst, probably remained in the solution. In other words, the dialysis was not enough. It can explain not only the peaks around $\delta = 7.5\sim 8.0$ as the benzene protons of HOBt, but also the disappearance of H-a peak as the creation of ionic bonding between the amino group of glycol chitosan and hydroxyl group of HOBt^[14]. Even if it is taken into account, the added protected PL must be reacted perfectly.

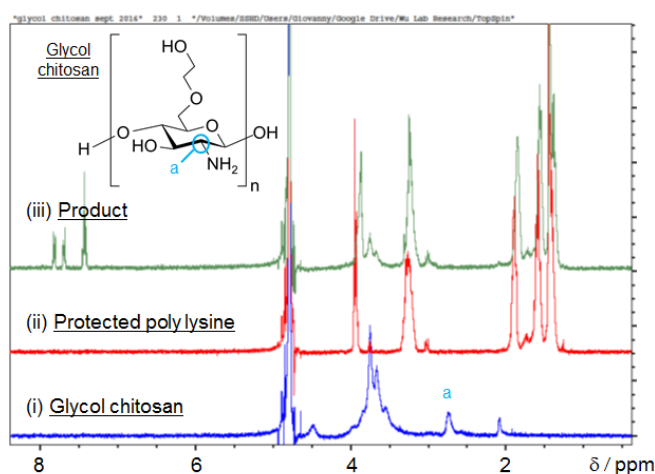


Fig. 4 ^1H NMR peak (i) Glycol chitosan (ii) Protected poly lysine (iii) Glycol chitosan with protected PL (product)

3.4 Attaching the EDTA-2Na on the glycol chitosan and removal of Boc protection

In this part, the experiments were not carried out, therefore discussion is only written.

EDTA-2Na must be attached through the same process as the former one. However, many amino groups in poly lysine are not protected, resulting in EDTA-2Na possible attachments with poly lysine as well. Higher protection rate should be obtained for the whole synthesis. As for the dialysis, it needs to be used the proper membrane. Otherwise, unreacted substance may not be removed as well.

4. CONCLUSION

Modified glycol chitosan was synthesized by attaching Boc protected poly lysine. Protection ratio was about 17%. Added protected PL must be reacted perfectly. Almost all synthesis steps used the water solvent because it was easy to treat and it does not damage the human compared to using toxic organic solvent.

ACKNOWLEDGEMENTS

I would like to express my sincere gratitude to my supervisor, Professor Benjamin Wu for providing me this precious experience. I would like to thank Yulong Zhang, Chase Linsley, Giovanni F. Acosta-Vélez and all of laboratory's members for supporting me and giving advice. This study was also supported by Japan-US Advanced Collaborative Education Program.

REFERENCES

- [1] Juliê M., André G.P., Larissa S.R., Andressa R.P.L., Ana C.P. and Marco A.C., Effect of an acrylic resin combined with an antimicrobial polymer on biofilm formation, *Journal of Applied Oral Science*, Vol.20, No.6, pp.643-648 (2012)
- [2] Pereira-Cenci T., Del Bel Cury A.A., Crielaard W. and Ten Cate J.M., Development of *Candida*-associated denture stomatitis: new insights, *Journal of Applied Oral Science*, Vol.16, No.2, pp.86-94 (2008)
- [3] Radford D.R., Sweet S.P., Challacombe S.J., Walter J.D., Adherence of *Candida albicans* to denture-base materials with different surface finishes, *Journal of Dentistry*, Vol.26, No.7, pp.577-583 (1998)
- [4] Kuroki K., Hayashi T., Sato K., Asai T., Okano M., Kominami Y., Takahashi Y. and Kawai T., Effect of self-cured acrylic resin added with an inorganic antibacterial agent on *Streptococcus mutans*, *Dental Materials Journal*, Vol.29, No.3, pp.277-285 (2010)
- [5] Nikawa H., Egusa H., Makihira S., Yamashiro H., Fukushima H., Jin C., Nishimura M., Pudji R.R. and

- Hamada T., Alteration of the co-adherence of *Candida albicans* with oral bacteria by dietary sugars, *Oral microbiology and immunology*, Vol.16, No.5, pp.279-283 (2001)
- [6] Paleari A.G., Marra J., Pero A.C., Rodriguez L.S., Ruvolo-Filho A. and Compagnoni M.A., Effect of incorporation of 2-tert-butylaminoethyl methacrylate on flexural strength of a denture base acrylic resin, *Journal of Applied Oral Science*, Vol.19, No.3, pp.195-199 (2011)
- [7] Shibata T., Hamada N., Kimoto K., Sawada T., Sawada T., Kumada H., Umemoto T. and Toyoda M., Antifungal effect of acrylic resin containing apatite-coated TiO₂ photocatalyst, *Dental Materials Journal*, Vol.26, NO.3, pp.437-444 (2007)
- [8] Imazato S., Kinomoto Y., Tarumi H., Ebisu S. and Tay F.R., Antibacterial activity and bonding characteristics of an adhesive resin containing antibacterial monomer MDPB, *Dental materials*, Vol.19, No.5, pp.313-319 (2003)
- [9] Pesci-Bardon C., Fosse T., Serre D. and Madinier I., *In vitro* antiseptic properties of an ammonium compound combined with denture base acrylic resin, *Gerodontology*, Vol.23, No.2, pp.111-113 (2006)
- [10] Joseph M.A., Diana N.Z., Kathy T., Sheng L.G., Bruce O.F. and Nancy J.L., Synthesis and characterization of dimethacrylates containing quaternary ammonium functionalities for dental applications, *Dental materials*, Vol.28, No.2, pp.219-228 (2012)
- [11] Nikawa H., Egusa H., Kawabata R., Yatani H., Mikihiro S., Fukushima H. and Hamada T., *Candida* Adherence and Biofilm Formation on Oral Surfaces, *Japanese journal of medical mycology*, Vol.46, pp.233-242 (2005)
- [12] <http://georgebest1969.typepad.jp/blog/2015/06/>
- [13] Juthathip F., Akashi M., Kida T. and Suwabun C., Chitosan-Hydroxybenzotriazole Aqueous Solution: A Novel Water-Based System for Chitosan Functionalization, *Macromolecular rapid communications*, Vol.27, No.13, pp.1039-1046 (2006)
- [14] Fatemeh J., Mahmood T., Hamid G. and Samad K., Guanidine hydrochloride as an organocatalyst for N-Boc protection of amino groups, *Tetrahedron letters*, Vol.52, No.12, pp.1260-1264 (2011)
- [15] <http://people.virginia.edu/~owp3a/docs/protocols/Buffer%20recipes.pdf>
- [16] http://www.ls.toyaku.ac.jp/~bioinfo/bioinformatics/cgi-bin/buffer_calc.cgi
- [17] <https://www.thermofisher.com/order/catalog/product/2980>

SYNTHESIS OF OCTAHEDRAL PLATINUM-CUPPER NANOCRYSTALS

Chisato Atsumi

Department of Crystalline Materials Science, Graduate school of Engineering, Nagoya University
atsumi.chisato@c.mbox.nagoya-u.ac.jp

Supervisor: Yu Huang

Department of Materials Science and Engineering, HSSEAS, UCLA
yhuang@seas.ucla.edu

ABSTRACT

Bimetallic alloy nanocrystals (NCs) have received great attention because of superior catalytic abilities to their monometallic counterparts. Recently, manipulation of the catalytic selectivity has been a centered topic in advanced catalysis. The properties of a nanocrystal are heavily influenced by its shape, so making uniform NCs in shape, size is important to control of the catalytic selectivity of NCs. In this work, the way to prepare well-dispersed Pt-Cu alloy NCs with octahedral structures for catalysts was explored by changing the composition of stabilizing agent and reducing agent.

Undisclosed

LOCAL FEEDING APCVD GRAPHENE GROWTH ON CU AND CU:NI FOILS

Naoki Kamimura

Department of Quantum Engineering, Graduate School of Engineering, Nagoya University
kamimura.naoki@g.mbox.nagoya-u.ac.jp

Supervisor: Ya-Hong Xie

Department of Materials Science and Engineering, Graduate School of Engineering, University of California, Los Angeles
yhx@ucla.edu

ABSTRACT

The growth of high-quality single crystal graphene by chemical vapor deposition on copper (Cu) or copper-nickel (Cu:Ni) has not always achieved control over domain size and morphology, and the results vary from lab to lab under presumably similar growth conditions. A method for large single-grain graphene growth on a Cu:Ni alloy using a local precursor feeding setup has been reported [1]. In this experiment, we explored the way of growing large single grain graphene and important parameters were optimized to improve quality of graphene for local feeding graphene growth.

1. INTRODUCTION

Graphene and other two-dimensional materials have attracted plenty of attention and high expectations have been placed on them by academia and industry since the discovery in 2004 [2]. Monolayer graphene has unique and fascinating properties, such as high transparency, high thermal conductivity, high electrical conductivity, high Young's modulus and high specific surface area [3,4]. Over the past decade, theoretical and experimental investigations on graphene showed such extraordinary performances in various applications, such as optoelectronics and electronics, and so on, which responds remarkably to the expectations [5-7]. However graphene's excellence would not be fully realized before high-quality single-crystalline graphene (SCG) is available.

As well as one of the applications, this experiments' objective is EDS devices using micro mechanical response of graphene nano-ribbon. A suspended single crystalline

graphene nano-ribbon is needed to achieve better ESD devices performance. Control of the nucleation and growth of graphene during the chemical vapor deposition (CVD) process is important to achieve large, high-quality single crystals [8-12]. Much attention has been paid to the process details, with the emphasis on the parameters of carbon precursors, hydrogen, copper, temperature and pressure for the conventional CVD graphene growth [13]. As such, turning the C:H ratio [13], changing the hydrocarbon and H₂ gas pressures [14] and smoothing the Cu surface before growth [15,16] have been used to grow graphene with desirable quality. However, the wide variation in domain size, shape, film quality from lab to lab suggests that crucial growth parameters still remain unknown or uncontrolled.

Recently, in order to realize large single grain graphene, a method using a local precursor feeding setup has been reported [1]. However, few details about the actual local feeding setup and the yield were given.

In this research, we struggled to achieve large single grain graphene with a local precursor feeding setup, which was optimized a little by little. Important parameters were also optimized to allow local graphene growth. Local growth of graphene was achieved for several substrate-nozzle distances (0.1 inch, 0.25 inch, 0.30 inch, 0.35 inch and 0.60 inch) near atmospheric pressure (86.5hPa) for low precursor flow rate (5cm³/min). Local growth on both Cu and Cu:Ni foil is possible for these optimized parameters. Argon-diluted Methane as a carbon precursor was fed through quartz-nozzle placed above the growth substrate in the 10cm diameter quartz tube for the localized precursor feeding. Cu and Cu:Ni-alloy substrates were used.

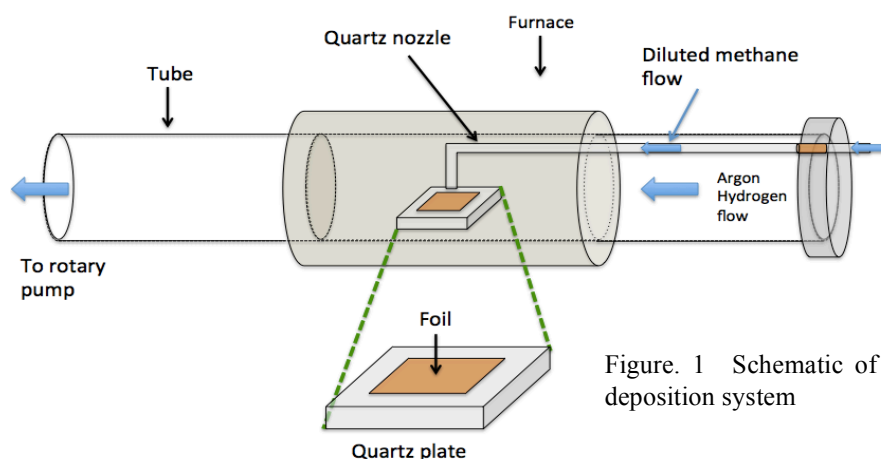


Figure. 1 Schematic of local feeding chemical vapor deposition system

2. EXPERIMENTAL

2.1 Local Feeding Chemical Vapor Deposition System

A schematic of Local Feeding Chemical Vapor Deposition System is shown in Figure. 1. All graphene growth experiments in this research were carried out in this system. The CVD system consists of the furnace, quartz tube, quartz nozzle and quartz stage as Figure. 1 shows. A local precursor feeding setup was implemented using a conventional tube-furnace, modified to allow local precursor feeding. The furnace can control the temperature from room temperature to around 1100°C. For graphene growth from a controlled nucleus, the 0.1 inch diameter small feeding quartz nozzle was set above the foil in the 10 cm diameter quartz tube for the localized precursor feeding. At the center of the precursor flow, the concentration of precursor gas is the highest and it decreases with the distance from the center owing to the dilution by Ar and H₂.

One end of the tube is connected to the gas inlet of Argon (Ar) and Hydrogen (H₂) and the nozzle which flows diluted methane as a precursor gas. The quartz nozzle is connected to the metal tube with copper gasket in the furnace. The other end of tube is connected to the rotary pump and the gas inlet of the air. A foil is placed on the quartz stage under the nozzle. By adding quartz plates to the quartz stage, the distance between the nozzle and foil can be changed.

2.2 Substrate and Precursors

Cu foil and Cu:Ni foil are used as a substrate in this experiment.

For the Cu foils, Cu foil (25 μm, 99.8% for graphene growth, Alfa Aesar) was cut to 4×4cm and washed by acetone, isopropyl alcohol (IPA) and DI water. After washing, the Cu foil was put into polishing solution for 30s to make the foil surface smoother because the foils had a lot of grooves. Polishing solution consisted of 400ml DI water, 60ml acetic acid, 40ml nitric acid and 0.5ml hydrochloric acid. Then, the foil was rinsed by DI water again and dried up using nitrogen gas.

As for Cu:Ni foil, the Cu foil was cut and washed as well as Cu foil. After that, the Cu foil was electrochemically polished to reduce the surface roughness by using polishing

solution for 45s. Cu:Ni foils were prepared by electroplating of Ni foil (0.25mm, 100×100mm, annealed, 99.5%) and solution (Nickel plating solution semi-bright finish, Alfa Aesar) on Cu foil followed electrochemically polishing process. Then, the foil was rinsed by DI water again and dried.

2.3 Graphene growth condition

A foil is placed on the quartz stage under the nozzle as shown in Figure. 1. After taking the nozzle into the furnace, the furnace was evacuated with all mass flow controller turned off. Pressure reached a value below ten millitorr to ensure there was no air leakage because under this pressure - the remaining oxygen was found to be negligible to prevent oxidization of the foil. After pumping down, the needle valve and ball valve were closed. The rotary pump and Pirani gauge was turned off after closing both valves.

Argon fill-up established the current atmosphere inside the furnace for heat-up and growth after pumping down. Basically mass flow rates for hydrogen and argon were set to be 50sccm and 1000sccm on each due to Ref. [1] except experiments about hydrogen dependency mentioned later. After reaching ambient pressure or slightly higher (Mechanical pressure gauge), the ambient air valve was fully opened. The correct temperature for the following growth was set. Heat-up takes approximately 40 minutes.

As graphene growth step, desired flow rate was set for the mass flow controller feeding to the quartz nozzle. For small flow rates and short growth time it can be necessary to fill up the piping with methane before the actual growth. Otherwise the methane does not reach the nozzle before the end of the growth step.

Heating is turned off after the end of the growth step. The furnace was cooled down under 10 millitorr followed pumping down after growth.

2.4 Analysis

For analysis, a hot plate was used for getting better contrast. The area covered by Graphene cannot be oxidized after oxidization using hot plate. Then, the sample was analyzed with optical microscopy, Raman spectroscopy and Scanning Electron Microscopy (SEM).

Raman spectroscopy is a common technique for grapheme characterization. This method is popularly used to characterize the quality and the layer number of graphene. The technique involves the bombardment of a material's surface with monochromatic photons. Graphene has three distinct peaks, the G peak ($\sim 1587\text{cm}^{-1}$), the D peak ($\sim 1350\text{cm}^{-1}$) and the 2D peak ($\sim 2700\text{cm}^{-1}$), whose positions, widths, and heights can be used to quantify the various qualities of the substance. The D peak is located at $\sim 1350\text{cm}^{-1}$. The peak is the result of vibrational mode in sp^3 bonded carbon. The presence of this vibrational mode indicates the presence of defects in the structure of grapheme. The presence of sp^3 bonds suggest that the grapheme is folded such a way that some of the carbon atoms are now bonded of four neighbors instead of the typical three in graphene. The intensity of this peak is related to the number of defects present. This band is not normally present in CVD grown graphene. The G peak is located at $\sim 1587\text{cm}^{-1}$ in the graphene spectrum. The peak corresponds to the in-plane vibrational model involving sp^2 hybridized carbon atoms. This means that the carbon atoms are bonded to three neighbors. This peak has the ability to vary with the number of layers of grapheme that are present. As the number of grapheme layers increase, the peak shifts to layer energies due to softening of the planar carbon bonds. What is useful about the G peak is that its intensity and width remains relatively constant, in comparison to the 2D peak with varying layers of grapheme and into graphite. The 2D peak is known as an overtone of the D peak, however, it is not related to the physical defects of the grapheme itself. It is located at $\sim 2700\text{cm}^{-1}$. The 2D peak is comprised of four different peaks. In single layer grapheme however, only one of those peaks dominant, which results in a strong and sharp peak. This peak is believed to be a result of a zone-boundary vibrational model.

3 RESULTS

3.1 Optimization

After several growth, the parameter of methane from the nozzle, hydrogen and argon flow rate were optimized in order to gain graphene and the temperature was set up at 1050°C . 5 sccm diluted methane (mixed Ar/ CH_4 gas with 5% of methane) was fed through the nozzle, introduced into the growth chamber with 1,000 sccm Ar and 50 sccm H_2 . For LPCVD growth, any graphene were not observed because the turbulence caused by hydrogen and argon gas flow prevented the methane flow from the nozzle reaching to the foil straight. Therefore, APCVD was used with every experiment. Moreover, the height from the nozzle to the foil was made changed by using quartz plates.

3.2 The distance dependency

Three types of graphene growth was conducted at the different height (0.1 inch, 0.25 inch and 0.35 inch) with the copper foil.

H_2 and Ar were purged followed by pinging down to less than 10 mTorr. After the pressure in the furnace reach the atmospheric pressure, the temperature was increased to 1050°C and fixed for 30 minutes with 50 sccm H_2 and 1000 sccm Ar so that the copper foil was annealed. After annealing 5 sccm CH_4 from the nozzle was fed through the nozzle for 10 minutes. Cooling down process was conducted with H_2 and Ar to prevent oxidization of the copper foil for 6 hours. After growth, the samples were oxidized using the hot plate at 180°C for at least 10 minutes for better contrast and observed with optical microscopy and Raman spectroscopy.

Time	CH_4	H_2	Ar	Comment
10 mins	-	-	-	Pumping down
25 mins		50	1000	Purge
30 mins	-	50	1000	Increasing temperature
30 mins	-	50	1000	Annealing
10 mins	5	50	1000	Growth
6 hours	-	50	1000	Cooling down

Figure. 2 Recipe of local feeding APCVD grapheme growth with the copper foil at the different height (0.1 inch, 0.25 inch and 0.35 inch)

As a result, for growth at the height; 0.10 inch and 0.25 inch a white spot and a circle were observed with each foil and for growth at the height; 0.35 inch the shiny area was observed homogenously.

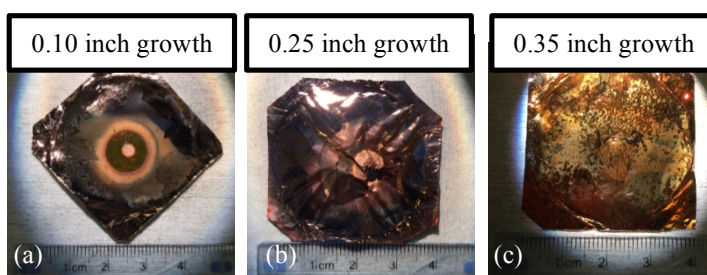


Figure. 3 Results from local feeding APCVD on the copper foil after oxidization with height; (a) 0.10 inch, (b) 0.25 inch and (c) 0.35 inch.

Each foil was analysed using optical microscopy, Raman spectroscopy and the area covered by graphene was calculated using imageJ (Figure. 5, 7).

For growth at the height; 0.10 inch, a lot of star-shape graphene were observed in the area between $3800\ \mu\text{m}$ and $6000\ \mu\text{m}$ from the center, which were gradually increasing as getting far from the center (Figure. 4 (a)). Approximately at $6000\ \mu\text{m}$, graphene shape changed from star-shape to random-shape (Figure. 4 (b)) and the covered area was increasing getting far from the center without changing the graphene shape (Figure. 4 (c)).

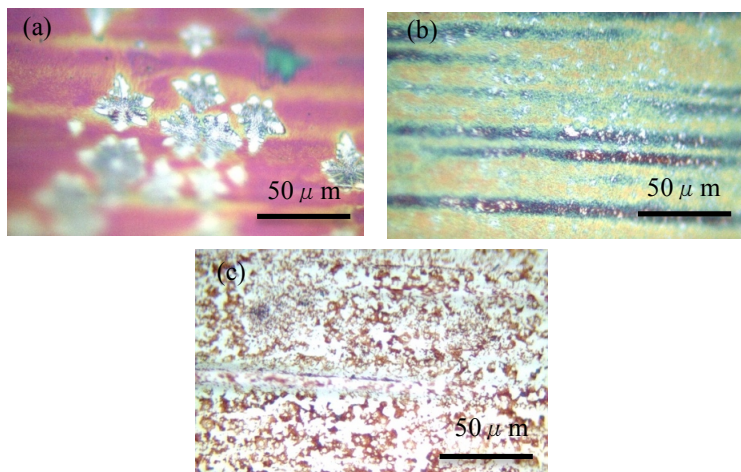


Figure. 4 Optical microscopy images from local feeding APCVD on copper foil with height; 0.10 inch after oxidization. (a) Star-shape graphene flakes formed in the area of 5400 μm from the center (b) Random shape graphene formed in the areas of 6500 μm (c) Random shape graphene formed in the areas of 12500 μm

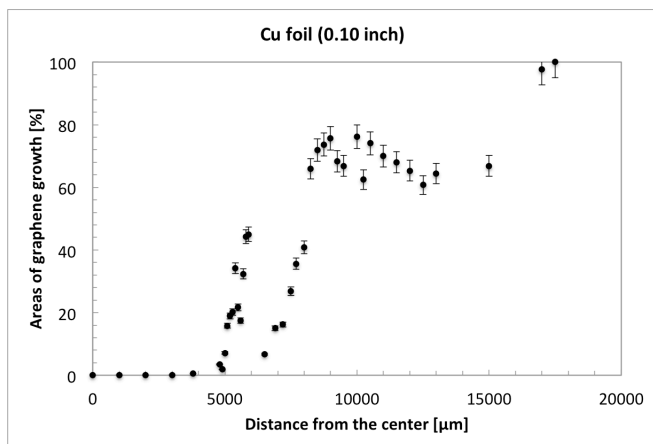


Figure. 5 Distance from the center vs. area covered by graphene from local feeding APCVD on copper foil with height; 0.10 inch

For growth at the height; 0.25 inch growth, a lot of star-shape graphene were observed on the entire area on the foil. Area covered by graphene was increasing as getting far from the center. Moreover, the nucleation density was getting higher as getting far from the center (Figure. 6).

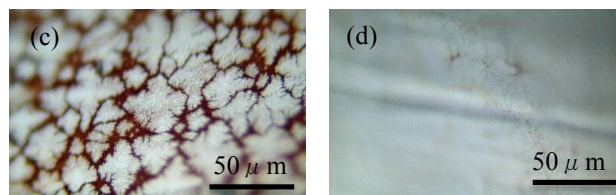
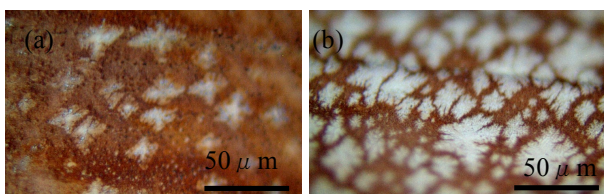


Figure. 6 Optical microscopy images from local feeding APCVD on copper foil with height; 0.25 inch after oxidization. Star-shape graphene formed in the area of (a) 4100 μm, (b) 6100 μm and (c) 7100 μm from the center. (d) Overlapping graphene formed in the area of 9600 μm

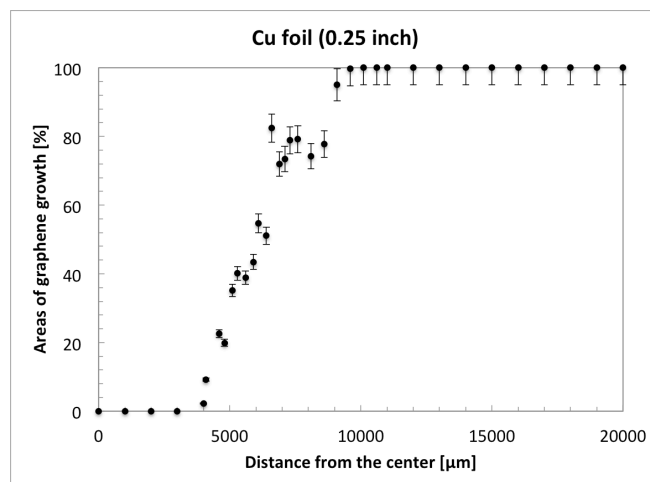


Figure. 7 Distance from the center vs. area covered by graphene from local feeding APCVD on copper foil with height; 0.25 inch

For growth at the height; 0.35 inch, there were un-oxidized areas, which means areas covered with graphene, very randomly on the entire foil (Figure. 6). Moreover, most of graphene observed were single-layer graphene.

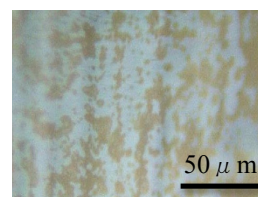


Figure. 8 Randomly graphene covered area with growth at the height; 0.35 inch

3.3 hydrogen dependency

According to some papers, the hydrogen flow rate made an effect to graphene shape for conventional graphene CVD growth [14,17]. Three types of growth depending on hydrogen flow rate were conducted for local feeding APCVD growth with height; 0.1inch. Only the hydrogen flow rate was changed to 50 sccm, 150 sccm or 1000 sccm fixing CH₄ and Ar flow rate at 5 sccm and 1000 sccm.

As a result, a lot of hexagonal shape graphene were observed on the foils with the 150 sccm and 1000 sccm H₂ flow rate instead of star-shape graphene (Figure. 9). The domain size was 2~3 μm and 5~10 μm on each. SEM images of star-shape graphene with 50 sccm H₂ and hexagonal shape graphene with 150 sccm H₂ is shown in Figure. 10.

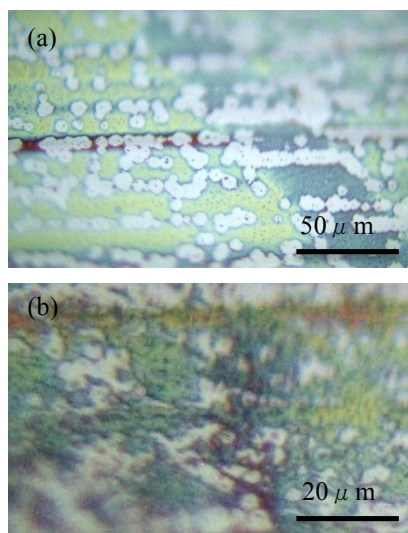


Figure. 9 Optical microscopy image of hexagonal graphene flakes with (a)150 sccm hydrogen flow and (b) 1000 sccm hydrogen flow

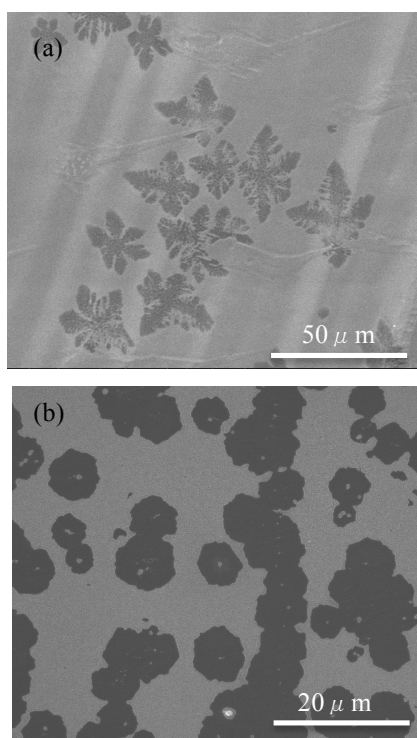


Figure. 10 (a) SEM image of star shape graphene flakes. (b) SEM image of hexagonal shape graphene flakes for 150 sccm H₂ flow rate growth.

Unfortunately, it was difficult to control the density of nucleation seeds for graphene growth exactly, but it is clear

that the regular hexagonal shape was observed only under high enough hydrogen pressure at least under our grow condition.

4. DISCUSSION

For local feeding APCVD graphene growth under the condition; 5sccm methane, 150 sccm hydrogen, Argon1000 sccm at 0.1 inch height and 1050°C, a lot of hexagonal shaped graphene were observed. From this result, we might 2 important information for local feeding APCVD graphene growth on the copper foil.

3.1 The Effect of hydrogen

From results, the difference of graphene shape was caused by hydrogen flow rate. Basically, graphene growth is strongly dependent on the hydrogen contribution, which serves a double role as an activator of surface-bound carbon that leads to monolayer growth and as etching reagent that controls the size and morphology of the resulting graphene domains. It is reported that the growth rate has a mazimum as a function of hydrogen partial pressure. Moreover, the orphology and size of graphene domains change along with hydrogen partial pressure [14].

In this experiment, the reason why the star shape graphene were observed for the growth at the height; 0.10 inch with 50 sccm hydrogen flow seems to be caused by the shortage of hydrogen. On the other hand, for the growth at the height; 0.10 inch with 150 and 1000 sccm hydrogen flow, graphene had the hydrogen enough to be etched and formed hexagonal shape.

For the growth at the height; 0.10 inch with 1000 sccm hydrogen flow, the graphene domain size is smaller (2~3 μm) compared to growth at the height; 0.10 inch with 150 sccm hydrogen flow (5~10 μm). If the hydrogen flow rate is too much high, hydrogen should etch graphene too much, which means the graphene domain size decreases.

3.2 Nozzle-substrate distance

According to results, the white spot in the center and the circle seem to be caused by the distance between the nozzle and substrate. There is no white spot and circle as for 0.35 inch growth. If the nozzle is made too close to the foil, the precursor gas flow should be like the jet flow. Therefore, any graphene growth are not observed. In my opinion, the distribution of methane flow from the nozzle on the foil surface depends on the distance very much. Obviously the nucleation density was changed due to the difference of nozzle-quartz distance. Moreover, even on the same foil the nucleation density was changed depending on the area observed. Though we are able to get large only *single* grain graphene with the super-concentrated precursor gas flow, changing

the nozzle-quartz distance might be a key point to get large *multi* grain graphene on the copper foil.

3.3 Surface condition

Low nucleation density is needed to get larger single grain graphene. I think the smoother surface is essential to get low nucleation density because most hexagonal graphene were observed in grooves on the foil. By increasing the temperature as much as possible or optimized polishing with the solution, we should be able to get the smoother surface.

5. CONCLUSION

The influence of different growth-parameters was studied, especially about hydrogen and the height between the nozzle and foil. Precursor flow rate, background-pressure and substrate material were optimized for the experimental setup. Moreover, the difference of hydrogen flow rate and nozzle-substrate distance showed the different graphene growth on each foil. Dependencies about the substrate-nozzle distance and hydrogen flow rate were studied to gain a better understanding of the local feeding growth mechanism. A possible explanation for the dependencies based on the fluid mechanics inside the furnace was found.

ACKNOWLEDGEMENTS

First of all, I would like to thank Prof. Xie for giving me a great chance. All the discussion and advise he gave me through this program must be precious. I would like to thank Jimmy very much for the invitation to this project and his supports. And I would like to thank Hannes from University of Stuttgart, Germany for proceeding with this project together. And I would like to thank all members of his laboratory for supporting me. This study was also supported by Japan-US Advance Collaborative Education Program.

REFERENCES

- [1]. T. Wu *et al.*, 'Fast growth of inch-sized single-crystalline graphene from a controlled single nucleus on Cu-Ni alloys', *Nature materials*, **15**, no. 1, 43-47, 2016
- [2]. Novoselov KS, Geim AK, Morozov SV, Jiang D, Zhang Y, Dubonos SV *et al.*, 'Electric Field Effect in Atomically thin Carbon Films', *Science* **306**, 666-669 (2004)
- [3]. Allen MJ, Tung VC Kaner RB. 'Honeycomb carbon: a review of graphene', *Chem* **110**, 132-145 (2010)
- [4]. Soldano C, Mahmood A, Dujardin E. Production, 'properties and potential of graphene', *Carbon* **48**, 2127-2150 (2010)
- [5]. Waldmann, D. *et al.*, 'Bottom-gated epitaxial graphene', *Nature Mater.* **10**, 357-360 (2011)
- [6]. Liu, Y. *et al.*, 'Plasmon resonance enhanced multicolor photo detection by graphene', *Nature Commun.* **2**, 579 (2011)
- [7]. Liao, L. & Duan, X, 'Graphene for radio frequency electronics', *Mater. Today*, **15**, 328-338 (2012)
- [8]. X. Li *et al.*, 'Large-Area Synthesis of High-Quality and Uniform Graphene Films on Copper Foils', *Science* **324**, 1312-1314 (2009)
- [9]. S. Bae *et al.*, 'Roll-to-roll production of 30-inch graphene films for transparent electrodes', *Nat. Nanotechnol.* **5**, 574-578 (2010)
- [10]. N. C. Bartelt, K. F. McCarty, *MRS Bull.* **37**, 1158-1165 (2012)
- [11]. A.W. Tsen *et al.*, 'Tailoring Electrical Transport Across Grain Boundries in Polycrystalline Graphene', *Science* **336**, 1143-1146 (2012)
- [12]. P.M. Ajayan, B. I. Yakobson, *Nat. Mater.* **10**, 415-417 (2011)
- [13]. S. Bhaviripudi, X. Jia, M. S. Dresselhaus, J. Kong, 'Role of kinetic factors in chemical vapor deposition synthesis of uniform large area graphene using copper catalyst', *Nano Lett.* **10**, 4128-4133 (2010)
- [14]. I. Vlassiuk *et al.*, 'Role of Hydrogen in Chemical Vapor Deposition Growth of Large Single-Crystal Graphene', *ACS Nano* **5**, 6069-6076 (2011)
- [15]. Z. Yan *et al.*, 'Toward the Synthesis of Wafer-Scale Single-Crystal Graphene on Copper Foils', *ACS Nano* **6**, 9110-9117 (2012)
- [16]. H. Wang *et al.*, 'Controllable Synthesis of Submillimeter Single-Crystal Monolayer Graphene Domains on copper Foils by Suppressing Nucleation', *J. Am. Chem. Soc.* **134**, 3627-3630 (2012)
- [17]. I. Vlassiuk *et al.*, 'Graphene Nucleation Density on Copper: Fundamental Role of Background Pressure', *J. Phys. Chem.* **117**, 18919-18926 (2013)

<3> Research Presentations

- For 2016 Short-term course
---The 18th JUACEP Workshop



- For 2016 Medium- and Long-term course
---The 19th JUACEP Workshop





The 18th JUACEP Workshop for 2016 Short-term course students

Date: Thursday, October 6, 2016

Venue: IB015

[Timetable]

13:00 Opening address: Prof. Umehara, JUACEP Leader

13:05-13:20 **Kazuya Sato**, *mentored by Prof. Zhong He,
University of Michigan*

“Effects of scatter angle overestimation in Compton images
of partial energy deposition events” (Undisclosed)

13:20-13:35 **Chisato Atsumi**, *mentored by Prof. Yu Huang,
UCLA*

“Synthesis of octahedral Pt-Cu nanocrystals” (Undisclosed)

13:35-13:50 **Takaharu Katsu**, *mentored by Prof. Benjamin Wu,
UCLA*

“Synthesis of biopolymer compound with selective
antimicrobial activity for denture applications” (P.43)


13:50-14:00 Completion Ceremony

**10 minutes presentation + 4 minutes Q&A each*


Presentation of JUACEP program October 6th, 2016

Synthesis of biopolymer compound with selective antimicrobial activity for denture applications

Takaharu Katsu



Ohtsuki laboratory
Department of Crystalline Materials Science,
Nagoya University, Japan



Supervisor; Benjamin M. Wu, DDS, PhD
Department of Bioengineering,
University of California Los Angeles, U.S.A.

1

Outline

- I. Introduction
- II. Experimental part ①; Protection of amino group of poly lysine
- III. Experimental part ②; Synthesis of amide bond (1)
- IV. Conclusion

2

Outline

- I. Introduction
 - Back ground; problem of denture
 - Previous research
 - The aim and materials for the synthesis of antimicrobial polymer
 - The selection of synthesis steps
 - Scheme of my experiment
- II. Experimental part ①; Protection of amino group of poly lysine
- III. Experimental part ②; Synthesis of amide bond (1)
- IV. Conclusion

3

Back ground; problem of denture

Acrylic resin

- physical property
- mechanical property
- esthetic property
- △ reservoirs of microbial

The problem of denture

- i. adhesion
- ii. growth and formation of biofilm
- iii. chronic inflammatory ex. denture stomatitis

Fabrication of the resins on which microorganisms do not adhere

4

Previous research

antifungal agents antiseptics resins

- × toxicity for oral mucosa
- × damage the mechanical property
- × lose the effectiveness

alternative... cationic polymers


ex. Poly(2-tert-butylaminoethyl)methacrylate (PTBAEMA)

CC(C)(C)CN(C)CCOC(=O)C(C)C

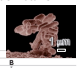
monomer

Julie MAARA et al., J. Appl. Oral Sci., 20(6), 643-648 (2012)


(1) *Staphylococcus aureus*

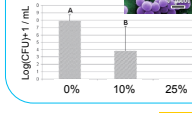
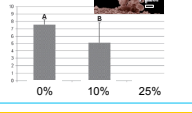
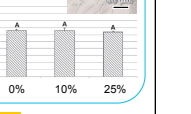


(2) *Streptococcus mutans*



(3) *Candida albicans*



No selective antimicrobial activity

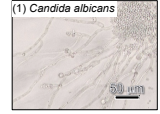
5

The aim and materials for the synthesis of antimicrobial polymer

Aim; selective antimicrobial activity for denture applications


◆ **Microorganisms**

(1) *Candida albicans*

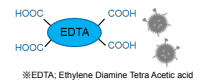


stomatitis

(2) *Fusobacterium*




bacterial acute pharyngitis



EDTA

※EDTA: Ethylene Diamine Tetra Acetic acid



Poly lysine

Chitosan

NC(CO)N

- Biocompatibility
- Non-toxicity
- Many amino group

Attaching EDTA and ε-poly lysine on the chitosan through amide bonding

6

The aim and materials for the synthesis of antimicrobial polymer

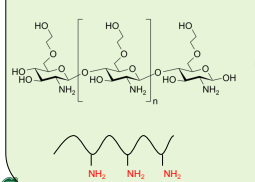
Aim: selective antimicrobial activity for denture applications

Glycol chitosan was modified by grafted EDTA-2Na and poly lysine for selective antimicrobial activity.

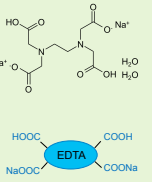
※EDTA-2Na, Ethylene Diamine Tetra Acetic acid disodium salt, 2-hydrate

○ Easy treatment
○ Without toxic organic solvent

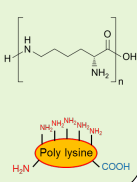
Glycol chitosan



EDTA-2Na



ε-poly lysine



The selection of synthesis steps

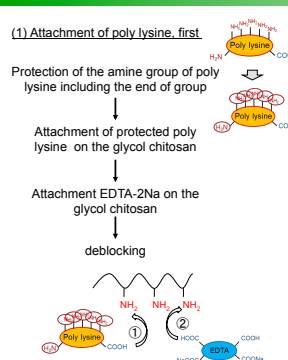
(1) Attachment of poly lysine, first

Protection of the amine group of poly lysine including the end of group

Attachment of protected poly lysine on the glycol chitosan

Attachment EDTA-2Na on the glycol chitosan

deblocking



(2) Attachment of EDTA-2Na, first

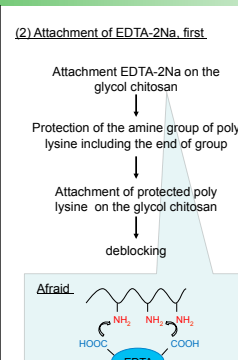
Attachment EDTA-2Na on the glycol chitosan

Protection of the amine group of poly lysine including the end of group

Attachment of protected poly lysine on the glycol chitosan

deblocking

Afraid!



The selection of synthesis steps

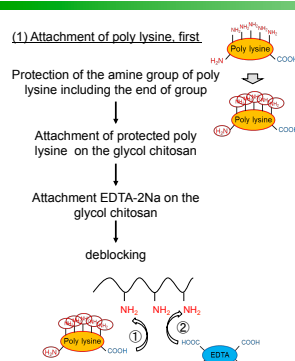
(1) Attachment of poly lysine, first

Protection of the amine group of poly lysine including the end of group

Attachment of protected poly lysine on the glycol chitosan

Attachment EDTA-2Na on the glycol chitosan

deblocking



(2) Attachment of EDTA-2Na, first

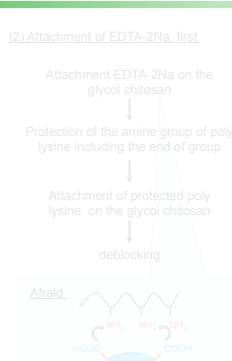
Attachment EDTA-2Na on the glycol chitosan

Protection of the amine group of poly lysine including the end of group

Attachment of protected poly lysine on the glycol chitosan

deblocking

Afraid!



Scheme of my experiment (1)

① Protection of amino group of poly lysine

ε-poly lysine (ε-PL) + (Boc)₃O → Protected PL

Reagents: Gu-HCl, EtOH/H₂O (1:1), overnight, r.t.

※(Boc)₃O, di-tert-butyl dicarbonate ※Gu-HCl, Guanidine hydrochloride

② Synthesis of amide bond (1)

Protected PL + Glycol chitosan → Amide bond

Reagents: HOBt, EDC, EtOH/H₂O, pH4.7-6.0, overnight, r.t.

※HOBt, 1-Hydroxybenzotriazole ※EDC, 1-Ethyl-3-(3-dimethylaminopropyl) carbodiimide

Scheme of my experiment (2)

③ Synthesis of amide bond (2)

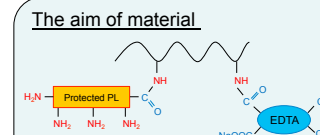
Protected PL + EDTA-2Na → Amide bond

Reagents: 1) HOBt, EDC, 2) H₂O/EtOH, pH4.7-6.0, overnight, r.t.

④ Deblocking

1N HCl, 3 h, r.t.

The aim of material



Outline

- I. Introduction
- II. Experimental part ①; Protection of amino group of poly lysine
 - Scheme
 - Result of ¹H NMR
 - Discussion
- III. Experimental part ②; Synthesis of amide bond (1)
- IV. Conclusion

Synthesis ①; Protection of amino group of poly lysine

ϵ -PL 0.250 g $(\text{Boc})_2\text{O}$ 1.27 g Gu-HCl 0.556 g EtOH 1.5 mL H_2O 1.5 mL

Molecular ratio
 ϵ -PL : $(\text{Boc})_2\text{O}$: Gu-HCl = 1 : 35 : 35

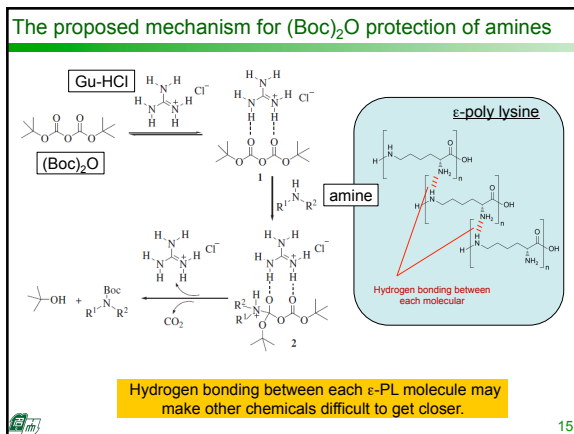
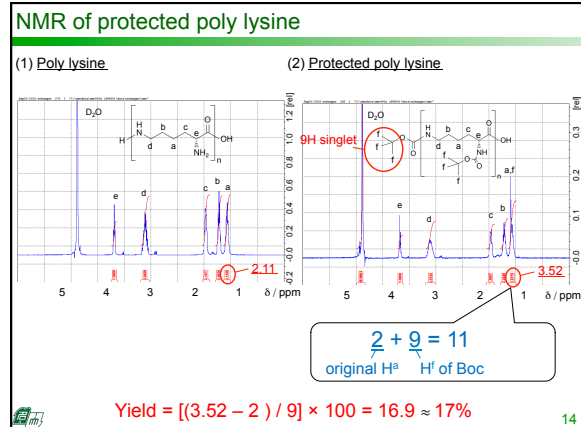
stirred
 solution

stirred at r.t. for over night
 dialysis
 lyophilization over night
 protected ϵ -PL powder

dialysis lyophilization protected ϵ -PL powder

protected ϵ -PL powder \rightarrow ^1H NMR

13



- ### Outline
- I. Introduction
 - II. Experimental part ①; Protection of amino group of poly lysine
 - III. Experimental part ②; Synthesis of amide bond (1)
 - Scheme
 - Result of ^1H NMR
 - Discussion
 - IV. Conclusion
- 16

Synthesis ②; Synthesis of amide bond (1)

Glycol chitosan 0.010 g HOBt 0.013 g MES buffer 1 mL Protected PL 0.072 g MES buffer 1 mL EDC 0.019 g MES buffer 1 mL

pH = 5.2

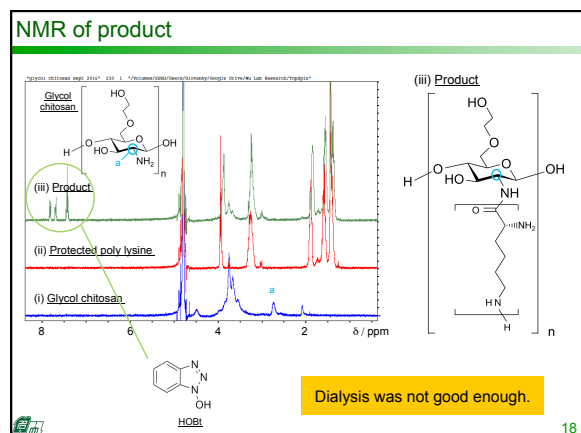
solution solution

Molecular ratio
 Glycol chitosan : HOBt : EDC = 1 : 2 : 2
 Protected PL: 3 mol% of Glycol chitosan

stirred at r.t. for over night
 dialysis
 lyophilization over night
 Glycol chitosan with protected ϵ -PL

Glycol chitosan with protected ϵ -PL \rightarrow ^1H NMR

17



Outline

- I. Introduction
- II. Experimental part ①; Protection of amino group of poly lysine
- III. Experimental part ②; Synthesis of amide bond (1)
- IV. Conclusion



19

Conclusion

- Modified glycol chitosan was synthesized by attaching Boc protected poly lysine.
- Protection ratio was about 17%.
- Protected poly lysine was attached on the glycol chitosan
- Almost all synthesis steps used the water solvent



20

The 19th JUACEP Workshop

**Research presentations by the 2016
long- & medium-term course students of
JUACEP at Univ. Michigan/UCLA**

Date: 13:00, Friday, March 31, 2017

Venue: IB 013

Timetable

- 13:00 Opening address: Prof. Umehara, JUACEP Leader
- 13:05-13:20 **Naoki Kamimura**, *mentored by Prof. Ya-Hong Xie, UCLA*
 “Local Feeding APCVD Graphene Growth on Cu and Cu:Ni Foils” (P.48)
- 13:20-13:35 **Kota Konishi**, *mentored by Prof. Wei Lu, Univ. Michigan*
 “Development of Three Dimensional Imaging Techniques Using Optical
Microscope” (P.51)
- 13:35-13:50 **Toshiya Sawaki**, *mentored by Prof. Richard Laine, Univ. Michigan*
 “Development of Transparent YSZ Thin Films” (P.53)
- 13:50-14:05 **Akira Tsuji**, *mentored by Prof. Pramod Reddy, Univ. of Michigan*
 “High Resolution Resistive Calorimetry Made of a Capillary Tube”
(Undisclosed)
- 14:05-14:20 **Keisuke Goto**, *mentored by Prof. Katsuo Kurabayashi, Univ.
Michigan*
 “Therapeutic Sepsis Biomaker Screening with Localized Surface
Plasmon Resonance Biosensors” (P.57)
- 14:20-14:30 Completion Ceremony

**10 minutes presentation + 4 minutes Q&A each*

Inquiry... JUACEP Office 052-789-2799



The 19th JUACEP Workshop
2017/03/31

LOCAL FEEDING APCVD GRAPHENE GROWTH ON CU AND CU:NI FOILS

Naoki Kamimura
Supervisor : Ya-Hang Xie



1

Contents

UCLA

1. Objective
2. Local Feeding Chemical Vapor Deposition System
3. Growth Condition
4. Results
5. Discussion
6. Conclusion

2

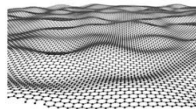
1. Objective of this experiment

UCLA

Graphene {
High transparency
High thermal conductivity
High electrical conductivity
High Young's modulus

Large-size single grain graphene

- High mobility
- Good mechanical properties



Wide range of applications

- Back-end of line integration (BEOL) devices
- Electrostatic Discharge protection device

3

1. Objective of this experiment

UCLA

Electrical mobility : μ

A method using a local precursor feeding setup
for large single grain graphene growth on a Cu:Ni-alloy has been reported [1].
: $\mu = 10,000 \sim 20,000 \text{ (cm}^2/\text{v}\cdot\text{s)}$

Conventional CVD graphene growth [2] : $\mu = 5,500 \text{ (cm}^2/\text{v}\cdot\text{s)}$
Exfoliated graphene flakes [3] : $\mu = 10,000 \text{ (cm}^2/\text{v}\cdot\text{s)}$

However,

Few details on the experimental setup to required C precursor distribution.
No information on the yield of the growth and repeatability of the process.

Preparation of the setup for reliable high yield growth
Growth of large single grain graphene

[1] T. Wu *et al.*, *Nature materials*, 15, 1, 43–47 (2016).

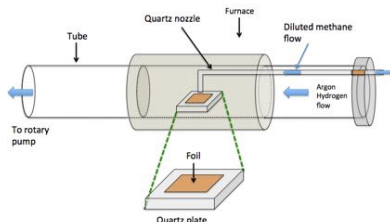
[2] Y.-P. Hsieh *et al.*, *RSC Adv.*, 7, 7, 3736–3740 (2017).

[3] K. S. Novoselov *et al.*, *Science*, 306, 5696, 666–669 (2004).

4

2. Local feeding CVD System

UCLA



Through the experiments, the setup had been optimized

Optimization	Merit
Gas-tight connection between the quartz nozzle and the feedthrough	Prevent gas leak
Atmosphere pressure CVD system	Reduce the random flow of background gas
Addition of quartz plates under the foil	Make nozzle-foil distance Changeable
Optimize the position of the foil placed in the center	Homogeneous temperature

5

3. Growth Condition

UCLA

i. Pretreatment

Cut Copper (25 μm , 99.8% for graphene growth, Alfa Aesar) to 4x4 cm²
Wash the foil by acetone, isopropyl alcohol (IPA) and DI water
Put it into polishing solution

ii. Growth

Time	CH ₄ [sccm]	H ₂ [sccm]	Ar [sccm]	Temperature [°C]	
10 mins	-	-	-	-	Pumping down
25 mins	-	-	1000	RT	Purge
30 mins	-	-	1000	RT ~ 1050	Heating
30 mins	-	-	1000	1050	Annealing
10 mins	5	-	1000	1050	Growth
6 hours	-	-	1000	RT	Cooling down

H₂ is set in the range of 0~1000 sccm.

From the experimental results, some parameters (CH₄, Ar flow rate, Temperature, Growth Time) are optimized.

iii. Contrast enhancement

Contrast enhancement for optical microscopy was done by selective oxidation on a hotplate.

6

3. Growth Condition

UCLA

After modification of the setup and some growth with various parameters, the influence of the **nozzle-substrate distance** ($l_{\text{nozzle-foil}}$) and the influence of **hydrogen flow rate** were observed.

Three types of growth were conducted to compare the results on each. The other parameters were fixed.

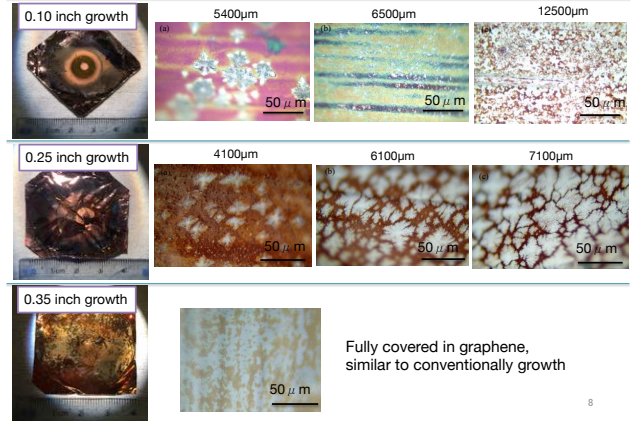
H ₂ [sccm]	l _{nozzle-foil} [inch]
50	0.1
50	0.25
50	0.35

H ₂ [sccm]	l _{nozzle-foil} [inch]
50	0.1
150	0.1
1000	0.1

7

4.1 Growth with the different height

UCLA



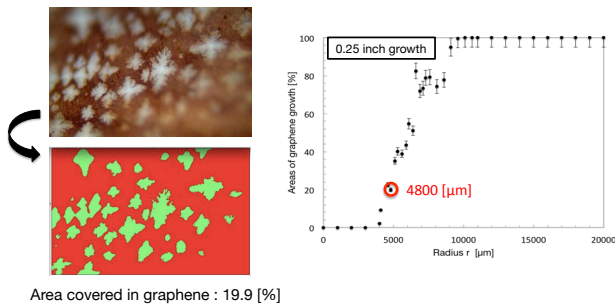
Fully covered in graphene, similar to conventionally growth

8

4.1 Growth with the different height

UCLA

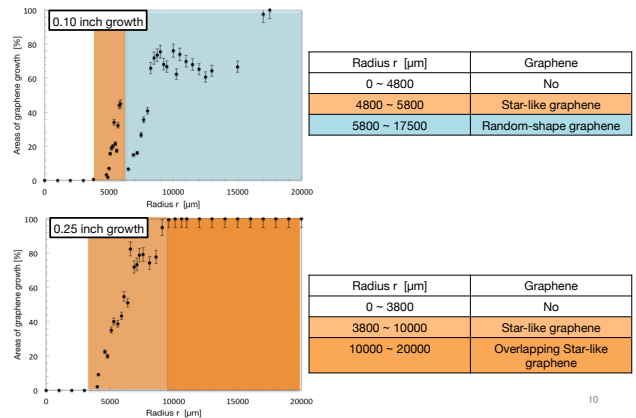
To get more detail about distribution of graphene, areas covered in graphene were calculated using *Fiji* on each area.



9

4.1 Growth with the different height

UCLA



10

4.2. Influence of the hydrogen flow rate

UCLA

5400µm	10000µm	5000µm	
H ₂ flow rate [sccm]	50	150	1000
Domain size [µm]	30~40	5~10	2~3
Graphene shape	Star-like	Hexagonal	Hexagonal

11

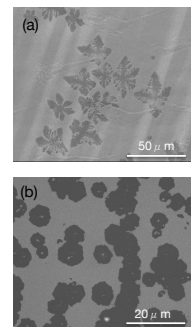
4.2. Effect of the hydrogen

UCLA

For graphene growth using CH₄ as a C precursor, H₂ plays an important role as a catalyst and as an etchant.

Condition difference of hydrogen flow rate

- (a) H₂ = 50 [sccm]
Star-like shape
H₂ works more as an etchant.
- (b) H₂ = 150 [sccm]
hexagonal shape
H₂ works more as a catalyst.



Ratio of CH₄ and H₂ partial pressure is important to determine the graphene shape and size.

12

5. Influence of partial pressure

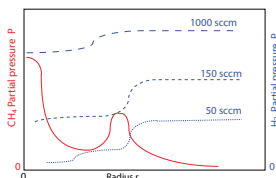
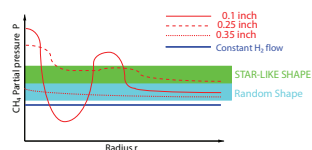
UCLA

Possible explanation for partial pressure of CH₄ and H₂

Assuming that H₂ flow is constant, the flow of CH₄ from nozzle could be influenced by the nozzle-foil distance.

Besides diffusion, the convection and probably turbulence in the local feeding gas stream leading the mixing of H₂ and CH₄.

A fix for the variability and low yield from the mixing issue is feeding both, H₂ and CH₄ locally.



13

6. Conclusion

UCLA

- A simple setup for local precursor feeding using a special sample holder was introduced.
- The important setup and process were determined.
- An explanation for low yield based on CH₄ and H₂ precursor mixing is given.
- The possible influence of different growth-parameters was studied, especially about hydrogen and nozzle-substrate distance.
- An alternative experiment for local graphene growth, feeding both CH₄ and H₂ locally, is proposed for the future work.

14

March 31st JUACEP WORKSHOP

Development of 3D imaging techniques using optical microscope

Kota Konishi

Department of Mechanical Engineering
University of Michigan



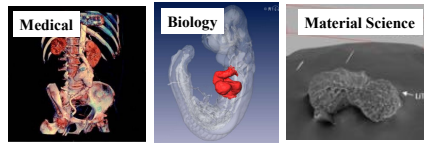
Advisor: Prof. Wei Lu



March 31st JUACEP WORKSHOP

Introduction

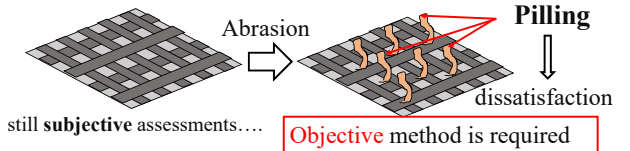
Three-dimensional (3D) imaging



Advantage

- Quantification
- Visualization

Evaluation of fabric abrasion



March 31st JUACEP WORKSHOP

Introduction



- Visualization
 - Quantification
- ⇒ Objective evaluation

For small specimen...

- μ-CT
- Confocal microscope
- TEM
- **Optical microscope**



- Low cost
- Easy accessibility
- Non destructive

March 31st JUACEP WORKSHOP

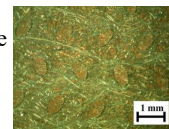
2

Objective

Fabric Sample

- Complicated structure
- Transparency

difficult to reconstruct 3D image



Make a 3D image of fabric material from 2D images using a ordinal optical microscope

March 31st JUACEP WORKSHOP

3

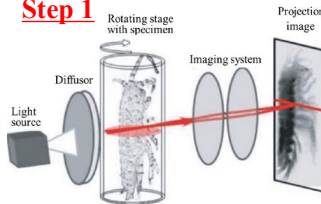
Method and Principle

Optical Projection Tomography (OPT)

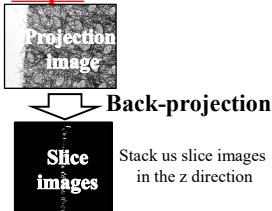
- Relatively new technique
- Only in the biology field
- Similar to CT principle

Procedure
1. Image acquisition
2. 3D reconstruction

Step 1



Step 2

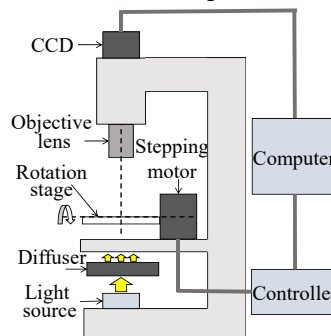


March 31st JUACEP WORKSHOP

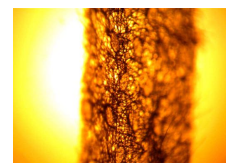
4

Method and Principle part1

OPT set-up



Projection images



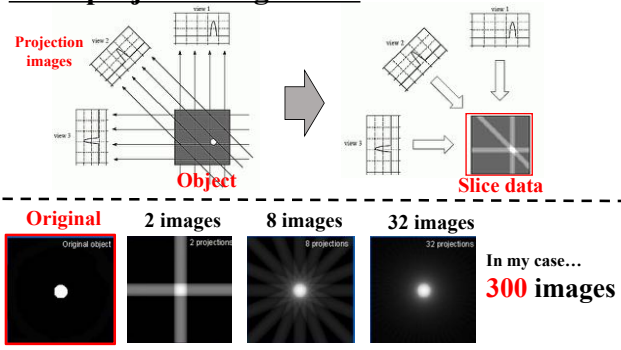
0.36° × 300 images

March 31st JUACEP WORKSHOP

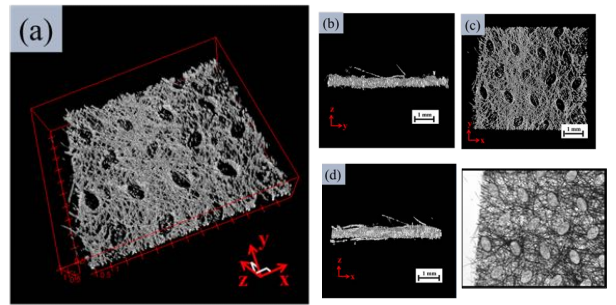
5

Method and Principle **part2**

Back-projection algorithm

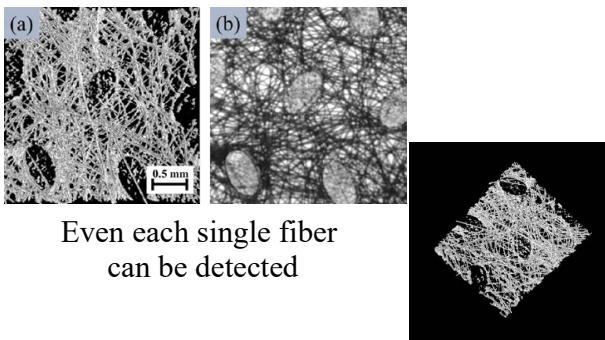


Results



3D visualization was successfully performed

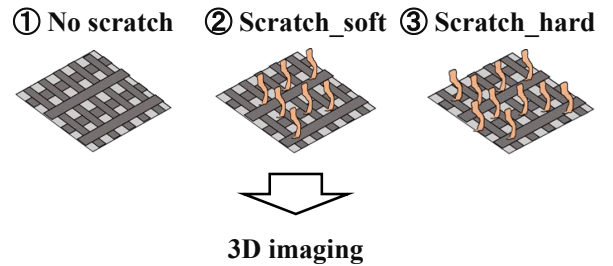
Results



Even each single fiber can be detected

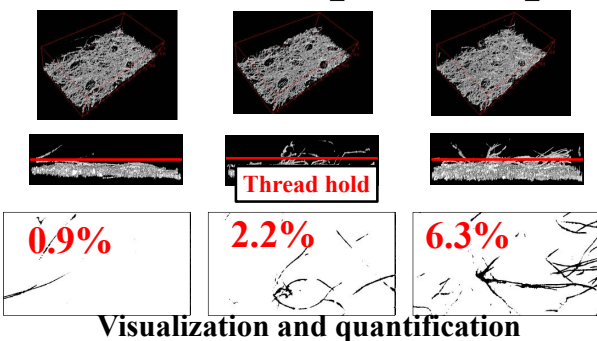
Application

Prepare different scratch-level fabrics



Application

① No scratch ② Scratch_soft ③ Scratch_hard



Visualization and quantification

Conclusion

- 3D imaging of fabric material was successfully performed using **ordinary optical microscope** and **some free software** *Contribution to my lab*
- Application for the evaluation of fabric abrasion is proposed using 3D imaging *Contribution to the society*



Development of transparent YSZ films

Department of Mechanical Engineering and Science
 Graduate School of Engineering
 Nagoya University
 M1 Toshiya Sawaki

Materials Science and Engineering
 University of Michigan
 Prof. Richard Laine

Outline



1. Introduction
2. Purpose
3. Experimental
4. Results & Discussion
5. Conclusion
6. Future work

1. Introduction Ceramics



Ceramics

- Good mechanical property
- Good thermal property
- Big scale production
- Capability for different shape



Optical ceramics

Application

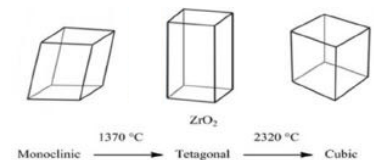
- YAG
 - ZrO₂
- ➔
- High power lasers
 - Cellphone surface

1. Introduction YSZ



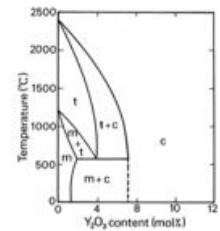
Zirconia

Cracks caused
 by phase changing



Yttria stabilized zirconia (YSZ)

Yttria dopant stabilizes cubic structure and prevent cracks



1. Introduction Conventional research



Transparent YSZ materials

Transparent 8 mol % Y₂O₃ doped ZrO₂ materials have been fabricated by hot isostatic pressing.

YSZ thin films

YSZ thin films have been prepared by several kinds of deposition methods.

Need in obtaining transparent YSZ thin films without special methods to achieve low cost and time-effectiveness.

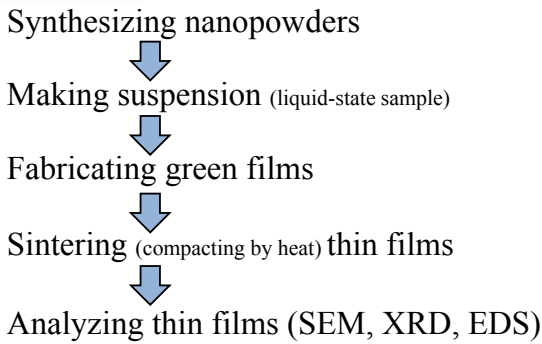
2. Purpose



To develop transparent YSZ thin films by tape-casting

3. Experimental Flow 

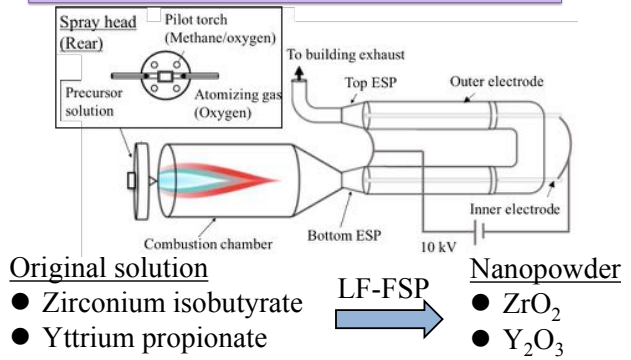
Flow



Nagoya University

3. Experimental Nanopowder synthesis 

Liquid feed flame spray pyrolysis (LF-FSP)



Nagoya University

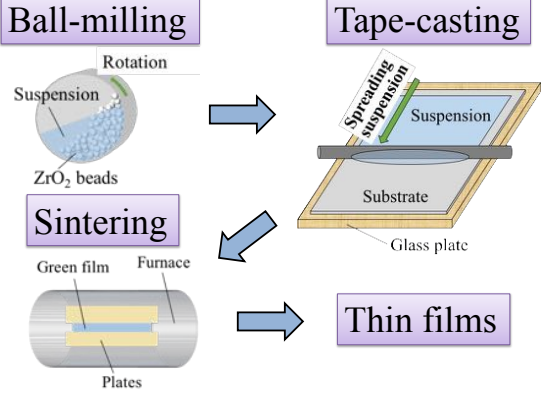
3. Experimental Suspension making 

Suspension composition

- Powders
give the properties
- Dispersant
disperses and solves particles homogeneously
- Plasticizer
softens suspension and make uniform thickness
- Binder
binds particles and prevents crack when drying.
- Solvent
solves ingredients

Nagoya University

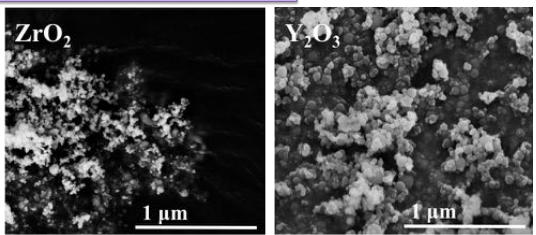
3. Experimental Film fabrication 



Nagoya University

4. Results & Discussion Nanopowders synthesis 

SEM of nanopowders

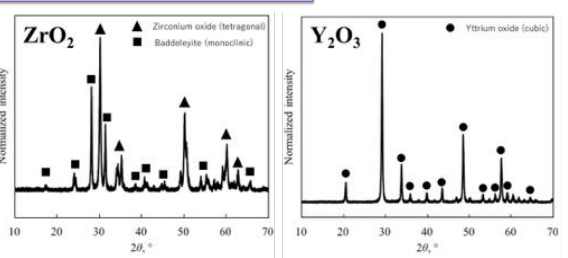


The average particle sizes were under 100 nm and spherical. Generally, smaller particles reduce sintering temperature and time compared to micron sizes.

Nagoya University

4. Results & Discussion Nanopowders synthesis 

XRD of nanopowders



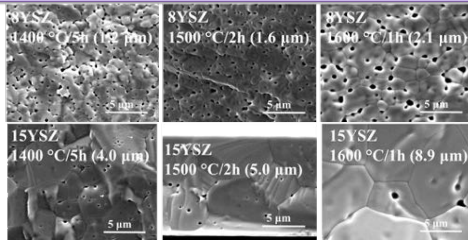
ZrO_2 powers have tetragonal phase because of rapid quenching of LF-FSP method.

Nagoya University

4. Results & Discussion Thin films property



8 and 15 mol % Y_2O_3 doped ZrO_2 (8YSZ and 15YSZ) thin films



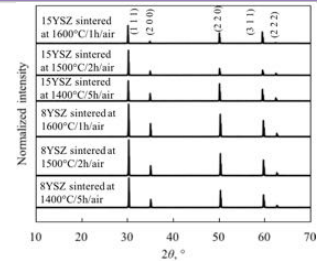
Higher sintering temperatures and higher Y_2O_3 dopant induced more densification and grain growth.
But, grain growth makes it difficult to fabricate thin films

Nagoya University

4. Results & Discussion Thin films property



XRD of 8YSZ and 15YSZ thin films



All peaks showed almost the same peak positions as cubic yttrium zirconium oxide even if the yttria dopant or sintering temperatures were changed.

Nagoya University

4. Results & Discussion Thin films property



8 and 15 mol % Y_2O_3 doped ZrO_2 (8YSZ and 15YSZ) thin films



Transparency of 15 YSZ thin films was higher than that of 8YSZ thin films because of lower porosity.

Nagoya University

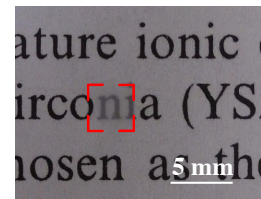
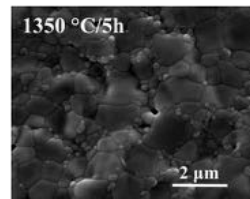
4. Results & Discussion 8YSZ/ TiO_2 thin films



8YSZ doped 3 mol % TiO_2 (8YSZ/ TiO_2) thin films

SEM fracture surface

Image



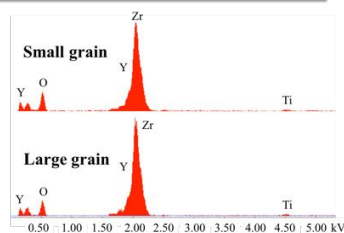
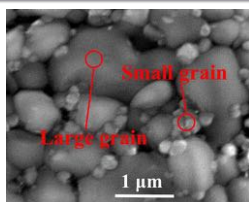
Small grains covered pores and increased transparency.
But 8YSZ/ TiO_2 stuck to plates strongly and fell apart because TiO_2 diffused to plates.

Nagoya University

4. Results & Discussion 8YSZ/ TiO_2 thin films



EDS of grain difference of 8YSZ/ TiO_2 thin films



	Small grain		Large grain	
Element	Wt. %	At. %	Wt. %	At. %
O	20.40	58.88	19.90	58.13
Y	13.08	6.79	13.94	7.33
Zr	65.05	32.92	64.76	33.18
Ti	1.46	1.41	1.40	1.37

No difference was detected.
Further work will be needed.

Nagoya University

5. Conclusion



- YSZ thin films were fabricated using nanopowders synthesized by LF-FSP.
- Show the possibility that TiO_2 dopant eliminates pores in YSZ thin films and increases the transparency.

Nagoya University

6. Future work



- Clarify how to make thin films intact.
- Clarify the mechanism of TiO_2 .
- Find out best composition and sintering condition.

19th JUACEP Workshop
2016.03.31
IB013

Therapeutic Sepsis Biomarker Screening with Localized Surface Plasmon Resonance Biosensors

Nagoya University
Dept. Micro-Nano Systems Engineering
1st year graduate student
Keisuke Goto

University of Michigan
Dept. Mechanical Engineering
Professor
Supervisor: Katsuo Kurabayashi



Introduction -Background-

Biomarkers in our body

- Proteins which play important roles in disease prediction and monitoring
- e.g. "cytokines" ... mediators and modulators in the immune system.

Quantification of cytokine provide immune response, hence it provides clinically and immunologically useful information related to acute inflammation and infectious disease.

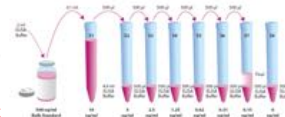
CitH3 -novel biomarker for early diagnosis of sepsis-

- Sepsis ... major threat to human health (sepsis causes organ dysfunction → 250,000 annual deaths in U.S.)
- CitH3 is revealed as a potential new biomarkers for early diagnosis of sepsis

ELISA -standard immunoassay-

- Fluorescent based measurement
- lack of the real-time information
- Minimum assay time (sampling to detection)
- 3 - 8 hours

Prohibits detection of the early on-set and transient status of sepsis for the treatment



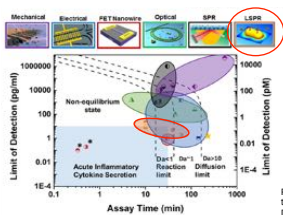
Introduction -Research Motivation-

Label-free biosensing

- Avoid labeling process → allows us to quantify biomarkers information
- Provide real-time information

Localized Surface Plasmon Resonance (LSPR) Biosensor

- Surface Plasmons** ... Resonant oscillation of the conduction electrons within the metallic nanostructures excited by incident light.
- highly sensitive to the change of local environment of metal nanoparticles
- Great promise to achieve high sensitivity and rapid assay



Pengyu et al. (2015) Label-free cytokine micro- and nano-biosensing towards personalized medicine of systemic inflammatory disorders, Adv. Drug Deliv. Rev. (2015)

Develop LSPR sensor to detect CitH3 within 1 hour assay time.

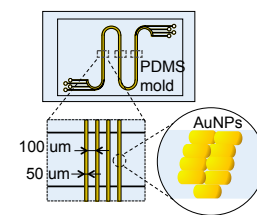


Method and Materials -Microchip fabrication-

Microchip fabrication

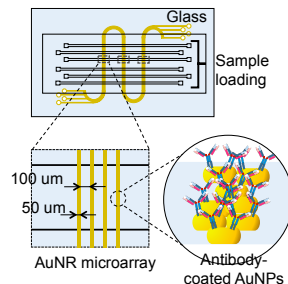
① Building sensor platform (gold nanoparticle AuNPs)

- Piranha treatment** ($H_2SO_4 : H_2O_2 = 3:1$)
 - O₂ plasma (30W)**
- Remove organic residue
 - Make surface hydrophilic
 - Negative charge on the glass surface → capture AuNPs in colloidal stock solution



② Attaching specific receptor (antibody) on sensor platform

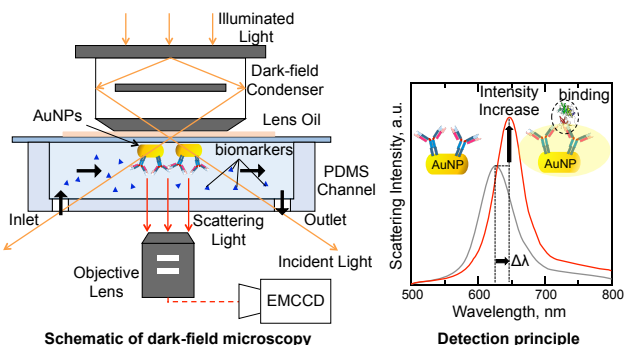
- Build a linker** (C16) between AuNPs and receptor (antibody)
- Receptor conjugation** on AuNPs surface, enhanced by EDC/NHS chemical reaction



Method and Materials -Dark-field Microscopy-

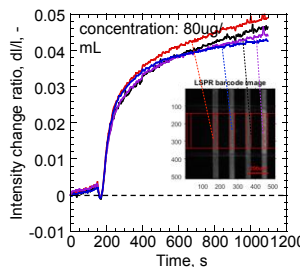
Dark-field microscopy

- Nanoscale is detectable (AuNPs ~ 80nm)
- Collect only scattering light



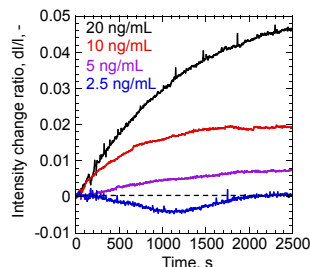
Results -Real-time CitH3 measurement-

CitH3 real-time monitoring



Monitoring receptor conjugation

Same dI/I from different sensor spots → consistent amount of conjugated receptors on the sensor surface.



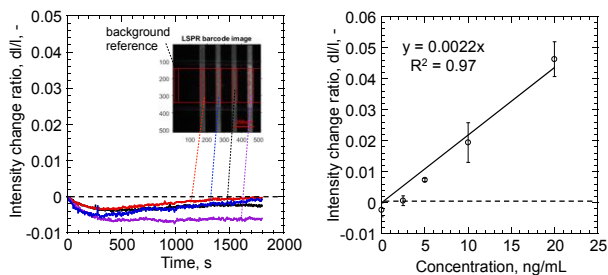
Detection of target molecule (CitH3)

Got different dI/I from each concentration of target molecules.



Results -Discussion-

Calibration curve



LOD: Limit of detection

$LOD = 3\sigma/k_{slope}$

σ : standard deviation of background signal

k_{slope} : slope of regression of calibration curve

LOD = 3 ng/mL

(ELISA : 0.1 ng/mL)

Conclusion

Conclusion

- We developed new immunoassay platform to detect CitH3, which is a novel biomarker for early diagnosis of sepsis.
- We achieved 40 min assay (5 times lower than standard method)
- We got calibration curve of CitH3 and LOD of 3ng/mL.

Future direction

- Further investigation in gold structure to improve sensitivity is needed.
- Future astronaut medical devices or immunological platform in space
Real-time monitoring → Fast and can reveal the nature of immune system
Simple detection scheme → Easy to use

<4> Findings through JUACEP

- Students' reviews
- Questionnaires (in Japanese)

Findings through JUACEP

Name: Chisato Atsumi

Affiliation at home country: Department of Crystalline Materials Science, Graduate School of Engineering, Nagoya University

Participated program: Short course 2016

Research theme: Specific peptide recognition against metal alloy surfaces

Advisor at the visiting university: Prof. Yu Huang

Affiliation at visiting university: Department of Materials Science and Engineering, HSSEAS, UCLA



-Research in UCLA

I would like to appreciate Prof. Yu Huang and JUACEP for giving me such a wonderful opportunity. The laboratory was very large and had a lot of apparatuses. Although the field of research in her group was similar to that of mine in Japan, my research here was completely different from that in Japan. So I read many papers to understand my theme and I learned how ignorant I am.

I was working with my mentor who is a candidate for Ph. D and a visiting student from China. I was lucky to have lab mate who started internship earlier than me, so she taught me how to do experiments. And mentor helped me when I wanted to use the analytical instruments which I didn't permit to use by myself. However, I sometimes bemoaned because I couldn't advance my experiments in my pace, it was up to my mentor and he was very busy. At that time, I ask other lab mates to help. All members in Yu Huang's group were very friendly and nice to me. My poor English sometimes caused problem, but they assumed and understood what I meant.

-Life in LA

The time I spent in LA was absolutely great. The campus of UCLA is very beautiful and the city around campus is very safe and convenient. And there are a lot of place to see in LA, moreover in the cities near LA. I went out many places on weekends. The most impressive thing for me is the comfortable weather in LA, always sunny, not so hot nor cold thorough a year. U.S.A. is a huge country, so everything such as road and food was huge. When you think the place is close on the map, it's very far. So it was sometimes convenient to go somewhere without car.

I lived in the apartment like a dormitory sharing one bedroom with another girl and kitchen and living room with other 3 girls. On the first day, I was very nervous because living alone in the foreign country and sharing my room with others was completely new experience for me, and I didn't know well about the place I would live in. The people living there was not only students, and they were from various countries. So talking with roommate was very interesting. We soon became friends and talked a lot. Every night was like a night of school trip. I satisfied with the environment here. Though I was nervous at first, thanks to many friends who helped me, I gradually accustomed to the life in LA and I could really enjoy my stay. There were so many small troubles here, but I could manage it every time. In the end, I couldn't understand why I was so nervous.



Findings through JUACEP

Name: Takaharu Katsu

Affiliation: Crystalline Materials Science, Nagoya University

Participated program: Short course 2016

Research theme: Synthesis of biopolymer compound with selective antimicrobial activity for denture applications

Advisor at the visiting university: Prof. Benjamin M. Wu, DDS, PhD

Affiliation at visiting university: Bioengineering, UCLA



I studied at UCLA for 2 months. I researched almost the same field as in Japan, but approached the aim through a different method. Furthermore, it was a new project in the lab, so I needed to search a lot of things. It was a little difficult, but it made me tough and strong. This has been a good experience for my future life.

As for the LA life, I visited many places and did a lot of things such as going to a Major League Baseball game, Hollywood, Santa Monica, Universal Studio Hollywood, San Francisco, and I even did surfing during weekends. I studied hard on weekdays, and I enjoyed a lot on the weekends.

This was the first time living without parents and I was especially afraid of cooking, but I actually enjoyed making dinner in the large kitchen. There is a Japanese supermarket near the house, so I was able to buy rice and other Japanese food. We shared the house with 4 people and they are all UCLA students. They kindly helped us adjust to this lifestyle. The room was big, clean, and quiet; moreover the weather in LA is very nice, especially since there is no rain and low humidity. It was so comfortable. On the last day, we had a sushi party at our house with roommates and Japanese JUACEP students. We enjoyed the Japanese traditional food.

Everything helped me improved. I spent a wonderful time there. I will never forget this experience. In the future, if possible, I would like to live and stay in LA again.

Finally, I really appreciate everyone who supported me, Prof. Wu, Prof. Ohtsuki and my lab mates, family, friends, and JUACEP whom all gave me such a special experience.



Life in Ann Arbor

Name: Kazuya Sato

Affiliation at home country: Quantum science and energy engineering

Participated program: Short course 2016

Research theme: Effect of scatter angle overestimation in Compton images of partial deposited energy

Advisor at the visiting university: Prof. Zhong He

Affiliation: Nuclear engineering and radiological Sciences



When I entered the US, I was very concerned about the life there. I am not good at speaking English, therefore I thought that I might not be able to even start my study. It was contrary to my expectations, and I had lived a happy life there. Not only for my study, but I did some activity like canoeing, golf, Frisbee golf, swimming in a lake etc.

Everything was impressive, especially people around Ann arbor. They are very kind and I was always helped when I encountered some problems. At the same time, I regret that I just did say "Thank you" and could not do a thing for the people.

Though I don't know how I can make the most of this experience at present, I am convinced that the experience should be useful someday in the future.



My findings through JUACEP

Name: Toshiya Sawaki

Mechanical Science and Engineering

Nagoya University, Mechanical Engineering

Participated program: Medium course: August 2016~ January 2017

Research theme: Development of transparent YSZ thin films

Advisor at the visiting university: Prof. Richard M Laine

University of Michigan, Materials Science and Engineering



In my case, I changed my research area from Mechanical Engineering to Materials Science. Everything was new for me, and it was hard to catch up with other students in my laboratory at first. But thanks to the support of professor and members in the laboratory, I could proceed my research. In particular, my knowledge about the research owes a lot to the class which I took. My professor was in charge of the class. Although I needed to do my homework every week and three examinations as other students in the class do, those experiences helped me to understand deeply the background of my research. A lot of people helped me to proceed my research. When I asked some questions resulted from my research, my professor and the members always took time and explained to me thoroughly. In addition, I am very thankful to people in charge of the experimental equipment. In University of Michigan, some of devices are shared by students in the engineering department, so I also needed to take training for use. Without their kindness and profitable advice, I could not master any equipment.

During my stay in United States, I experienced really a lot of things except for my research. But I would like to introduce two main things here.

Michigan stadium!!

The first thing is the Michigan stadium. University of Michigan is famous for a strong football team. Almost all students in the university have fun to watch football match. This stadium is so big that people call that "Big house". This stadium can accommodate one hundred thousand people at most. I went there to watch not only football game but also the performance of brass band. To be honest, I did not know the rule of football very much, but I enjoyed the match with my friends.



The second thing is the Halloween. In this season, even grocery stores sell Halloween stuffs like pumpkin dolls. Some people wear their Halloween costumes and walk around the city. I did not wear my costume, but when I went to the orchestra concert of Japanese video game "Final Fantasy", I could see many people wearing the character's costume made by themselves.

As often said, Japanese culture is a little unique compared to those of foreign countries. For example, I felt the difference about the ambitiousness. This is just my opinion, but I felt that students in University of Michigan have their own clearer dreams or purpose than Japanese students including me. Most of them also have reasons for their acting. I felt that I need to think about my purpose and act for realizing my dream. At this point this exchange program was beneficial for me.

Around my apartment!!



The best experience ever

Name: Kota Konishi

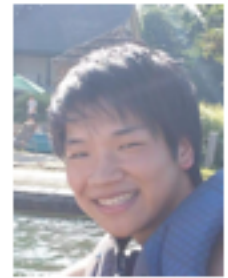
Affiliation at home country: Mechanical and Science Engineering, NU

Participated program: Medium course (Aug.2016-Jan.2017)

Research theme: Development of 3D reconstruction technics using a microscope

Advisor at the visiting university: Prof. Wei Lu

Affiliation at visiting university: Mechanical Engineering, Univ. of Michigan



I would say the best experience in my school life have been studying at the University of Michigan though the JUACEP problem. A year ago, my friend from UM highly recommended this JUACEP option, and I took his opinion. He was totally right. This experience will be helpful not only for the rest of my Master's studies but also for working at a company. I really appreciate my friend encouraging me to study abroad, JUACEP office giving me this opportunity, my parents supporting me financially, and professor Lu accepting me into his group.

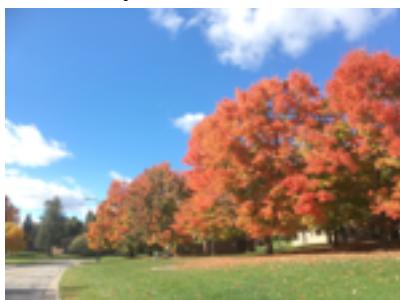
The University of Michigan is one of the finest universities in the world and the surrounding city, Ann Arbor, makes it a great city for studying abroad (besides the severe winter). People in Ann Arbor are very kind and generous. For example, when I had difficulty locating housing, my friend's friend let me stay at his house for 2 weeks even though I was a complete stranger to him. We have since become great friends.

Academically, my research topic was "3D imaging". Since this was totally different from the research in Japan, I had a hard time proceeding on my work at UM. Thanks to my lab mate, however, I managed to complete the research. He was always helpful when I was in trouble. Even though my topic has nothing to do with his research, he tried to understand me and provided some advice. Of course, If I haven't asked my lab mate for assistance, I wouldn't have learned anything. I learned therefore that the most important thing is be an active person.

Besides the research, I traveled, played basketball, watched football, and cooked. I did so much, and can't describe it all. I also experienced some cultural differences. I like the "How are you" culture, and I found that people are interactive everywhere. And people were willing to let newcomer in their group, so I even played basketball on a team. I really liked how friendly people at UM were. On the other hand, what I didn't become accustomed to was the lack of punctuality. Even classes begin ten minutes late, and the 10 minutes is called "Michigan time". In terms of punctuality, Japan is the best country. Through finding cultural differences, I can now look at Japan from a different perspective.

I visited several places in the US. The most amazing trip was one to Las Vegas on Thanksgiving break. We enjoyed the gorgeous atmosphere, like water fountain shows, and saw an entertainment show called 'Blue Man Groupe'. It was totally worth the money. We additionally visited Red rock canyon, Antelope canyon, and the Grand Canyon. I was touched with the nature's magnificence.

Last but not least, this experience definitely affected my career vision and made me be a more active person. I am so thankful for all the people who are related to this JUACEP program. I had not only many precious experiences, but also made many great friends. I highly recommend studying abroad if you have a chance. Thank you.



Findings through JUACEP

Name: Akira Tsuji

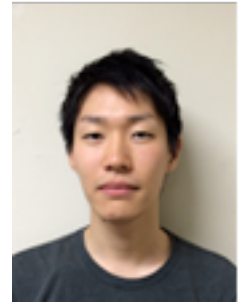
Affiliation at home country: Aerospace Engineering, Nagoya Univ.

Participated program: Medium course 2017

Research theme: High resolution resistive calorimetry made of a capillary tube

Advisor at the visiting university: Prof. Reddy, Prof Meyhofer

Affiliation at visiting university: Mechanical Engineering, Univ. of Michigan

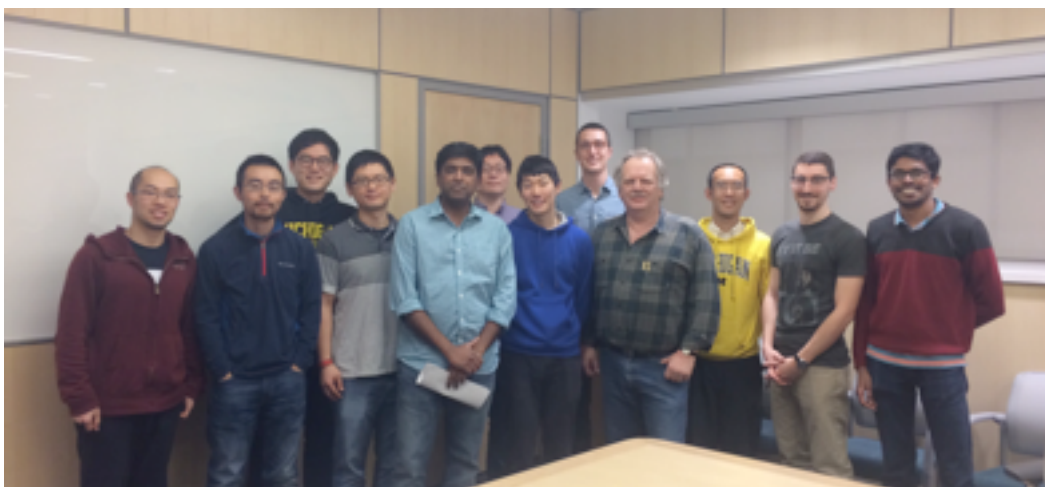


First of all, I am very grateful to Prof. Reddy and Prof. Edger for admitting me to stay at Nanoscale Transport lab. They gave me an opportunity to conduct a very interesting and challenging research. There, I was working on high resolution resistive calorimetry made of a capillary tube with Sunghoon, my TA, and development of low noise lock-in amplifier with Rohith, my TA. Especially, former topic was very challenging and interesting. Through these research, I was be able to learn electronic circuit, how to use spectrum analyzer, and micro-fabricated calorimeter. My TA Sunghoon and Rohith helped me a lot with the experimental side. Besides them, all lab mates have been helpful at all time. I would like to thank all of members in the lab for help me a lot.

I was able to visit some places. In Chicago, I ate deep dish pizza and saw “Bean”. Niagara falls were simply amazing. I was awed into silence when I saw those really up close. Boston had a good atmosphere, and I had a certain valuable experience there. Detroit was a thrilling city. The city is known as the most dangerous city in the US, and there were so many abandoned building. I spent New Year’s Eve in Times Square! It was crazy and perfect experience, but never again! New York was best city for me.

House share life is one of the best experiences in the U.S. We had 7 people in a small house! There were a lot of races in the house, and they were all good people. We have talked what happened the day, about own country, etc. almost every night, sometimes over beer. Everybody has own culture and thinking, and I was able to know these. I’m sure that this experience will have a positive influence in my life. I surprised that one of them (Andrew) was so good at Smash Bro. 64!

Through this program, I was able to learn a lot of things not only academic things but also cultural things, and it will be helpful to broaden my horizons.



Findings through JUACEP

Name: Naoki Kamimura

Affiliation at home country: Quantum Engineering, Nagoya University

Participated program: Medium 2016



Research theme: Local feeding APCVD graphene growth on Cu and Cu:Ni foils

Advisor at the visiting university: Prof. Ya-Hong Xie

Affiliation at visiting university:

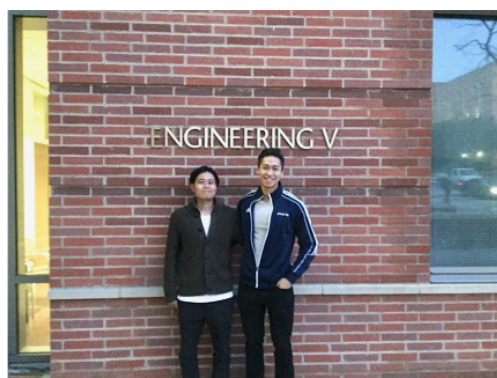
Materials and Science Engineering, University of California Los Angeles

My experience through JUACEP was precious to me no matter whether I was on campus or off campus. Fortunately, I was able to meet many people with multicultural background due to the rich diversity of Los Angeles. One thing I found interesting is that every single student I met, despite the difference in nationality, was very ambitious and had clear academic goals at UCLA. In fact, they had specific reasons why they came to the university and the desire to accomplish their worldwide career goal after graduating. On the other hand, since I was born and raised in Japan as well as many of my friends and family, I only had Japanese way of thinking before I came here. By immersing myself into a multinational environment, I could broaden my perspective and also opened up my mind toward future goal and career.

Moreover, I would like to talk about my experiments at UCLA. I had been able to join UCLA for a total of six months as a visiting graduate researcher (VGR) under the supervision of Prof. Ya-Hong Xie. Our group was composed of four small research groups, each group worked on their own research. I worked with another VGR from Germany, a UCLA Ph. D student and a undergraduate student, focusing on local feeding APCVD graphene growth on Cu and Cu:Ni foils. Our group had many group discussions including professor, so I was able to be involved to the project in deep. My professor always asked us to conduct experiments and explain the results on the basis of physics very seriously. I really liked his professional approaches to the well-unknown phenomena. Furthermore, I was able to do experiments comfortably in the lab because my lab mates were very cooperative to me, especially when using new equipment and software. Unfortunately, I was not able to get large single-grain graphene, which is the biggest target for our group during my stay at UCLA but we just found several hints to get large single-grain graphene. Of course, the objective of the stay is to get results in the experiment. However, more importantly, I am grateful for the time doing the worthwhile work and heading toward the same goal with my valued peers and professor as one team. This experience at UCLA will for sure have good effects in my coming life. Lastly, I hope that my peers can do well and fabricate large single-grain graphene in near future.

As for the off-campus activity, I enjoyed a lot of things such as soccer, surfing, music concert and so on. Although there are plenty of things I have learned, felt and lived, I cannot mention all in detail because I only have A4 size sheet. Therefore, I would like to write down some of the places I visited, where I made unforgettable memories in each trip. Along with the experiments at UCLA, I had a chance to visit San Francisco, Santa Barbara, San Diego, Las Vegas, New York, Boston, Arizona and Cancun in Mexico. Honestly, every trip was amazing for me. Depending on the city, I could obviously see the difference in people's life style, culture, music, fashion, safeness, weather and so on. While I was able to see wonderful but strange places and people, it made me realize the vast diversity of the United States and how big the world is.

In the end, I would like to thank Jimmy, Hannes and Kazu for making my adventure such a special time of my life. And also I would like to express my appreciation to Prof. Xie, Prof. Saito and staffs of JUACEP for giving me this meaningful opportunity.



Findings through JUACEP

Name: Keisuke Goto

**Affiliation at home country: Micro-Nano System Engineering
Nagoya University**

Participated program: Long course 2016

**Research theme: Therapeutic Sepsis Biomarker Screening with Localized
Surface Plasmon Resonance Biosensors**

Advisor at the visiting university: Prof. Katsuo Kurabayashi

**Affiliation at visiting university: Mechanical Engineering,
University of Michigan**



This exchange program could change my entire life. In Japan, I was wondering why we did research, and lost my way. However, Professor Katsuo taught me the importance of having a clear vision for research and it completely changed my thought towards engineering and research. Throughout the supervision under him and his colleagues, I could build my strong mindset as a researcher and engineer such as problem solving and designing the research and experiment. If I did not come to Michigan, if I did not come to his lab, I would not be able to figure out my ethical question towards the research. Although I did not have any experience and knowledge about his research field, thanks to his and his colleagues' help, I could finish my project and slightly drive the research by myself. It is a great honor to work with them.

Thanks to my friends who I met in U.S., I had an absolutely great time with them. I went to kayak, BBQ, parties, and everything that I saw in U.S. was amazing. Also, it was fortunate for me to meet again my friend that I met in UK 2 years ago in U.S. During Thanksgiving break, we went to New York and New Haven because he was in Yale University. We really enjoyed watching Macy's parade and having Thanksgiving party. People that I met in U.S. were very kind and warm, so I cannot thank you enough.

The most exciting thing that I experienced in U.S. is definitely viewing rocket launch at Kennedy Space Center. Falcon 9, which is the rocket SpaceX developed, ascended to the space. This was the first reflight from KSC pad 39A since 2011, when the space shuttle Atlantis lifted off on the final flight of NASA's shuttle program. When I stared into the light ascending to the sky, I was like a kid in a candy store. This experience ignited my heart and determined my future dream. This is the second change of my life happened during JUACEP.

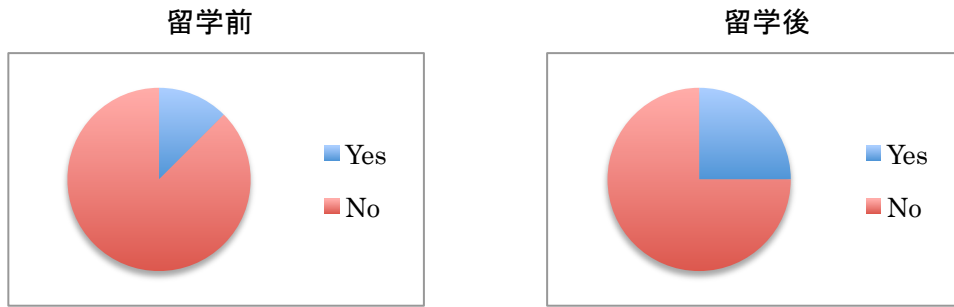
By the way, this was the first time for me to live by myself. Before I came to Ann Arbor, I did not know even how to cook and housework. But finally, I could survive somehow, haha. It was also a great experience for me.

I could not make it clear my future career, but I found the direction that my compass showed through this exchange program. I will never forget anything that I felt, experienced and thought through the life in Michigan.

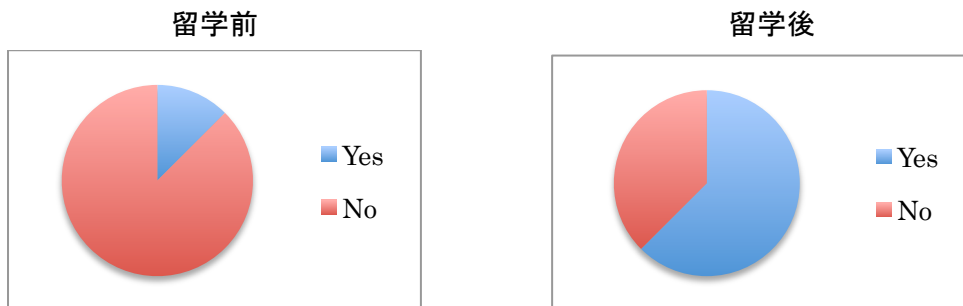


派遣プログラム参加者に行ったアンケート結果

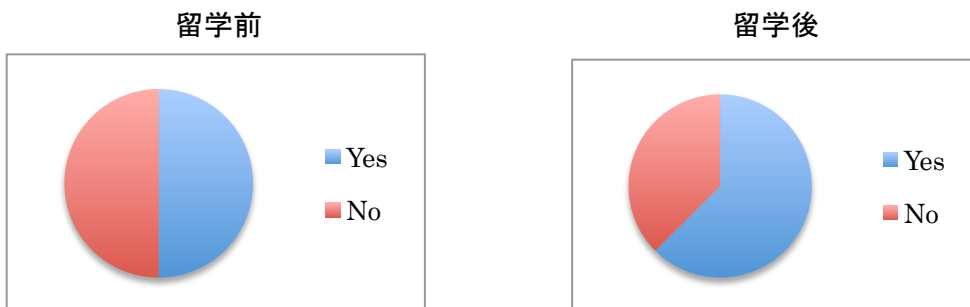
＜博士課程進学に興味がある＞



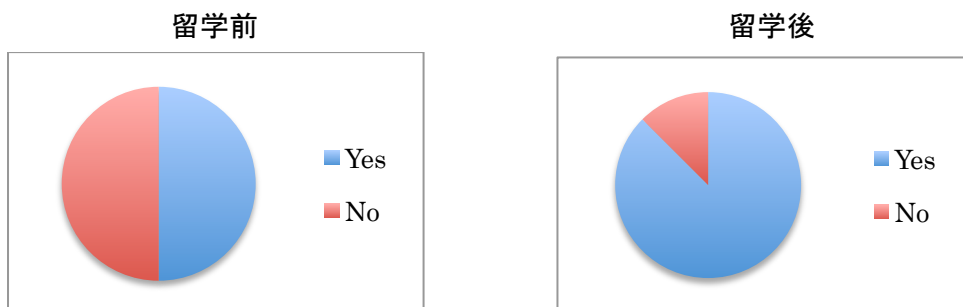
＜外国の大学での博士課程進学に興味がある＞



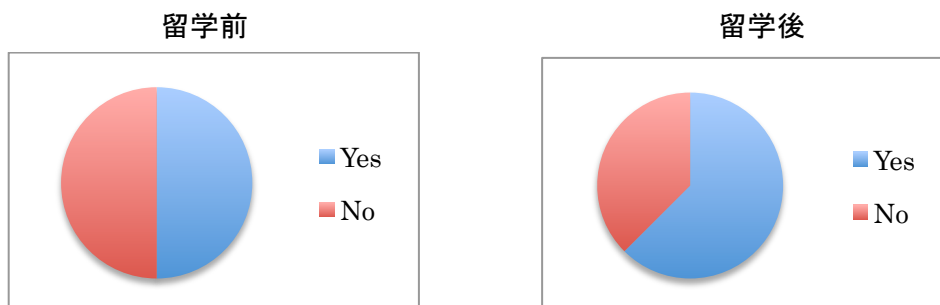
＜日本での外資系企業への就職に興味がある＞



＜外国での日系企業への就職（海外勤務）に興味がある＞



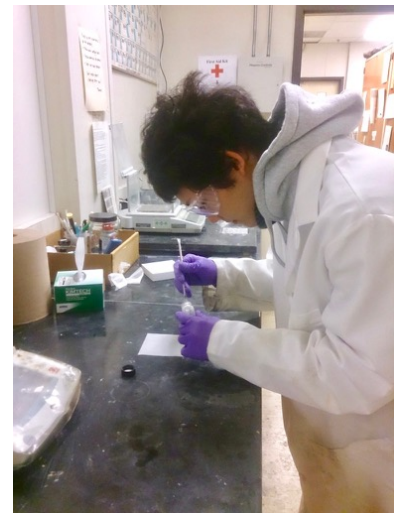
＜外国での日系以外の企業への就職に興味がある＞



1. このプログラムの良かった点 (○) と改善してほしい点 (×) について

- 自分で学びたい分野を決め、自由に教授にアプライさせてもらったので、興味のある研究ができた。
- 留学中も近況報告を課せられないため、リラックスして研究を行えた。
- 研究というしっかりした軸を持って留学することができる。海外留学生の中には、はっきりとした目的がないまま留学しているという人が少なくなかったため、このことは強みではないかと感じた。
- 事務の方が、留学に行くまでのサポートを手厚くしてくれる。(VISA 取得など)
- 留年せずに、短期間で留学できたこと。
- 住みやすく安全な町にある UCLA とミシガン大学から選べること。
- 他の留学方法に比べ留学への敷居が低いこと。また研究に集中出来ること。研究に対する文化が日本と異なっており、その文化に深く携われたことは自分の知見・考え方を広げるのに有意義であった。
- 教授の下で研究に従事できて単位を取得できる点。
- 奨学金があること。
- UCLA/ミシガンから名大に來ている JUACEP 留学生と渡航前に交流できたので現地で心強い。

- × 単位に関して言えば、半年間という期間で 2 単位しか付与されないのは少ないと思う。
- × 家賃や保険など学業面以外の支出が多かったため、金銭面のサポートがもう少し欲しかった。
- × 奨学金が足りない。家賃でほとんど消えるか、家賃にも満たない。物価が予想以上に高い。
- × 工学研究科の教員方への認知度の低さ (私の量子工学専攻ではあまり周知がされておらず、手続き等の際大変であった。)
- × 受け入れ先を決める時、協定校間のプログラムで行くことを伝えても受け入れてもらえず大変苦労した。短期間住める家を探すのは難しく、家賃も物価も高かったため、奨学金が足りない。支給額も少ない上に、手続きもほとんど自分で行っており、プログラムで行く必要性が感じられないと思いました。時期がよくないと思います。
- × 到着してからの宿探しは本当に苦労する。研究に集中できない。最初の数週間の滞在先の確保だけでもしていただけると助かる。また基本的に情報の伝達が遅いまたは不十分であった。奨学金が円支給であると為替の変動によって実質支給額が変動するため、ドル支給だとありがたかったです。
- × 受け入れ先を探す際のサポートが乏しい点。



- × アパートを探すのが大変。現地到着後は、入学シーズンでもあるので、春ごろからアパートのサポートが始まれば、住居探しの苦勞も減るかもしれない。
- × 宿の確保について、名古屋大学で確実に手配してほしいと感じた。ミシガンの学期の関係で、2か月間(8, 9月)のみのリースは皆無。運よく3週間だけのリースができたのでその分の宿代は比較的抑えることができたが、それでもホテル生活が長く、金銭的に大きな負担を強いられた。この点で、2ヶ月コースの人には厳しいプログラムだと思う。
- × 保険や DS2019 についての過去の例や情報があるともう少し楽だった。
- × 受け入れ先研究室を決定する際のコンタクトのサポート

2. 講義「国際共同教育外国語演習」についての感想（受講者のみ）

- ・ とても有意義だった。英語でのプレゼンテーションの機会が初めてであったため、一度でも経験しておくことが留学後も役に立った。また他の留学希望者との交流もあり、自分の留学に対する気持ちを整理することができた。
- ・ 事前に自分の研究を留学先で説明する良い練習になった。
- ・ 講義中はアカデミックな視点で、アドバイスをいただけたので良かった。
- ・ 英語で発表した経験がなかったため、毎回の授業の準備に長い時間がかかり大変でした。しかし、終わってみると、大変ためになり授業を受けてよかったと思います。先生は優しく丁寧に添削してくれ、受講者のみんなもやる気があり一生懸命取り組んでいたもので、雰囲気がよく刺激になりました。
- ・ 基本的な英語でのプレゼンのコツや、テクニックを学べたので良かった。実際、留学直前の国際学会で役に立った。
- ・ 少人数による授業で、一人一人に的確なアドバイスをしていただき、非常に有益だった。留学中にどのように生かされたかはよくわからないが、留学前に英語に慣れるという意味で効果があったと思う。
- ・ 現地で日本の研究内容の紹介をプレゼンする機会があり、授業でやったことを生かした。
- ・ 英語に限らずプレゼンテーションには慣れが必要であり、この授業では毎週発表の機会を与えてくれたため、人前で話すことに抵抗が少なくなった。



3. その他、自由コメント

- ・ ミシガン大学という工学部の中でもレベルの高い学校で研究生活する機会は滅多にないと思う。その意味で JUACEP に参加できたことは良かった。新しい知識が身に付けられることはもちろん

んだが、日本に帰った後の研究への姿勢を考えさせられるいい機会にもなった。

- ・ ミシガン大学が存在するアナーバーという町は、アメリカの中でもかなり安全で生活しやすい。コンビニこそ日本ほどはないものの、市民が無料で利用出来る公共バスが充実しているため、スーパーや食事、デパートに簡単に行ける。特にアナーバーで出会った人々は優しく困った時に助けてくれる。留学初期は研究に関連する人々を始め、色々な人々にお世話になった。ミシガン大学を選んで良かった。
- ・ 留学の手続きに関して、わからないことやトラブルが多く、事務室には大変お世話になりました。海外の教授とメールでやりとりする経験はなかったので、1通送るだけでもこの文面で問題はないか、失礼ではないか不安でした。自主的にやることも勉強にはなるとは思いますが、はじめの時点でもっと詳しく手続きについて教えて頂ければスムーズに進むのではないかと思います。M1の前期は授業も多く、行くまでがすごく大変だった。過去の先輩の手続きにおける前例など先に説明してほしかった。
- ・ JUACEP を通じて非常に貴重な経験をさせていただきました。この場を借りて JUACP に携わった全ての方々に感謝の意を表します。また私自身非常に有益であったと考えているため、ぜひ来年度以降もプログラムを継続させ、より多くの人に同様の経験を得る機会を設けることができることを願います。
- ・ 科学への、工学への見方が180度変わり、忘れられない留学となりました。
- ・ 自分にとっては初めての、1ヶ月超の海外生活。一人でアメリカに入国を果たし、大学に足を運ぶまでは不安しかなく、プレッシャーで押しつぶされそうになっていたことを今でも覚えています。バスの乗り方すらも覚束ない中、大学周辺の人たちはとても優しい人ばかりで、判らないことを質問すると、親切にいろいろ教えてくれました。同じ研究室の仲間たちは非常に高い向学心を持ち、刺激を受け、2か月という短い期間ながら、一定の成果を出せたのもラボのメンバーの協力によるところが大きいように思います。この経験やモチベーションを維持したまま、日本での学習、研究に還元していきたいと思っています。
- ・ 個人差はあるだろうが、語学留学と比べると、研究室に籠っている時間が長いため、英語を話す機会が少ない。語学力の向上は、意識して勉強していないとある程度のところまでしか行けないと思う。
- ・ 渡航者に、来年以降の受け入れを自分のところの教授にお願いしてくるよう決めておくといいと思う。研究室決めのハードルが多少なりとも下がると思う。
- ・ 準備段階ではわからないことだらけで終わりも見えない中、サポートありがとうございました。
- ・ 海外で2か月生活するという、貴重な体験をさせていただき感謝しております。
- ・ 留学なんて微塵も考えていなかった僕に留学のチャンスを与えてくれてありがとうございました。



Copyright © JUACEP 2017 All Rights Reserved

Published in August 2017

JUACEP

Japan-US Advanced Collaborative Education Program

Graduate School of Engineering, Nagoya University

Furo-cho, Chikusa-ku, Nagoya 464-8603, Japan

+81-52-789-2799

JUACEP@engg.nagoya-u.ac.jp

<http://www.juacep.engg.nagoya-u.ac.jp>

